Isolation and characterisation of umbilical cord blood serum exosomes

by

Sphesihle Mkhize

Submitted in fulfilment of the academic requirements of

Master of Science

Discipline of Biochemistry

School of Life Sciences

College of Agriculture, Engineering and Science

University of KwaZulu-Natal

Pietermaritzburg

South Africa

July 2023

PREFACE

The research contained in this dissertation was completed by the candidate while based in the Discipline of Biochemistry, School of Life Science of the College of Agriculture, Engineering and Science, University of KwaZulu-Natal, PMB, South Africa. The research was financially supported by the National Research Foundation (NRF) as well as Next Biosciences.

The contents of this work have not been submitted in any form to another university and, except where the work of others is acknowledged in the text, the results reported are due to investigations by the candidate.

Signed: Prof C.U. Niesler

Date: 08 January 2024

DECLARATION 1: PLAGIARISM

Note that two declaration sections are required if there are papers emanating from the dissertation/thesis. The first (obligatory) declaration concerns plagiarism and the second declaration specifies your role in the published papers.

I, Sphesihle Mkhize, declare that:

(i) the research reported in this dissertation, except where otherwise indicated or acknowledged, is my original work;

(ii) this dissertation has not been submitted in full or in part for any degree or examination to any other university;

(iii) this dissertation does not contain other persons' data, pictures, graphs or other information, unless specifically acknowledged as being sourced from other persons;

(iv) this dissertation does not contain other persons' writing, unless specifically acknowledged as being sourced from other researchers. Where other written sources have been quoted, then:

a) their words have been re-written, but the general information attributed to them has been referenced;

b) where their exact words have been used, their writing has been placed inside quotation marks, and referenced;

(v) where I have used material for which publications followed, I have indicated in detail my role in the work;

(vi) this dissertation is primarily a collection of material, prepared by myself, published as journal articles or presented as a poster and oral presentations at conferences. In some cases, additional material has been included;

(vii) this dissertation does not contain text, graphics or tables copied and pasted from the Internet, unless specifically acknowledged, and the source being detailed in the dissertation and in the References sections.

Signed: Sphesihle Mkhize

Date: 16 July 2023

DECLARATION 2: PUBLICATIONS

Details of contributions to publications/conferences that form part and/or include research presented in this thesis.

Mkhize, S. & Niesler, C. (2023). *Isolation and characterization of Umbilical Cord Blood Serum exosomes*. 2nd STELLENBOSCH EXTRACELLULAR VESICLE SEMINARS & WORKSHOP, Stellenbosch, South Africa; 22-33 February 2023.

Mkhize, S. & Niesler, C. (2022). *Cord blood serum exosome isolation and characterization for wound healing and drug delivery.* Postgraduate Research Symposium 2022 (PRIS22) oral presentation, University of KwaZulu-Natal, South Africa; 8 December 2022. Prizes won: 3rd place, Most Impactful Research, as well as lucky draw.

Mkhize, S., Niesler, C., Buthelezi, K., Montague, C., Holt, Y., Nkosi, N., Ramela, L., Mati, L. (2022). *Lyophilisation of umbilical cord blood serum – a comparison of epithelial growth factor content to non-lyophilised serum to indicate similar potency.* 29th SATS & 6th SATiBA Congress, Stellenbosch Institute of Advanced Studies, South Africa; 11-13 November 2022. Prize won: best poster presentation.

Signed: Sphesihle Mkhize

Date: 16 July 2023

ABSTRACT

Exosomes are small lipid-bound extracellular vesicles (30 – 150 nm in diameter) that are released via the endosomal pathway to mediate communication with target cells through the delivery of specific cargo. This cargo can include proteins, such as growth factors, as well as nucleic acids, such as regulatory miRNA and coding mRNA, which can collectively influence biological processes such as cellular proliferation and migration. Exosomes are present in multiple bodily fluids, including amniotic fluid, urine, plasma, serum, and saliva; they therefore have applications in biomarker development, immune system modulation, regenerative medicine, cancer therapeutics and drug delivery. Umbilical cord blood serum (UCBS) contains many growth factors, and cytokines and has been shown to be efficacious in the treatment of corneal damage and ocular surface disorders; it is commercially available as Optiserum, a 20% dilution of UCBS. The current study aimed to isolate and characterise exosomes from the cord blood serum in Optiserum. The Optiserum samples were provided by Next Biosciences (Midrand, South Africa). Exosomes were isolated from Optiserum using PEG6000 and characterised using tunable resistive pulse sensing (TRPS), transmission electron microscopy (TEM) and immunocytochemistry (ICC). The effect of these exosomes vs. UCBS on cell proliferation was determined using the standard MTS assay. Total protein and epidermal growth factor (EGF) levels were then determined using the Bradford assay and Quantikine EGF ELISA respectively, while cytokine levels were measured using the Bio-Plex Pro Human Cytokine Screening Panels (27-plex and 48-plex). Exosomes, characterised by their cup-shaped morphology and expression of Cluster of Differentiation 81 (CD81), with a mean diameter of 111 ± 12 nm and an average concentration of 6 x 10^9 ± 3 x 10^9 vesicles/ml were successfully isolated from Optiserum. The average total protein concentration in exosomes was determined to be 1 ± 0.1 mg/ml, compared with 14.7 ± 2.5 mg/ml of the original Optiserum (indicating 7% of total protein in the exosome fraction). To determine the effect of the UCBS-isolated exosomes on cell proliferation over 24

hours, human embryonic kidney 293 (HEK293) cells were cultured in the absence or presence of 1 x 10^3 – 1 x 10^8 exosomes in serum free medium (SFM); serum containing medium (SCM) was used as a positive control, whereas SFM was used as a negative control, for proliferation. Exosomes were taken up by HEK293 cells and observed to increase cell proliferation in comparison with cells cultured in SFM alone; specifically, cells cultured in SFM containing 1 x 10^8 exosomes promoted cellular proliferation to levels that exceeded the proliferative effect of SCM. Protein analysis revealed exosome enrichment of β-Nerve Growth Factor (b-NGF) and Interleukin-15 (IL-15) when compared with the matched Optiserum batch. Both the Chemokine Growth-Regulated Protein–α (GRO-a) and Tumor Necrosis Factor–α (TNF-α) were present at comparable levels in the exosomes and the Optiserum from which they were isolated. In conclusion, exosomes can be successfully isolated from cord blood serum and, despite containing a fraction of the total protein that exists in the original serum, they can promote proliferation of HEK293 cells. This may be related to the demonstrated enrichment of specific proteins as well as ability to deliver cargo directly to the target cell. Future studies will continue to explore the mechanism of action and will additionally include cargo loading with proteins of interest as well as the analysis of the effect of UCBS-derived exosome on *in vitro* and *in vivo* wound healing models.

ACKNOWLEDGEMENTS

It is with great pleasure that I thank the following parties who have made it possible for me to complete my thesis. Each and every one of you played an impeccable role during my Masters degree and I wish to extend my wholehearted gratitude for I would not have made it this far without you. May God bless you all abundantly.

It goes without saying that my most utmost appreciation goes to my supervisor Prof. Carola Niesler. Prof., there's a reason why the honours students are always fighting to be in your lab every year. At some point I was one of those students and choosing you was the best academic choice of my life. You have always understood us as students, and you have always been the one academic we turn to since undergrad. I thank you so much for allowing me to be a part of your team and holding me by the hand throughout my academic journey thus far. Thank you for the emotional, financial, as well as academic support. I truly appreciate all that you have done for me. I wish you many more blessed years so you can continue touching more lives as you have mine.

To Dr. Celia Snyman, possibly the most passionate scientist I know, I would like to thank you so much for your support. Till this day I believe you're the most experienced and valuable researcher in our faculty and I am grateful that you never shy away from sharing your expertise. You were always willing to help in troubleshooting my failed experiments and were always excited even more than me when I finally got good results. Thank you Celia.

I would also like to thank UKZN PMB microscopy unit (MMU) team, especially Tivana Moonsamy, for assisting me with microscopy. I spent the last semester doing a single experiment and without Tivana I was not going to get the amazing ICC images which I desperately needed in order to conclude lab work.

To Mangaliso Goge, it would take the entire thesis if I were to write down all you have done for me. From the late-night walks from res to the lab for scratch assays to being my only friend, you have been a very crucial part of my life. I truly appreciate you and hope we will continue to be blessings in each other's lives. Ngiyabonga maGoge.

Thank you to the NRF and Next Biosciences for the much-needed financial assistance, without which I know not where I would be.

To my grandmother, MaThabethe, thank you so much MaTee for always looking after the family in my absence. You have shown me unmatched motherly love and emotional support. You are the only reason why going back home was sometimes a mind refresher.

To my brother, Siyabonga Mkhize, thank you for being my mentor, friend, therapist, brother, and father figure. Your presence in my life will always be appreciated Bafo.

Lastly, I'd like to thank myself. It truly has not been an easy one. From dealing with the pandemic, to the looting, to the anxiety, to the depression, to the ADHD, to the addiction, to the burnout; the list goes on, but I kept pushing even when I saw no apparent reason for doing so. I hope life is kinder from now on, but may I remember to be even kinder to myself.

TABLE OF CONTENTS

PREFACE ii
DECLARATION 1: PLAGIARISM iii
DECLARATION 2: PUBLICATIONS iv
ABSTRACT v
ACKNOWLEDGEMENTS vii
TABLE OF CONTENTS ix
LIST OF FIGURES xi
LIST OF TABLES xiii
LIST OF ABBREVIATIONS xiv
Chapter 1: Introduction 1
1.1. Exosomes 1
1.1.1. Exosome biogenesis 3
1.2. Characterisation 4
1.2.1. Nanoparticle tracking analysis (NTA) 5
1.2.2. Tunable Resistive Pulse Sensing (TRPS) 6
1.2.3. Flow Cytometry 10
1.2.4. Electron Microscopy 11
1.2.5. Immunocytochemistry (ICC) 12
1.3. Isolation 13
1.3.1. Differential centrifugation 13
1.3.2. Density gradient centrifugation 14
1.3.3. Size exclusion-based methods 15
1.3.4. Size exclusion chromatography 15
1.3.5. Ultrafiltration 16
1.3.6. Polymer-based precipitation 16
1.3.7. Immuno-affinity purification 17
1.4. Therapeutic applications 18
1.4.1. Immunity 18
1.4.2. Regeneration 19
1.4.3. Cancer biomarkers/diagnostics 19
1.4.4. Drug Delivery 20
1.5. Umbilical Cord Blood Serum 22

1.5.1. UCBS Exosomes 23
1.6. Aims and Objectives 24
Chapter 2: Materials and Methods 25
2.1. General lab reagents and procedures 25
2.1.1. Reagents 25
2.1.2. Cell culture 27
2.2. EV Isolation 28
2.3. Tunable resistive pulse sensing (TRPS) (Refer to Appendix 1 for labelled device parts) 29
2.4. Transmission Electron Microscopy 30
2.5. Cell proliferation assay (MTS assay) 31
2.5.1. Standard curve 31
2.5.2. HEK293 cell proliferation in the presence of exosomes 32
2.6. Internalisation of exosomes by HEK293 cells 32
2.6.1. Exosome membrane labelling and uptake 32
2.6.2. Immunocytochemistry 33
2.7. Protein quantification 33
2.7.1. Determination of total protein concentration 33
2.7.2. ELISA 34
2.8. Statistical analysis 36
Chapter 3: Results 36
3.1. TRPS Optimisation 36
3.1.1. Important parameters 39
3.1.2. Analysis 46
3.2. Optimisation of the analysis of biological extracellular vesicles using TRPS 51
3.3. Characterisation of UCBS extracellular vesicles 55
3.3.1. TRPS 55
3.3.2. Transmission electron microscopy 57
3.3.3. Internalisation by HEK293 cells 59
3.3.4. Effect on cell proliferation 62
3.3.5. Protein Content Analysis 65
3.4. Summary 71
Chapter 4: Discussion 72
Appendix 1: Labelled Exoid device parts 76
References 77

LIST OF FIGURES

Figure **Page**

Figure 1.1: Illustration of extracellular vesicle sizes in comparison to commonly known human cells (adapted from [16]).... 2
Figure 1.2: A schematic diagram of exosome formation. 4
Figure 1.3: NTA basic principle 6
Figure 1.4: Size profile of vesicles isolated from umbilical cord blood serum generated using TRPS 8
Figure 1.5: Nanopore classes and their particle diameter detection range.... 9
Figure 1.6: Microscopy-based characterisation of exosomes.... 11

Figure 2.1: Isolation of vesicles from Optiserum 29
Figure 2.2: Standard curve used for the MTS assay cell quantification.... 31
Figure 2.3: Standard curve used for protein concentration estimations 34

Figure 3.1: Using the Exoid TRPS instrument.... 38
Figure 3.2: Correlation between applied voltage and baseline current.... 40
Figure 3.3: Unclogging a nanopore. 42
Figure 3.4: Examples of interferences in current and noise due to operating the Exoid near electronic devices.... 43
Figure 3.5: Correlation between pressure and the particle rate.... 45
Figure 3.6: Particle rate plots generated using CPC200 calibration particles run at 3 different pressures.... 47
Figure 3.7: Accuracy of the Exoid TRPS equipment 49
Figure 3.8: Workflow to achieving accurate estimation of particle size and diameter using the Exoid TRPS equipment. 50
Figure 3.9: Effect of filtration on sample vesicle profile. 54
Figure 3.10: EV-containing samples analysed using the Exoid.... 56
Figure 3.11: Transmission electron micrographs of various samples mounted on different TEM grids.... 58

Figure 3.12: HEK293 cells negative CD81 control 59
Figure 3.13: HEK393 cells incubated in SFM displaying endogenous CD81 60
Figure 3.14: Uptake of PKH26-stained exosomes by HEK293 cells. 61
Figure 3. 15: Effect of UCBS-isolated exosomes on HEK293 cell proliferation 63
Figure 3.16: Effect of UCBS on cell proliferation. 64
Figure 3.17: Levels of EGF in exosomes compared to the original Optiserum from which they were isolated 66
Figure 3.18: Cytokines found in higher levels in Optiserum compared to the exosomes 68
Figure 3.19: Cytokines enriched highly in exosomes compared to the original Optiserum from which they were isolated 69
Figure 3.20: Cytokines present in comparable levels in exosomes compared to the original Optiserum from which they were isolated.. 70

LIST OF TABLES

Table **Page**

Table 1.1: Exosome isolation techniques 18
Table 1.2: Exosome cargo loading methods. 21

Table 2.1: TRPS reagent information 25
Table 2.2: Cytokines detected using the Bioplex 27-plex and the 48-plex systems. 35

Table 3.1: Age and pregnancy duration of umbilical cord blood donors from which Optiserum batches was produced. Batch numbers refer to the Optiserum batch that was utilised to isolate the EVs. 52

LIST OF ABBREVIATIONS

Abbreviation	*Expansion*
AD	Alzheimer's Disease
Alix	ALG-2-Interacting protein X
BACE1	β Secretase 1
BBB	Blood-Brain Barrier
BSA	Bovine Serum Albumin
CCD	Charge-Coupled Device
CD63	Cluster of Differentiation 63
CD81	Cluster of Differentiation 81
CD9	Cluster of Differentiation 9
CO2	Carbon Dioxide
COVID 19	Coronavirus Disease 19
CPC100	Calibration Particles Carboxylated 100
CPC200	Calibration Particles Carboxylated 200
CryoEM	Cryogenic Electron Microscopy
CTACK	Cutaneous T cell- Attracting Chemokine
DMEM	Dulbecco' Modified Eagle's Medium
EGF	Epidermal Growth Factor
ESCRT	Endosomal Sorting Complex Required for Transport
EVs	Extracellular Vesicles
FBS	Foetal Bovine Serum
fPBS	Filtered Phosphate-Buffered Saline
HCl	Hydrochloric Acid
HEK293	Human Embryonic Kidney 293
hUCBS-MSC	Human umbilical cord blood-derived mesenchymal stem cell
ICC	Immunocytochemistry
IFC	Imaging Flow Cytometer
IgG3	Immunoglobulin 3
IL-9	Interleukin 9
ILVs	Intraluminal Vesicles
MIF	Macrophage Migration Inhibitor Factor
MIP-1b	Macrophage Inflammatory Protein 1-β
miRNA	MicroRNA/ microRibonucleic Acid
mRNA	Messenger RNA/ messenger Ribonucleic Acid
MVs	Microvesicles
MVB	Multivesicular Body
NTA	Nanoparticle Tracking Analysis

PBMC	Peripheral Blood Mononuclear Cell
PBS	Phosphate-Buffered Saline
PDGF-bb	Platelet-Derived Growth Factor- β β
PEG	Polyethylene Glycol
PMT's	Photomultiplier Tubes
RANTES	Regulated upon Activation, Normal T Cell Expressed and Presumably Secreted
RIPA	Radioimmunoprecipitation
RMS	Root Mean Square
SA-PE	Streptavidin-Phycoerythrin
SCF	Stem Cell Factor
SCGF-b	Serum Stem Cell Growth Factor β
SCM	Serum-Containing Medium
SEM	Scanning Electron Microscopy
SFM	Serum-Free Medium
SOP	Standard Operating Procedure
TEM	Transmission Electron Microscopy
TRPS	Tunable Resistive Pulse Sensing
TSG101	Tumor Susceptibility Gene 101
UCB-MSC	Umbilical Cord Blood Mesenchymal Stem Cell
UCBS	Umbilical Cord Blood Serum
UCB	Umbilical Cord Blood
UPS	Uninterrupted Power Supply

Chapter 1: Introduction

1.1. Exosomes

Four decades ago, two studies reported the release of small extracellular vesicles (~50 nm) by immature red blood cells [1, 2]. Initially, these extracellular vesicles were thought to be no more than cellular waste carriers, but subsequent studies proved that this was very far from accurate [3]. Evidence suggested that they participate in an array of biological processes including immunity, carcinogenesis, and regeneration. These vesicles would later be termed exosomes by the groups that conducted the studies [4].

Contemporarily, exosomes are widely defined as extracellular vesicles (EVs) within the 30-150 nm diameter size range [5]. However, the exact size range as well as nomenclature of exosomes has been met with controversy [6]. Various studies have reported contradicting exosomes size ranges. This has led to widespread concerns as to whether the term ‘’exosome’’ is appropriate; recent suggestions indicate that they could rather be referred to as ‘’small extracellular vesicles’’; however, for the sake of consistency and for the purposes of this study, they will be referred to as exosomes [7].

Exosomes are now accepted to act as important mediators of inter-cellular communication and signalling [8]. This makes them a very interesting research subject because understanding how they facilitate this communication could enable us to utilise exosomes for various therapies and understand disease progression. Exosomes facilitate cellular communication by transporting cargo (which includes biomolecules such as proteins, lipids, and miRNA) to a target cell and then inducing physiological changes through changes in gene expression which ultimately modifies cellular processes such as proliferation and migration [9, 10]. Docking of these message carriers with their target cells can be in the form of endocytosis, fusion with the plasma membrane and phagocytosis. Sometimes, the exosomes do not even enter the cell, but elicit a biological cellular response by interacting with cell surface receptors [11]. Their presence in all body fluids therefore makes them interesting subjects for disease biomarker development research [12].

Other EVs, apart from exosomes, include apoptotic bodies and microvesicles (MVs); they differ from exosomes in terms of size and biogenesis. To understand what sets exosomes apart, it is important to understand EV biogenesis. MVs and apoptotic bodies, which both bleb directly from the plasma membrane, have respective size ranges of 100 nm to 1000 nm and 1000 nm to 5000 nm (Figure 1.1)[13, 14]. Exosomes and most MVs are therefore substantially smaller than apoptotic bodies as well as non-nucleated and nucleated adult cells. Moreover, larger vesicles (MVs and apoptotic bodies) formed via membrane budding express CD40, whereas smaller ones (exosomes) are generated through the endosomal pathway and express tetraspanins such as CD9, CD81 and CD63 [15].

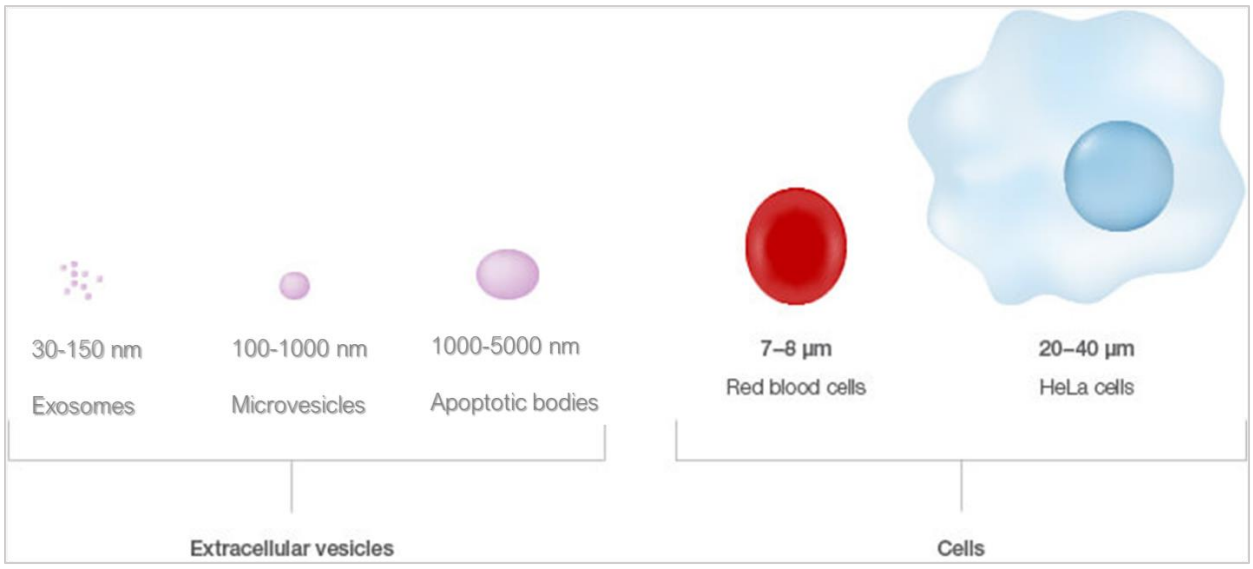

Figure 1.1: Illustration of extracellular vesicle sizes in comparison to commonly known human cells (adapted from [16]). Exosomes have a size range of 30 - 150 nm, followed by microvesicles with a size range of 100 – 1000 nm and lastly apoptotic bodies with a size range of 1000 – 5000 nm [16, 17].

1.1.1. Exosome biogenesis

Exosomal formation begins with the inward budding of the plasma membrane to form a lipid bilayer ring called the endosome (Figure 1.2, step 1). Membranous macromolecules such as lipid-anchored proteins, which would be on the extracellular region of the plasma membrane are then found on the inner region of the endosome membrane. As the endosome passes through various phases of maturation, it also undergoes inward budding which is similar to endocytosis. This results in the formation of multiple small vesicles in the endosome; these are called intraluminal vesicles (ILVs) and they contain cargo (Figure 1.2, step 2). The sorting of cargo into the ILVs is highly specific and is controlled by the endosomal sorting complex required for transport (ESCRT). At this point, the mature endosome is referred to as the multivesicular body (MVB) and it can now follow one of two fates (Figure 1.2, step 3). The first is that it can fuse with the lysosome, leading to the degradation of the ILVs. The alternative is fusion of the MVB membrane with the plasma membrane. This results in the release of ILVs into the extracellular space which are now termed exosomes [18-20].

Due to their production via the endosomal pathway, exosomes are enriched in multiple proteins characteristic of this pathway. These include the ALG-2-interacting protein X (Alix) and the Tumor Susceptibility Gene 101 protein (TSG101). These are cytosolic proteins found in exosomes and are responsible for MVB formation via association with the ESCRT [21-23]. Other proteins include flotillins (e.g., Flotillin 1) and annexins (e.g., Annexin A1) which are responsible for cargo sorting and exosome exocytosis respectively [24-26]. Lastly, proteins of the tetraspanin family (e.g., CD9, CD63 and CD81) have been reported to be highly abundant in exosomes along with metabolism-linked proteins (e.g., GAPDH) and cytoskeleton-linked proteins (e.g., β-actin) [27, 28]. The role of tetraspanins and β-actin in exosome formation have not been fully elucidated but GAPDH has been reported to be involved in ILV formation [28-30].

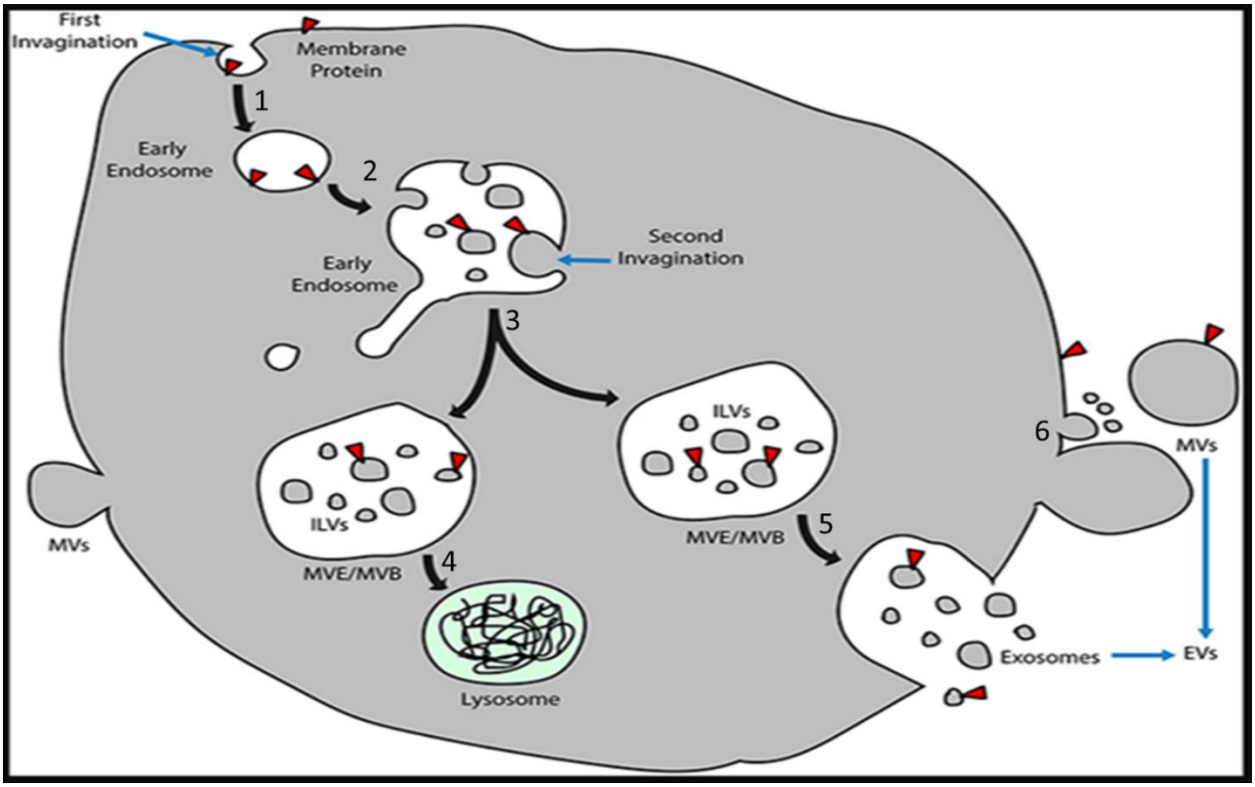

Figure 1.2: A schematic diagram of exosome formation. 1) Inward budding of the cell membrane forming the early endosome. 2) Early endosome undergoing further budding to form intraluminal vesicles (ILVs). 3) Early endosome matures into multivesicular body (MVB)/multivesicular endosome (MVE), which succumbs to one of 2 fates: 4) MVB fusion with the lysosome. 5) MVB fusion with the cell membrane to release ILVs into extracellular space. 6) Direct outward budding of cell membrane forming microvesicles (MVs). Adapted from [31].

1.2. Characterisation

Although techniques that determine the size profile, such as nanoparticle tracking analysis (NTA) or tunable resistive pulse sensing (TRPS), of an extracellular vesicle sample are a first step towards exosome characterisation, it is important to use additional methods to identify those aspects which make exosomes unique when compared with other EVs (other than potentially size). This is in part due to the fact that the reported size ranges of exosomes overlap with that of the MVs (see Section 1). Thus, it is important to include additional characterisation methods to confirm the purity of an isolated exosome sample.

As mentioned earlier, the exosome membrane contains proteins which would have been found on the plasma membrane of the original generating cell. These include flotillin-1 and the tetraspanins CD9, CD63 and CD81. These proteins are accepted as general

exosomal biomarkers because they are highly expressed on exosome membranes compared to other EVs. Tetraspanins are considered as markers of the endosomal pathway by which exosomes are produced [32]. They are also involved in an array of pathways associated with exosome production, specificity, uptake and cargo sorting [28, 33]. This information is key to the characterisation of exosomes where antibody-based techniques are used to detect these markers. Other methods, such as transmission electron microscopy (TEM) can be utilised to identify exosomes based on their specific morphology [34]. These techniques will all be discussed in more detail in the next sections.

1.2.1. Nanoparticle tracking analysis (NTA)

NTA is a widely used exosome characterisation method first utilised a decade ago for the characterisation of EVs [35]. The foundation of NTA is so-called Brownian motion. Particles moving in a liquid collide randomly with the water molecules. By projecting a laser beam through the sample, the NTA machinery tracks individual particles in the solution and correlates the speed and light scattering to their size (Figure 1.3A). Thus, NTA provides quantitative data which includes size, distribution, and concentration of vesicles [36]. Figure 1.3B depicts a typical NTA size profile for a range of EV samples. In a sample of pure exosomes, the peak is approximately 100 nm and none of the particles have a diameter greater than 150 nm, whereas in a sample that includes MVs, the profile shows peaks greater than 150 nm. This is an important consideration when it comes to assessing the efficiency of an isolation method; it is worth remembering that exosomes overlap in size with other EVs.

NTA can detect particles as small as 10 nm and as large as 2000 nm and sample preparation is very short. It however has a sample volume requirement of at least 250 µl. This might be challenging to accomplish depending on the vesicle yield as the method's detection range is $2 – 10 \times 10^8$ vesicles/ml and outside this range, the accuracy is reduced [37, 38]. Moreover, difficulty comparing data generated using NTA has been reported in literature. This is because it is heavily user-dependant and cannot distinguish clumped particles from large ones [39].

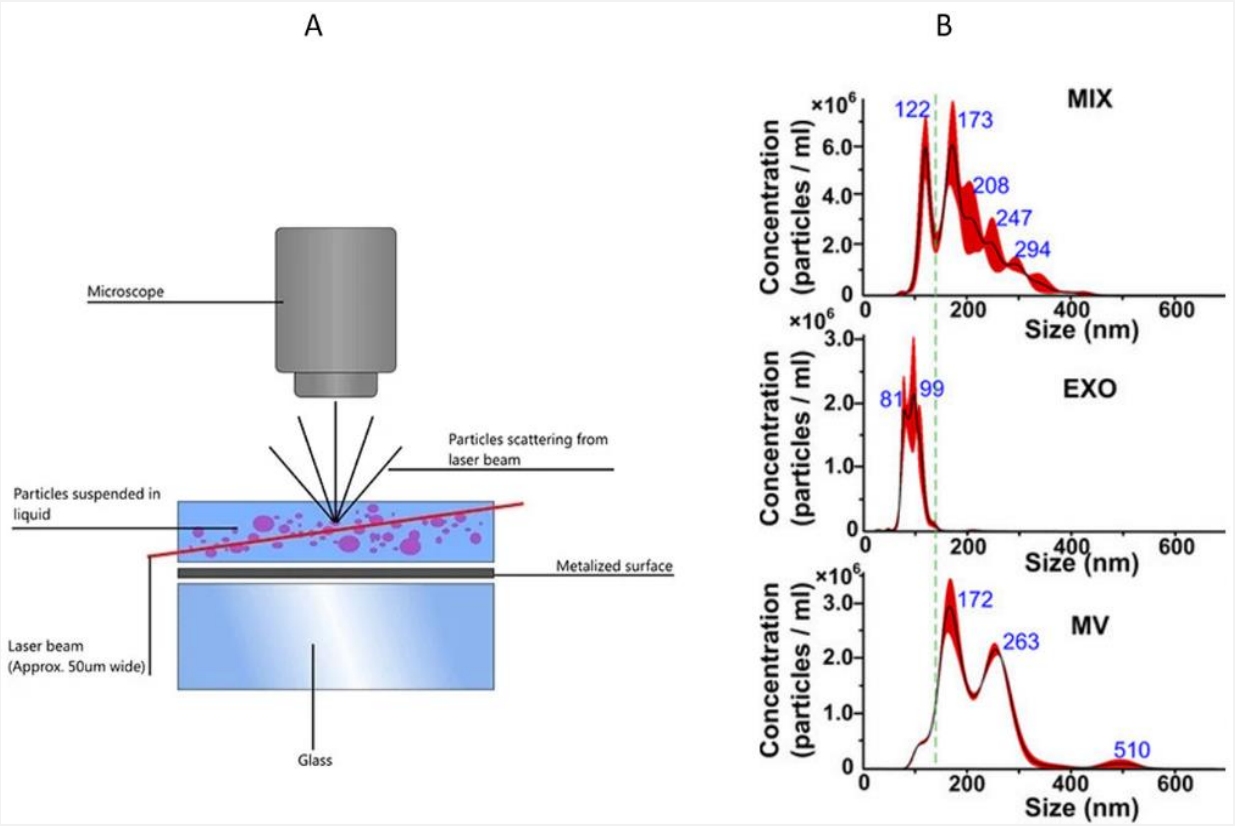

Figure 1.3: NTA basic principle. A) A laser beam is directed on particles suspended in a liquid. The scattered light is detected by a microscope and used to generate a size profile B) NTA Profile for a mixture of EVs (MIX), pure exosomes (EXO) and pure microvesicles (MVs) [36, 40].

1.2.2. Tunable Resistive Pulse Sensing (TRPS)

Contrary to detecting light scatter, tunable resistive pulse sensing (TRPS) electrically determines vesicle size distribution and concentration. Using voltage and pressure, the vesicles are passed through a nanopore in a non-conductive membrane. This membrane is located between two fluid cells containing an electrolyte, usually phosphate-buffered saline (PBS). When voltage is applied, an electrical baseline current is established in the nanopore. When pressure is applied it forces particles to progress through the pore. Because EVs such as exosomes are negatively charged, they also move through the nanopore via electric repulsion when the voltage is applied. As the particles move through the nanopore, the electrical current is disturbed and there is a temporary decrease in current. Both the frequency and magnitude of this disturbance (“resistive pulse’’) correspond to particle concentration and size respectively. This is quantified by the

software and compared to the blockades caused by standard polystyrene calibration nanoparticles of known concentration to establish a size profile based on the vesicles in the sample [41].

The Exoid (Izon Science, France) can be used for the purposes of TRPS of EVs. Quantitative data is generated, and typical results provide information about the concentration, diameter as well as size span of the isolated vesicles (Figure 1,4). Similar to NTA, the Exoid can provide information such as the particle diameter and the d-values. The particle diameter information provides the mean (with standard deviation) and mode diameters of detected vesicles. The d-values (d90, d50, d10) provide information about the minimum diameter that a certain percentage of the measured particles fall under. For example, the d90 value of 150 indicates that 90% of the particles have a diameter of 150 nm and below, while a d50 value of 98 indicates that 50% of the particles have a diameter of 98 nm and below [42]. However, unlike NTA, the Exoid generates additional data depicting the minimum particle size, maximum particle size, as well as the d90/d10 value (Figure 1.4). The d90/d10 value measures the spread of the particles and is directly proportional to the heterogeneity of the particles. Hence, the more homogenous the particles are, the closer this value will be to 1 [43]. Furthermore, following sample preparation for TRPS, only 35 µl volume of the diluted sample is required for analysis (unlike the 250 µl required in NTA). The method is highly accurate as it can characterise each vesicle passing through the nanopore rather than using an algorithm that utilises the average reading.

Sample: **621**
Measurement date: Friday, 11 March 2022 14:16

Sample Statistics

Particle diameter (nm)

Mean:	110 (Std Dev=41,6)	d50:	98		
Mode:	91	d10:	79	d90:	150
Maximum:	410	d90/d10:	1,90		
Minimum:	67	Span:	0,73		

Concentration [0-∞] (particles/ml)

Measured Concentration:	1,68e+09
Raw Concentration:	1,68e+10

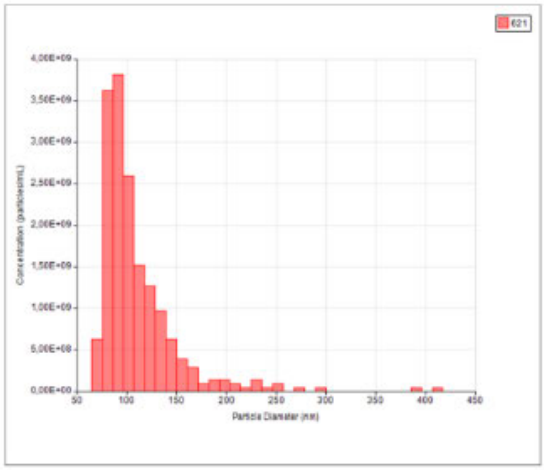

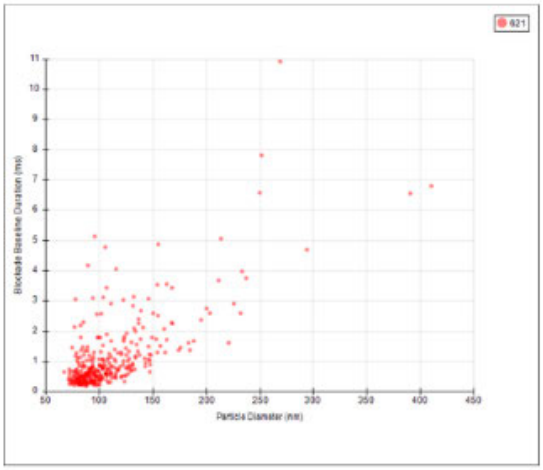

Figure 1.4: Size profile of vesicles isolated from umbilical cord blood serum generated using TRPS. The data was generated using sample 621 (denoting the Optiserum batch the exosomes were isolated from). The raw concentration represents the actual concentration in the original sample as it accounts for the fact that the sample measured was diluted prior to analysis.

As with NTA, one of the main challenges with TRPS is the inability to distinguish EVs from other non-EV particles such as lipoproteins [44]. Moreover, even though the method can detect vesicles ranging from 50 nm to 11300 nm, this requires the use of multiple nanopores which is time-consuming (Figure 1.5). This is because each nanopore can only quantify particles of a certain diameter range. For example, the NP100 class can quantify particles within the 50 nm – 330 nm size range. Although synthetic particles such as polystyrene beads may be easily quantified using the NP100, biological samples are highly heterogenous and the presence of larger particles and bio-particle aggregates

(which may be naturally present in sample or form during the vesicle isolation) cause blockade of the pore and prevent further quantification. Sometimes the blockade can be undone by applying negative pressure, but it is a futile exercise because it does not remove the particles larger than the pore and subsequent blockade becomes inevitable. This means that vesicle concentration in samples may be underestimated. An additional challenge is the short lifespan of the membranes (exacerbated by inevitable clogging which is sometimes irreversible) as well as the cost of replacement nanopores.

Class	Measurement Range (nm)	Calibraiton Particles	Target Conc. /mL
NP100	50-330	CPC100, 200	$5x10^{10}$
NP150	70-420	CPC100, 200	$5x10^{9}$
NP200	85-500	CPC200, 400	$5x10^{9}$
NP250	110-630	CPC200, 400	$2x10^{9}$
NP300	150-900	CPC400, 500, 800	$1x10^{9}$
NP400	165-1100	CPC400, 500, 800	$5x10^{8}$
NP600	275-1570	CPC500, 800, 1000	$5x10^{8}$
NP800	385-2050	CPC800, 1000	$1x10^{8}$
NP1000	490-2900	CPC1000, 2000	$5x10^{7}$
NP2000	935-5700	CPC2000, 4000	$5x10^{6}$
NP4000	1990-11300	CPC4000	$5x10^{5}$

Figure 1.5: Nanopore classes and their particle diameter detection range. Nanopore classes are grouped according to the range of particle size range that they can measure, the type of calibration particles to be used as well as the sample target concentration [45].

1.2.3. Flow Cytometry

Using multiple apparatuses including lasers and filters, flow cytometry optically qualifies exosomes based on how they scatter light or the fluorescence they emit based on the fluorophore and antibody used to detect them [46]. Although up to 12 different exosomal membrane markers can be detected using flow cytometry, most conventional flow cytometers are not ideal for exosome characterisation due to the small size of these vesicles and the fact that they have a low refractive index [47, 48]. Most commercially available flow cytometers have a resolution of 500 nm [49, 50].

To combat this hurdle, the exosomes would have to be captured using antibody-coated beads [51]. The optimised technique involves producing magnetic beads with a high affinity for a specific exosome marker (e.g CD9) by incubating streptavidin-coated beads with biotinylated antibodies against the first marker. This is followed by the capture of the exosomes by incubating the sample with the beads. The bead-bound exosomes are then labelled for a second marker such as CD81 via incubation with an anti-CD81 antibody. Flow cytometry is then performed on this bead-exosome conjugate. However, this method is not time-effective or cost-effective and may require additional steps such as size-exclusion chromatography or a sucrose cushion to remove unbound antibodies which cause background fluorescence [52].

An alternative would be to use an optimised high-end imaging flow cytometer (IFC) such as the AMNIS® ImageStreamXMk II which would be the most suitable for exosome characterisation as it has a 20 nm sensitivity [50]. These are similar to conventional flow cytometers, but their detectors use not photomultiplier tubes (PMT's) but rather charge-coupled device (CCD) cameras which have lower noise as well as more sensitivity [53]. However, these require a highly experienced user to configure the instrument and there is high variability between equipment, making data comparison challenging. Lastly, the calibration beads used for this method are generally polystyrene and/or silica nanospheres, but these can scatter up to 300-fold more light than exosomes [54]. This causes concern as to the accuracy of the calibration.

1.2.4. Electron Microscopy

Electron microscopes use an electron beam and have a high resolving power compared to traditional light microscopes; this is because the electron wavelength is about 100,000 times shorter than the photons of visible light and thus the magnification can be a 1000-fold compared to light microscopy. Extracellular vesicles can be analysed using Transmission Electron Microscopy (TEM), Scanning Electron Microscopy (SEM) and cryogenic electron microscopy (CryoEM) (Figure 1.6).

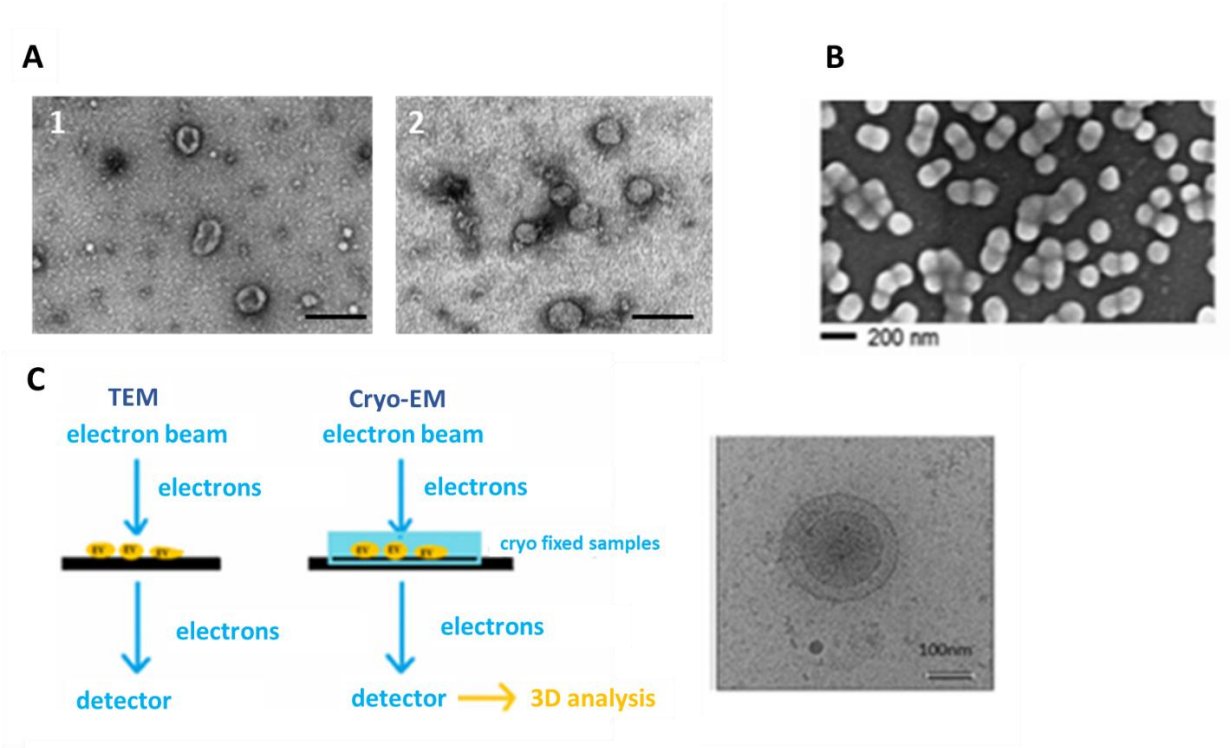

Figure 1.6: Microscopy-based characterisation of exosomes. A) Exosomes visualised using TEM depicting (A1) a cup-like morphology or (A2) round morphology [55, 56]. B) Exosomes visualised using SEM [34]. C) TEM principle versus Cryo-EM and the image of an exosome generated using Cryo-EM [57, 58].

In TEM, electrons are passed through the sample. This gives detailed information including the size of the exosomes as well as their membrane morphology. Depending on the sample preparation, exosomes appear to have a cup/doughnut shape or a round shape (Figure 1.6A1 and A2, respectively). When analysing samples, one is therefore looking for a specific morphology in order to confirm the exosome nature of the sample. The images produced are 2-dimensional and the resolution can be as little as 1 nm.

Sample preparation generally includes fixation using 2% paraformaldehyde where the formaldehyde causes the formation of permanent protein linkages which causes the preservation of the vesicle structure [59]. This is followed by mounting onto TEM grids (copper or nickel), rinsing with PBS, incubation with glutaraldehyde, rinsing with water, staining with uranyl acetate, air-dying and then finally imaging [60]. Although the method provides excellent ultrastructural information, these microscopes are costly, and TEM cannot provide data about the particle size distribution of a large number of exosomes.

Similarly, sample preparation for SEM includes fixation with formaldehyde (for optimum results [61]). Following fixation and dehydration, the sample is coated with a conductive metal, usually gold. The metal serves to scatter the electrons and from that scatter, external information about the exosomes can be obtained [62]. Although commonly used, gold provides low resolution images compared to the likes of tungsten or carbon [63]. SEM images provide detailed morphological information about exosomes (Figure 1.6B) as well as quantitative information such as particle size distribution.

Both TEM and SEM involve sample dehydration, and this can cause vesicle shrinkage. Cryo-EM combats this challenge as no sample fixation is involved and is a superior approach to TEM and SEM [58]. This method uses the TEM principle, but as there is no fixation there is less shrinkage of the exosomal membrane [64]. The sample containing exosomes is placed on a grid, vitrified then kept frozen in liquid nitrogen before imaging [65]. This method appears to be preferable due to its simplicity and the ability to clearly displays the exosome bilayer (Figure 1.6C). However, additional sample freezing equipment, not available in all institutions, is required [66, 67].

1.2.5. Immunocytochemistry (ICC)

This is a technique generally used in biomedical research for the identification of specific biomolecules such as proteins (in or on cells) using antibodies [68]. These cells are generally allowed to adhere onto glass slide coverslips before fixation and subsequent antibody labelling [69]. As mentioned in Section 1, exosomes are enriched in membrane proteins such as CD81 that are used as specific exosome biomarkers. Moreover, they're produced from the cell membrane and therefore have the same adhesion molecules the

cells use to adhere to the slide coverslips. Hence, ICC can be applicable in exosome detection [70]. Importantly, ICC cannot only be used to confirm the presence of exosomes but can also be used to confirm their internalisation by cells. To do this, the isolated exosomes are usually stained with a membrane dye, such as the PKH26 membrane labelling dye, before being incubated with cells prior to ICC. The possibility of false positives associated with the use of the membrane dyes must be addressed when using this approach, by including the appropriate negative controls [71, 72].

1.3. Isolation

Exosome isolation techniques capitalise on the various qualitative and quantitative aspects of these EVs. Techniques such as size exclusion chromatography, ultra-centrifugation and filtration are based on their size, while antibody-based techniques are based on the enrichment of certain proteins (such as tetraspanins) that exosomes display. Each isolation method has its advantages and disadvantages, some of which are highlighted in the following sections and summarised in Table 1.1.

1.3.1. Differential centrifugation

Making up more than 50% of all exosome isolation techniques reported in literature, this method is regarded as the gold standard for exosome isolation [73, 74]. The basic principle involves concentrating vesicles based on their size and density using a stepwise increase in centrifugal force [75]. The initial step involves the removal of high density and mass biounits such as cells and cell lysis products via centrifugation typically at 300 x g at 4°C for 10 minutes. This is followed by the removal of larger vesicles such as apoptotic bodies via centrifugation at 10 000 x g at 4°C for 30 minutes. Exosomes are then concentrated via ultracentrifugation at 100 000 x g at 4°C for 2 hours. A final wash step is added to remove contaminating non-vesicle proteins via another ultracentrifugation step (100 000 x g at 4°C for 2 hours). This final step increases purity, but decreases exosome yield [76].

There is no universal ultracentrifugation protocol as additional steps can be added to remove other cellular components and the ultracentrifugation step(s) can range from 100

000 x g to 200 000 x g [77]. These also depend on the biological fluid type as well as sample viscosity because viscous samples require extended centrifugation at higher centrifugal forces just as in exosome isolation from serum/plasma in comparison to conditioned medium [78].

The efficiency and length of the centrifugation also depends on the rotor's maximum rotation speed (k factor) and type of rotor (fixed angle rotor or swing bucket rotor) [79]. When using a fixed angle rotor, the sample particles travel longer before sedimentation compared to a swing bucket rotor. Hence, even though the sedimentation efficiency of a swing bucket rotor is lower, it is more suitable for separating samples with sedimentation coefficiency values that are similar, which is often the case in biological samples [79]. Surprisingly, the type of rotor can even affect the protein/RNA ratio of isolated vesicles [80].

The need for expensive and specialised equipment as well the long processing time makes this method less suitable for diagnostic purposes in environments such as hospitals [81]. Moreover, this method is plagued with vesicle contamination by lipoproteins and protein aggregates, a low reproducibility, and potential damage to the exosomes due to harsh centrifugal forces [79].

1.3.2. Density gradient centrifugation

Using ultracentrifugation for lengthy periods in a sucrose or iodixanol gradient, particles are separated based on their buoyant densities [82]. An iodixanol gradient is preferable because it is less harsh to the exosome's structural integrity compared to a sucrose gradient [73]. Generally, iodixanol solutions of increasing concentrations [e.g., 5% (w/v), 10% (w/v), 20% (w/v) and 40% (w/v)] are prepared and carefully layered in descending order from the bottom of a polyallomer centrifuge tube. This is followed by overnight ultracentrifugation (100 000 x g) at 4°C. The fractions are then carefully collected before a wash step involving a dilution in PBS and another ultracentrifugation for 3 hours at 4°C [83].

This method is applicable for the separation of particles with a diameter less than 2000 nm [84]. It is more favourable over classic ultracentrifugation as it is more efficient at separating exosomes from non-vesicle proteins and apoptotic bodies [79, 85]. However, it also results in low yield (≤ 25%) due to the use of large centrifugal forces [79, 86, 87]. Moreover, it is time consuming, requires expensive equipment and arduous [88, 89]. Thus, just like classic ultracentrifugation, applying it in a clinical setting would be challenging [90].

1.3.3. Size exclusion-based methods

The size range of extracellular vesicles, including exosomes, has been greatly studied and documented. Hence, methods, such as size exclusion chromatography and ultrafiltration, that capitalise on the exosomes' size are utilised [91, 92]. Generally, these are added as final steps following other techniques such as ultracentrifugation, but they can be utilised on their own [93].

1.3.4. Size exclusion chromatography

With size exclusion chromatography, samples are passed through a column containing porous beads in a buffer. The largest particles are eluted first, followed by smaller ones such as exosomes [94]. The researcher keeps small fractions of the eluted sample and subsequently determines which one contains the target particles [95]. No extensive force is applied as the samples pass through the beads via gravitational force only. Hence, this method preserves the structural integrity of the exosomes [96, 97]. The shortcomings associated with most methods such as ultracentrifugation are avoided using this method as it can separate exosomes from protein aggregates and lipoproteins [79]. Moreover, this method can easily be scaled up, and it has been shown that the height of the column is directly proportional to the separation efficiency [98, 99]. This method however results in low vesicle yield, worsened when it is used as a secondary step to techniques such as ultracentrifugation [100]. Should it be used as the sole isolation method the yield may still be affected due to sample dilution that is required before separation [101]. Hence, the vesicles may need an additional step to concentrate them [102].

1.3.5. Ultrafiltration

This method relies on commercial membrane filters that have varying pore sizes. These are generally 0.1, 0.2, 0.5 or 0.8 µm in diameter, allowing for the separation of particles as small as 100, 200, 500 and 800 nm respectively [79]. Since biological samples generally consist of a heterogenous mixture of particles this method is best used as an additional purification step following methods like size exclusion chromatography [103, 104]. For it to be used alone, the sample would have to be passed through a series of membranes in descending order of pore size [105]. The main disadvantage of this method is membrane clogging which traps the exosomes, thereby decreasing yield as well as destroying the costly filter [106]. Moreover, shear stress due to the force applied during filtration could potentially damage the exosomes [107].

1.3.6. Polymer-based precipitation

Polymers such as polyethylene glycol (PEG) have long been used for the precipitation of various biomolecules such as proteins and nucleic acids [108]. Various studies have successfully utilised PEGs of various molecular weights to isolate exosomes [109]. In fact, this is the second most-used vesicle-isolation method following ultracentrifugation [79]. It is preferable due to its simplicity and cost-effective nature [90]. PEG6000 or PEG-based commercial kits are generally used, with PEG6000 being a better option because it is significantly inexpensive and usually just as effective as commercial kits [110, 111]. PEG works via a water-exclusion mechanism whereby after incubating it with the sample, it binds the water molecules present and thereby decreases the solubility of the target molecules, such as exosomes [112, 113]. After this, the exosomes can be sedimented using low centrifugal forces [79]. The pellet is typically resuspended in PBS and subjected to downstream processing or can be cryopreserved [114-116]. However, it is preferable to pre-centrifuge the sample at 13 000 x g for 1 hour or filter through a 0.22 µm membrane to remove biological debris before adding PEG [117, 118]. The main drawback to this method is the lack of specificity. Hence it co-isolates non-vesicle proteins, lipoproteins and immunoglobulins [119].

1.3.7. Immuno-affinity purification

As the name suggests, this method utilises antibodies to capture exosomes [108]. Antibodies specific to exosome membrane proteins (such as CD9, CD81 and CD63) are coated onto magnetic microbeads and then added to a sample where they specifically bind to these proteins and therefore, by extension, to the exosomes. The magnetic bead-exosomes are then collected using a magnet. To separate the beads from the exosomes, ultracentrifugation (typically 10 000 x g for 1 hour at 4°C) is employed followed by incubation with an acidic buffer such as 0.2 M glycine, Tris–HCl, pH 2.8 [83, 120]. Due to the high specificity and selectivity associated with antibodies, this method yields highly pure exosome samples that are even negative for the lipoprotein markers ApoB and ApoA1 [121]. However, sample volume is limited, the method is time-consuming and the reagents used are expensive [122, 123]. Lastly, due to the lack of a universal exosome marker that is simultaneously highly selective, this method only isolates specific exosome subpopulations [122].

Table 1.1: Exosome isolation techniques

Method	Mechanism	Advantages	Disadvantages	Purity	Yield	References
Differential centrifugation	Ultracentrifugation separates particles based on their size and density	Gold standard	Time consuming Contamination from smaller debris and proteins. Requires expensive high-speed centrifuges.	**	*	[74]
Density gradient centrifugation	Ultracentrifugation in a density gradient separates particles based on buoyant density	Higher purity than classic ultracentrifugation	Laborious Time consuming Requires expensive high-speed centrifuges	***	*	[83]
Ultrafiltration	Porous membranes separate particles based on size	Simple	Clogging Sample loss Vesicle deformation	***	**	[92]
Size-exclusion chromatography	Particles passed through porous beads separated based on size	Exosome integrity Scalability	Low biological activity Lipoprotein contamination	***	***	[95]
Polymer-based precipitation	Water-exclusion results in precipitation	Simple Cost-effective Exosome integrity	Low purity	*	***	[119]
Immuno-affinity purification	Exosomes captured by magnetic beads coated with exosome-specific antibodies	Specificity Purity	Antibody availability and cost	***	**	[96]

The basic mechanism, advantages, and disadvantages of the most common vesicle isolation techniques were summarised. The yield and purity of each method were classified as low (*), medium (**), or high (***) based on literature.

1.4. Therapeutic applications

As of early 2023, there have been 72 completed clinical trials aimed at using exosomes for various applications such as vaccination, biomarker development and COVID-19 treatment [124]. Fortunately, no adverse effects have been reported with the therapeutic use of cord blood or cord blood-based products [125]. However, exosomes isolated directly from umbilical cord blood serum appear not to have been included yet.

1.4.1. Immunity

Various studies have demonstrated the potential application of exosomes as immune modulation tools. For example, it has been shown that when activated peripheral blood

mononuclear cells (PBMC) were treated with exosomes released by umbilical cord blood mesenchymal stem cells (UCB-MSC) it resulted in PMBC growth hinderance, decreased production of inflammatory cytokines and lastly, there was an increase in the number of naïve CD4+ and CD8+ T-cells as the deactivation of these cells increased [126]. UCB-MSC exosomes have also been shown to be able to transport miR-146a into macrophages. This mRNA is known to have anti-inflammatory properties, and in their study, this group demonstrated that it can support the survival in a septic mouse model [127].

1.4.2. Regeneration

The wound healing capabilities of exosomes have been demonstrated in various studies. Human umbilical cord blood-derived mesenchymal stem cell (hUCB-MSC)-derived exosomes move into the epidermis within 24 hours of being applied to skin samples from healthy African female donors. These exosomes were shown to increase the production of skin structural proteins such as elastin and collagen type 1 [128]. Since these proteins are the main structural components of the dermis, this suggests the potential application of exosomes as anti-aging agents and possibly for the treatment of conditions such as epidermolysis bullosa [129, 130].

1.4.3. Cancer biomarkers/diagnostics

Research suggests that exosomes play a crucial role in tumour development. They are involved in tissue enlargement via angiogenesis, migration, invasion, immune evasion and ultimately metastatic lesion formation [131]. Thus, detecting tumour-associated exosomes could be a great advantage for early cancer-diagnosis, especially if the liquid biopsy method could be applied to detect cancer-associated exosomes in various body fluids. For example, CD147 is a protein found on colon cancer exosomes and TGFβ2 (as well as miRNA's such as miR21 and miR-29b) is present in breast cancer exosomes isolated from breast milk [131, 132]. This offers an alternative approach to cancer detection. Exosomes may be superior to common liquid biopsy cancer targets such as

circulating tumour cells and circulating tumour DNA due to their abundance and stability [133].

1.4.4. Drug Delivery

The small size and specificity of exosomes, their ability to package cargo (in a non-randomized manner) using a well-organized cargo sorting system and delivering it to specific targets/cells, makes them a potentially potent candidate for vesicle-mediated drug delivery. Moreover, since biomolecule-based drugs like proteins and mRNA cannot be administered orally due to degradation susceptibility, exosomes offer an alternative drug delivery system [134-136].

During neurological drug design and optimisation, one of the major factors a researcher must consider is the likelihood of the drug crossing the blood-brain barrier (BBB). This is a barrier consisting of a lining of endothelial cells that separates circulatory blood from cerebrospinal fluid. This semipermeable junction prevents the entry of pathogens and other large or hydrophilic molecules that might be present in circulatory blood. Essential molecules such as amino acids, glucose and proteins are transported actively through the BBB via carrier, adsorption or receptor-mediated transport [137]. As demonstrated by Banks et al. (2020), exosomes are capable of crossing the BBB thereby addressing a major hinderance in the development of drugs that target the brain [138]. This means that exosomes may be one of the solutions for the delivery of potent drugs which cannot cross the BBB.

Various *in vitro* methods have been adopted to enable the insertion of specific therapeutic cargo into nanoparticles to enable targeted drug delivery. Liposomes, a type of artificial membrane-bound vesicle, are one of the common drug loading and delivery system. However, unlike exosomes, they are costly to produce, have low solubility as well as a short half-life [139]. Moreover, exosomes are more efficacious because they can be derived from the patient's own cells, limiting the possibility of immune rejection [140]. A range of exosome cargo loading methods exist; the basic principle underlying the technique, advantages, and disadvantages and examples of cargo loaded are outlined in Table 1.2.

Table 1. 2: Exosome cargo loading methods.

Method	Basic principle	Advantages	Disadvantages	Cargo	Reference
Passive loading via exosome-cargo incubation	Exosomes are incubated with the cargo at a specific temperature for a certain time period	Cost Time	Not ideal for hydrophobic cargo	Doxorubicin	[141]
Passive loading via exosome-secreting cell-cargo incubation	Exosome-secreting cells are incubated with the cargo which they traffic into exosomes	Cost Time	Lower loading efficiency	Paclitaxel	[142]
Saponin-mediated exosome membrane permeabilization	Detergent-like saponins permeabilise the lipid bilayer by complexing with cholesterol, allowing entry of co-incubated cargo	No membrane damage Ideal for hydrophobic cargo	Can limit therapeutic effects of exosomes Cargo degradation	Catalase	[143-145]
Sonication	Mechanical shear force using homogeniser probe is used to disrupt the membrane integrity ultrasonically	Higher loading efficiency	Membrane damage Nucleic acid degradation Exosome aggregation	Gemcitabine	[127, 146-148]
Electroporation	An electrical field is used to induce micropores on the exosomal membrane	Loading efficiency	Protein denaturation Membrane destruction Exosome aggregation RNA precipitation	Doxorubicin	[149]
Freeze-thawing	Cargo and exosomes are rapidly frozen in liquid nitrogen or -at 80°C and thawed at room temperature for at least 3 freeze-thaw cycles	Loading efficiency	Exosome enlargement Protein denaturation	Catalase	[143, 150-154]
Extrusion	Exosomes mixed with the drug are loaded into an extrusion machine which forcefully disrupt the exosome membrane as it pushes them through porous membranes	Reproducibility Time Vesicle deformation Loading efficiency	Negative effects unknown	Cas9	[143, 144, 151, 155-157]
Transfection	Cargo is loaded into exosomes directly or through the parent cell via cationic polymers or transduction- based commercial transfection kits	No protein cargo denaturation	Transfecting agents' toxicity	miR-125b2 and miR-155	[147, 150, 158-161]

The most common methods for loading different cargo into exosomes were summarised along with their basic principle and the advantages and/or disadvantages reported for each method. The references literature reported the basic principle, advantages, disadvantages, and/or the cargo they successfully loaded into the exosomes.

To combat the effects of Alzheimer's Disease (AD), Alvarez-Erviti et al. (2011) used electroporation to perforate exosomes and load them with siRNA which were specifically delivered to neurons, microglia, and oligodendrocytes in the brain. A 60% knockdown of β secretase 1 (BACE1), which is highly implicated in AD, was observed [140]. In a similar study, Faruqu et al. (2018) isolated exosomes generated by HEK293 cells and loaded them with siRNA. The encapsulation efficiency was approximately 10 – 20% and they successfully delivered this cargo in cancer cells [162]. Additionally, Kuate et al. (2007) also demonstrated the potential application of exosomes for vaccine development. The authors were able to show that exosomes isolated from 293T cell conditioned medium are ideal carriers of the corona virus S protein, which may be useful to induce high neutralising antibody production to combat diseases caused by this group of viruses, including the COVID-19 [163].

1.5. Umbilical Cord Blood Serum

Umbilical cord blood (UCB), blood from the umbilical cord and placenta, is rich in hematopoietic stem cells, which might explain its reported therapeutic effects [164-167]. Umbilical cord blood serum (UCBS) is the liquid component of UCB which is, in summary, produced by subjecting UCB (that has been allowed to clot at room temperature) to centrifugation in order to remove the red blood cells and debris [168]. There is variation in the production of UCBS across different studies [168, 169].

Nonetheless, UCBS has been shown to possess multiple therapeutic properties [170, 171]. For example, the treatment of severe dry eye with UBCS has been shown to be possible, and most importantly, safe [172]. It promotes corneal healing and reduces corneal clouding caused by chemical burns [173]. Moreover, it has been demonstrated that addition of 20% UCBS to artificial tears had an inhibitory effect on the frequency of de-epithelialisation associated with corneal erosion [174]. UCBS eye drops, used for the treatment various corneal defects including severe dry eye, corneal erosions, and neurotrophic keratitis, are therefore now commercially available. An example is

Optiserum (Next Biosciences, Midrand, South Africa), a product that consists of 20% (v/v) UCBS in saline. The dilution is aimed at mimicking the levels of TGF-β that are naturally found in tears to prevent possible complications such as inflammation and myofibroblast trans-differentiation [175]. The epidermal growth factor (EGF), which is one of the main mitogens implicated in wound healing as it activates the phosphatidylinositol pathway, induces actin microfilament system activation and membrane ruffle development [176-178]. EGF is generally accepted as a biomarker for UCBS for the purposes of quality and standardization.

1.5.1. UCBS Exosomes

Due to their natural role as mediators of cell communication, as well as their remarkable therapeutic implications, UCBS-derived exosomes have been investigated [179, 180]. Exosomes isolated from UCBS using ultracentrifugation have been reported to promote wound closure of human fibroblast cells as well as angiogenic activity in skin endothelial cells [181]. This could be due to the presence of pro-migration miRNA cargo, such as miR-376c-3p and miR-550a-5p, that have been discovered to be enclosed within the exosomes using qPCR [182]. However, it is worth noting that the beneficial properties of UCBS-derived exosomes may depend on the health of the infant. For example, exosomes isolated from UCBS of premature infants with bronchopulmonary dysplasia (characterised by abnormal lung development) have been reported to have anti-angiogenic properties against human umbilical vein endothelial cells (HUVECs) *in vitro* [179].

1.6. Aims and Objectives

The aims of this study were to isolate and characterise exosomes from umbilical cord blood serum (UCBS) and determine their effect on cellular proliferation *in vitro*.

To achieve this, the objectives were set as follows:

1. Isolation of extracellular vesicles from UCBS (using commercially available Optiserum as the UCBS source)
2. Characterisation of the extracellular vesicles to confirm their exosome nature and protein content using a range of techniques including:
    a. Tunable Resisitive Pulse Sensing
    b. Transmission Electron Microscopy
    c. Immunocytochemistry
    d. ELISA
3. Analysis of the effect of the isolated exosomes on HEK293 cellular proliferation (using the MTS assay).

Chapter 2: Materials and Methods

2.1. General lab reagents and procedures

2.1.1. Reagents

2.1.1.1. PEG6000

A 20% (w/v) PEG6000 stock solution, containing 0,5 M NaCl was made by dissolving 3 g PEG6000, (uniLAB, cat. 504018) and 0.44 g NaCl (MERCK, cat. SAAR5822320M) in 10 ml distilled water in a 15 ml falcon tube. This was followed by thorough vortexing until the crystals had fully dissolved before the volume was topped up to 15 ml and the tube was vortexed again. The solution was stored at 4°C until used.

2.1.1.2. TRP reagents

The reagents used for TRPS analysis are listed in Table 2.1 below:

Table 2.1: TRPS reagent information

Reagent	Mean particle diameter (nm)	Concentration (particles/ml)	Batch ID
Solution S	380	1.1×10^{11}	754647A
Calibration Particles Carboxylated 200 (CPC200)	210	8.3×10^{10}	9755H

2.1.1.3. PBS

Calcium and Magnesium-free Phosphate-Buffered Saline (PBS) stock solutions were prepared by dissolving 0.2 g KCL (MERCK, cat. 104936), 0.2 g KH_2PO_4 (MERCK, cat. SAAR5043600EM), 8.0 g NaCl, and 1.15 Na_2HPO_4 (MERCK, cat. 7558794) in 1 L distilled water before autoclaving at 120°C for 20 minutes.

2.1.1.4. Tris-HCl buffer

This was prepared in a 1L glass beaker by dissolving 121.14 g of Tris (Sigma – Aldrich, cat. 648310-M) using distilled water and mixing with a magnetic stirrer until the crystals completely dissolved. The pH was then adjusted to 8.5 using concentrated hydrochloric acid (or HCl; Sigma – Aldrich, cat. 7647-01-0) before distilled water was used to bring the volume to 1L. The solution was kept in a sealed clear-glass container at room temperature until use.

2.1.1.5. Uranyl acetate

Stock solutions of 2% (w/v) uranyl acetate were prepared under low light conditions by dissolving 1 g uranyl acetate (SPI-CHEM, cat. 1070911) in 50 ml double-distilled water in a flat bottom flask. The solution would then be stored a 4°C in the flask covered in aluminium foil to protected it from light.

2.1.1.6. Mowiol slide mounting medium

In a 250 ml glass beaker, 9.6 g Mowiol (Sigma – Aldrich, cat. 81381) was mixed with 24 g glycerol (Sigma – Aldrich, cat. 49770) before adding 24 ml distilled water and incubated at room temperature for 2 hours. Following this, 48 ml of the Tris-HCl buffer was added before mixing using a magnetic stirrer on a hot plate set to medium-low heat until most of the powder dissolved. The excess powder was pelleted using centrifugation in 15 ml falcon tubes at 5000 x g for 15 minutes. The supernatant was removed and stored in either 500 µl aliquots in Eppendorf tubes or 10 ml aliquots in 15 ml falcon tubes at -20°C until use.

2.1.1.7. Tissue culture medium

Serum containing medium (SCM) was prepared as follows: Dulbecco' Modified Eagle's Medium (or DMEM; Capricorn Scientific, cat. DMEM-HPA), containing 10 % Foetal Bovine Serum (FBS) (Capricorn Scientific, cat. FBS-GI-12A) and 2% Penicillin-Streptomycin (Lonza, cat. DE17-602E). Serum-Free Medium (SFM), which is simply SFM

without any FBS, was prepared as follows: DMEM (HyClone, cat. SH30243.01) containing 2% Penicillin-Streptomycin (Lonza, cat. DE17-603E)).

2.1.2. Cell culture

The Human Embryonic Kidney 293 (HEK293) cell line was donated by Prof Raymond Hewer (Biochemistry Discipline, School of Life Sciences, University of KwaZulu-Natal, South Africa). These were preserved in liquid nitrogen. Cells were kept sterile by employing aseptic techniques in a biosafety level 2 laminar flow cabinet (Haier Biomedical, product EN12469:2000).

2.1.2.1. Cell thawing

Cells in a cryovial were placed in warm water bath (~37°C) until only the sides were thawed but the centre remained frozen. These were then gently poured into a T75 tissue culture flask and warm SCM was added slowly to a final volume of 10 ml, and the flask was kept for 4 hours in a 37^{o}C and 5% carbon dioxide (CO_2) incubator (ESCO, serial. 2018-124079) to allow cells to adhere. Adherence was confirmed using the Olympus CKX41 brightfield microscope before the medium was removed the cells were rinsed in warm PBS and then 10 ml fresh tissue culture medium was added before the flask was placed back into the incubator.

2.1.2.2. Cell quantification and passaging

The medium from adherent cells in a T75 tissue flask was decanted followed by rinsing the cells twice with 1 ml warm PBS. This was followed by trypsinisation: 1 ml of the warm trypsin-versene mixture (BioWhittaker, cat. 17-161E) was added and allowed to cover the base of the flask evenly. The flask was placed back in the incubator for 10 minutes. Successful trypsinisation was confirmed by observing cellular detachment under the brightfield microscope. The trypsinisation was quenched by adding an equal volume (1 ml) of the tissue culture medium and mixing thoroughly via pipetting. A 20 µl sample was then removed for cell counting using a haemocytometer counting chamber, a brightfield

microscope (10 x objective) and a handheld analogue tally counter. From the calculated cell concentration, the desired dilution of cells was performed before cells were placed into a flask or plate as required.

2.2. EV Isolation

Extracellular vesicles were isolated from Optiserum batches, umbilical cord blood serum eye drops from Next Biosciences (http://surl.li/jbcrr). Optiserum is a product that contains 20% (v/v) umbilical cord blood serum and 80% (v/v) saline; it is stored at -20°C. A final 5% (w/v) PEG6000 concentration was used for isolation of EVs from 1 ml Optiserum samples.

The isolation protocol is summarised in Figure 2.1 below. Optiserum was thawed at room temperature and then centrifuged at 13 000 x g using a Beckman Coulter Allegra X-22R centrifuge with the F2402H rotor at 4°C. This step was aimed at removing larger vesicles and cellular debris. The supernatant was then mixed in a 3:1 ratio with 20% PEG 6000 to achieve a final PEG 6000 concentration of 5%. The solution was then mixed using a vortex and incubated on ice for 30 minutes. This was followed by centrifugation at 10 000 x g for 20 minutes at 4°C. The pellet was then resuspended in PBS or SFM. The pellet was vortexed to allow resuspension (in a volume equal to the volume of Optiserum used for isolation) until it was invisible (generally 10 seconds) and then stored at -20^{o}C before utilisation.

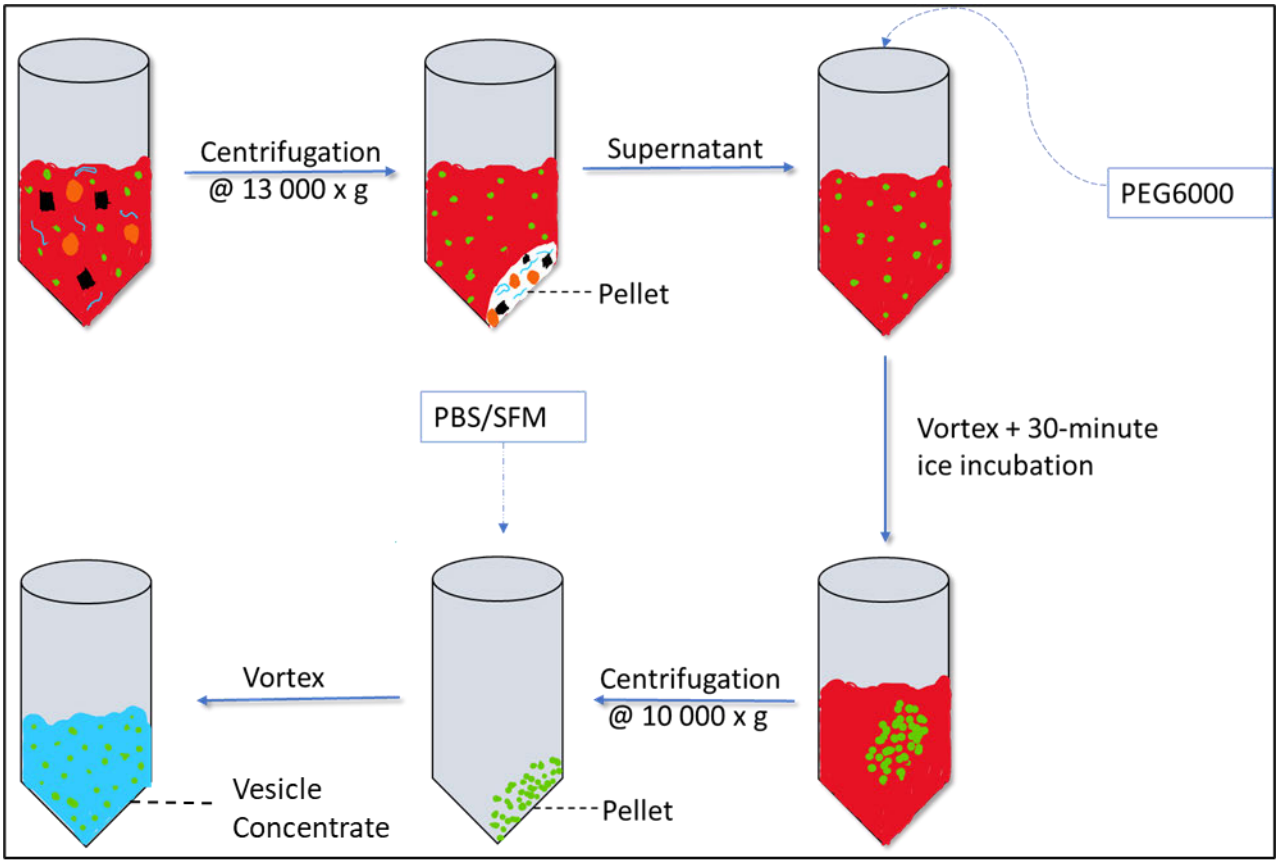

Figure 2.1: Isolation of vesicles from Optiserum. The sample was centrifuged at 13 000 x g before PEG6000 was added to the supernatant which was vortexed and incubated in ice for 30 minutes. This was followed by concentrating the vesicles to the pellet via centrifugation at 10 000 x g and the pellet was then resuspended via vortexing in either PBS or SFM.

2.3. Tunable resistive pulse sensing (TRPS) *(Refer to Appendix 1 for labelled device parts)*

The concentration of the isolated vesicles was determined using TRPS via the Exoid instrument (Version 1.0, serial. EXOID-062-R; this equipment is not available elsewhere in South Africa), from Izon Science, France. Prior to biological sample analysis, we optimised the system using polystyrene calibration particles (CPC200 and Solution S). As mentioned in Chapter 1, this equipment uses pressure and voltage to pass samples through a nanopore and this causes interferences in the current which is directly proportional to the particle size and concentration. Extracellular vesicles have a negative charge and are drawn towards the positive electrode across the nanopore. All samples and reagents were kept in ice throughout analysis.

Particle quantification using the Exoid was carried out as per our optimised standard operating procedure (Appendix 1). Briefly, the nanopore membrane stretch was kept at 47 mm. To ensure contact between the electrolyte solutions in the upper and lower fluid cells through the nanopore, the nanopore was wet using a 1/100 (v/v) dilution of the surfactant-containing Izon wetting solution in filtered PBS (fPBS), which was forced through the nanopore using 2500 Pa pressure for 10 minutes. Following removal of the wetting solution, the prevention of contaminants binding to the nanopore was carried out using 10% (w/v) filtered Izon coating solution in fPBS which was also forced through the nanopore using 2500 Pa pressure for 10 minutes. The nanopore membrane, the upper fluid cell, and the lower fluid cell were rinsed using filtered distilled water and blotted dry using lint-free paper towels. This was followed by the characterisation of the nanopore using CPC200 (Table 2.1) diluted 1/50 in fPBS. Samples (kept in ice) were diluted at least 1/1000 in fPBS before being analysed. Contrary to the normal sequence, the measurement conditions (pressure & voltage) were adjusted according to the sample rather than the CPC200. Analysis was only carried when the particle rate was at least 100 particles/minute, the RMS noise was less than 10 Pa and the current was between 120 nA – 140 nA. If the rate was still low despite applying sufficient pressure, a lower dilution (10-fold less than the previous) was used. Following sample analysis, calibration was then carried out using the same measurement conditions and nanopore as the samples. Data analysis was carried using the Izon Data Suite software.

2.4. Transmission Electron Microscopy

A drop of the sample was mounted on standard formvar-coated copper grids or carbon-coated copper grids, using a glass pipette, and allowed to stand at room temperature for 5 minutes before excess liquid was carefully blotted using Whatman no. 1 filter paper. Once the copper grids had dried, negative staining was performed using a drop of 2% uranyl acetate for 30 seconds before excess liquid was blotted again using Whatman no. 1 filter paper. Sample imaging was done using the JEM 1400 transmission electron

microscope (JOEL, serial. EM18480030). Images were generated using the Gatan Microscopy Suite software.

2.5. Cell proliferation assay (MTS assay)

2.5.1. Standard curve

In a 96-well plate; 0, 5000, 10 000, 20 000, 40 000 and 80 000 cells were plated in triplicate in a final volume of 100 µl tissue culture medium. These were allowed to adhere for 4 hours (37°C, 5% CO_2 incubator). Complete cell adherence was confirmed under the brightfield microscope by ensuring that there were no cells floating in the solution. Then, 100 µl fresh medium was added to each well, followed by the addition of 20 µl of the MTS reagent (CellTiter Aqueous One, cat. G3580) and the plate was put back in the incubator. Colour development was determined by measuring the absorbance after 3 hours at 490 nm using a SpectreMax ABS Plus spectrophotometer. A standard curve to be used for extrapolation was then constructed (Figure 2.2).

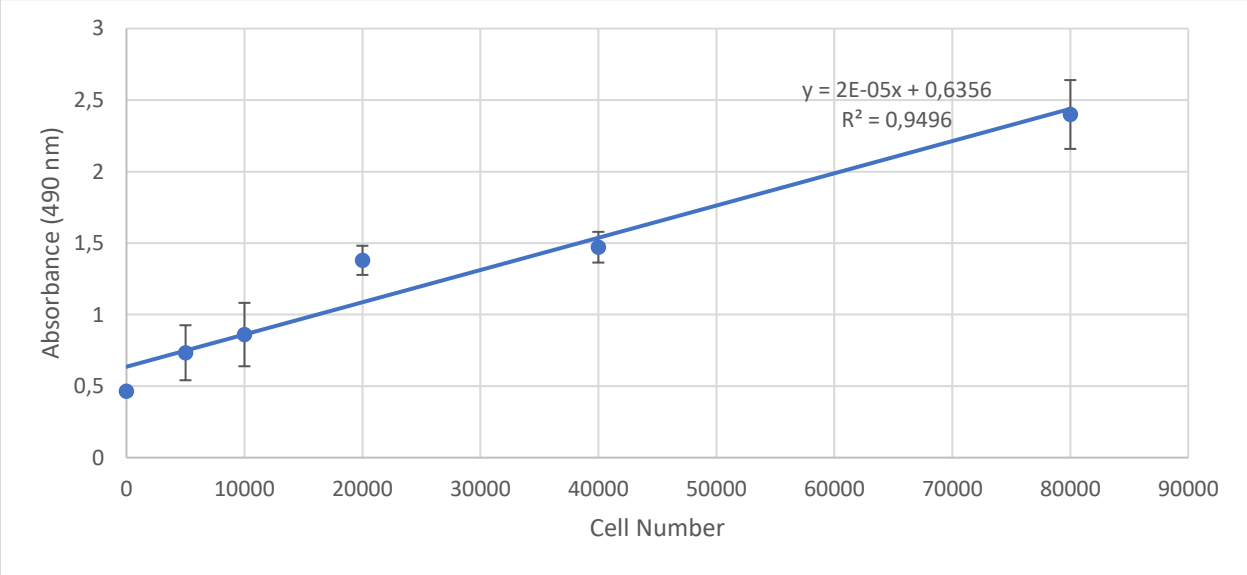

Figure 2.2: Standard curve used for the MTS assay cell quantification. The absorbance, resulting from the addition of the MTS reagent to HEK293 cells of increasing number, was measured at 490 nm. The values are an average of three replicates and the error bars were generated using the standard deviation.

2.5.2. HEK293 cell proliferation in the presence of exosomes

In a 96-well plate, 10 x 10^3 HEK293 cells were plated in a final volume of 100 µl tissue culture medium. They were allowed to adhere for 4 hours in the 37°C, 5% CO_2 incubator before the medium was removed and replaced with 200 µl of either fresh SCM, SFM or SFM containing 1 x 10^3 to 1 x 10^8 exosomes in duplicate. The plate was placed in the 37°C, 5% CO_2 incubator for 24 hours before addition of 20 µl of the MTS reagent. Colour development was allowed for 3 hours before the absorbance was measured as previously described (at 490 nm).

2.6. Internalisation of exosomes by HEK293 cells

2.6.1. Exosome membrane labelling and uptake

Exosome membrane staining was performed immediately before the vesicles were added to cells for uptake. Staining was done using the red-fluorescing PKH26 dye kit (Sigma – Aldrich, cat. MIDI26-1kt). The vesicles were concentrated to a pellet as described in Section 2; the pellet was resuspended in 500 µl SFM and the solution was directly added to an equal volume of the PKH26 membrane labelling dye (2 µl PKH26 dye in 500 µl diluent C). Dye uptake by the vesicles was allowed for 1 minute before quenching with 1 ml 1% bovine serum albumin [(BSA) Roche, cat. 107350860010 in SFM].

To examine the internalisation of the stained vesicles, fully confluent HEK293 cells were plated in a final volume of 100 µl SCM on 22 x 22 mm glass coverslips in a 6-well plate. The cells were allowed to adhere for 4 hours in a 37 °C, 5% CO_2 incubator. The medium was decanted, and the slides gently rinsed with 1 ml PBS three times before cells were immersed in 500 µl of the membrane-stained EV solution. To this, 500 µl SFM was added, and the plates were returned to the 37 °C, 5% CO_2 incubator for 24 hours before being rinsed thoroughly with 1 ml PBS three times. The cells were fixed using 1 ml 2% paraformaldehyde containing 0.1 % Triton X-100 (Sigma – Aldrich, cat. T9284) for 10 minutes and rinsed again with 1 ml PBS three times.

2.6.2. Immunocytochemistry

Following the vesicle uptake and fixation of the HEK293 cells, nonspecific antibody binding was reduced by coating the slides with 1 ml 5% donkey serum (Biowest, cat. S2170100), in PBS for 30 minutes. This was followed by an overnight incubation at 4°C with 500 µl mouse monoclonal anti-CD81 IgG_{2b} primary antibody (Santa Cruz Biotechnology, cat. sc-166029) diluted 1/400 in PBS. After washing cells again three times with 1 ml PBS, a light-protected 2-hour incubation with the 1/2000-diluted DyLight 488-conjugated AffiniPure donkey anti-mouse IgG secondary antibody (Jackson Immunoresearch, cat. CN-715-485-151) followed. The slides were rinsed again with 1 ml PBS three times before the cell nuclei were stained for 10 minutes using 1 ml of the Hoechst 33342 nuclear stain (Sigma – Aldrich, cat. B2261) in PBS (1/4000 dilution; stock concentration: 10 mg/ml). The slides were rinsed again with 1 ml PBS three times before being mounted onto glass microscope slides, using the mowiol mounting medium, prior to imaging using the Zeiss 710 LSM confocal microscope.

2.7. Protein quantification

2.7.1. Determination of total protein concentration

The protein concentration was measured according to Bradford (1976). A standard curve was prepared using BSA protein standards (5, 10, 15, 20, 30, 40, 50 µg) in duplicate. The standards were prepared from a 1 mg/ml BSA stock solution (Roche, cat. 10735086001) and each standard was made to a total of 100 µl using distilled water. Finally, 900 µl of the Bradford reagent (Sigma - Aldrich, cat. B6916) was added and absorbance of the 1 ml solution was measured at 595 nm using the IMPLEN NanoPhotometer C40 spectrophotometer, to generate the standard curve (Figure 2.3). For sample measurement, 0 – 100 µl sample was made to 100 µl using distilled water and 900 µl of the Bradford reagent was added before measuring absorbance at 595 nm. The protein concentration was then estimated via extrapolation using the standard curve. Colour formation, when the Bradford reagent was added, was immediate.

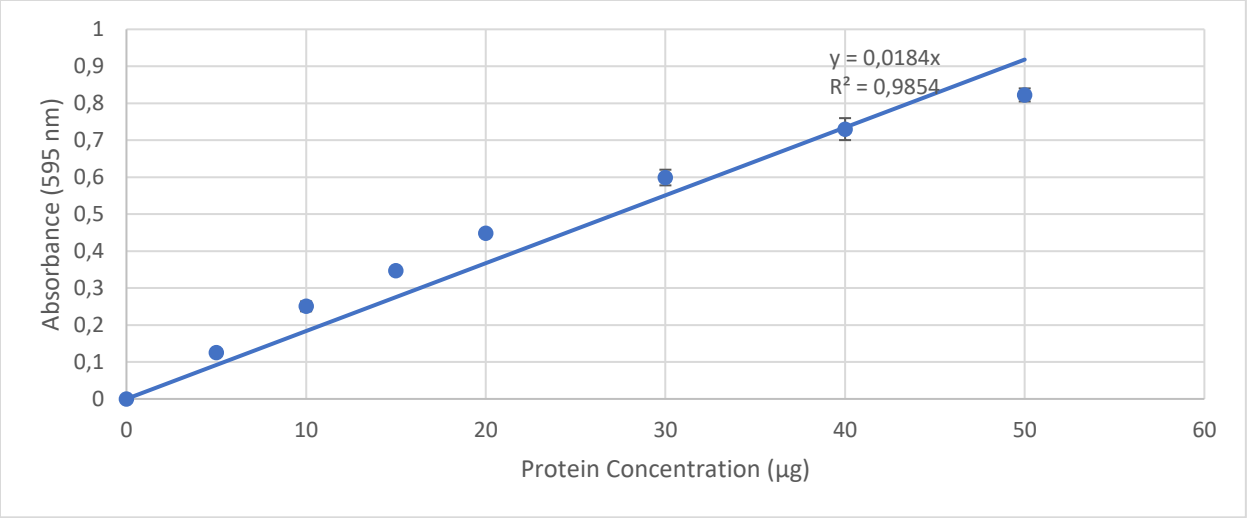

Figure 2.3: Standard curve used for protein concentration estimations. The absorbance of (BSA) standards (0 - 50 µg) was measured in duplicates at 595 nm. The values are an average of two replicates and the error bars were generated using the standard deviation.

2.7.2. ELISA

2.7.2.1. EGF quantification

To measure the levels of EGF, the Quantikine sandwich ELISA kit (R&D Systems, cat. DEG00) was used as per manufacturer's instructions. Briefly, 50 µl of the RD1-6 reagent was added in each well before the addition of 200 µl of the appropriately diluted sample (Optiserum and vesicle samples were diluted to 1:1 with the RD6N diluent; the EV samples had been lysed using a 1/10 dilution with the radioimmunoprecipitation (RIPA) buffer (Sigma – Aldrich, cat. R0278). The appropriate negative controls/blanks were included: RD6N diluent, saline in RD6N diluent, and RIPA buffer in RD6N diluent. The wells were covered in an adhesive plastic strip and incubated at room temperature for 2 hours on a Stuart SB3 shaker set to 8 RPM. The wells were aspirated and washed by adding 300 µl of the wash buffer for a total of 4 washes. Excess liquid was removed by blotting the plate on a paper towel before adding 200 µl of human EGF conjugate to each well and the plate was covered and incubated for 2 hours like before. The wash step was repeated before adding 200 µl of the substrate reagent and incubating the plate at room temperature for 20 minutes in the dark. This was followed by the addition of 20 µl of the stop solution in each well. The plate was placed on a white surface to visualise wells

where colour change, from blue to yellow, had not occurred or was not homogenous. In such instances, the colour change was aided by gently pipetting the liquid in the well up and down, while cautiously avoiding touching the bottom of the wells with the pipette tip. Lastly, the absorbance at 450 nm was measured as soon as possible but no later than 30 minutes after the addition of the stop solution. The values of the blanks were subtracted from the appropriate samples.

2.7.2.2. Cytokine screening

Following the manufacturer's instructions, cytokine screening was carried out using the Bio-Plex Pro Human Cytokine Screening Panel (Bio-Rad Laboratories, USA), 48-plex (cat. 12007283). The 48-plex screens for 48 cytokines (Table 2.2).

Table 2.2: Cytokines detected using the Bioplex 27-plex and the 48-plex systems.

48 - Plex	IL-1b, IL-1ra, IL-2, IL-4, IL-5, IL-6, IL-7, IL-8, IL-9, IL-10, IL-12 (P70), IL-13, IL-15, IL-17, Eotaxin, Basic FGF, G-CSF, GM-CSF, IFN-g, IP-10, MCP-1, MIP-1, PDGF-bb, MIP-1b, RANTES, TNF-a, VEGF, CTACK, GRO-a, HGF, ICAM-1, IFN-a2, IL-1a, IL-2ra, IL-3IL-12 (P40), IL-16, IL-18, LIF, MCP-3, MIF, MIG, b-NGF, SCF, SCGF-b, SDF-1a, TNF-b, TRIAL and VCAM-1	48

Eighteen Optiserum batches were used for analysis. Analysis was carried out on the Optiserum and the exosomes isolated from 14 matching batches. The exosome samples were lysed using a 1:1 dilution using the Bio-Rad cell lysis kit (cat. 171304011).

To begin the assay, a 1x stock solution of the fluorescently labelled magnetic beads was prepared and vortexed for 30 seconds at medium speed before 50 µl was loaded on each well of the assay plate. The plate was washed twice using 100 µl wash buffer (1x solution in deionised water), before 50 µl of the samples, blanks, standards, and controls were loaded. Because the exosomes are resuspended in SFM during isolation (and were lysed using the Bio-Rad cell lysis kit before analysis), and Optiserum is 20% UCBS solution in

saline, the following controls were included: SFM diluted 1:1 with Bio-Rad cell lysis buffer, as well as saline. Following loading, the plate was covered in sealing tape and incubated for 30 minutes at room temperature for with medium shaking. The sealing tape was removed, and the plate was washed three times using 100 µl of the wash buffer. This was followed by the addition of 25 µl of the detection antibodies (1x solution in diluent HB), before the plate was sealed and incubated at room temperature for 30 minutes as before. The plate was again washed three times using 100 µl of the wash buffer before the addition of 50 µl of 1x streptavidin-phycoerythrin (SA-PE) in assay buffer, in each well, before sealing and incubating at room temperature for 10 minutes with medium shaking. The SA-PE was removed by a final wash step before the addition of 125 µl of assay buffer in each well before incubating the plate at room temperature for 30 seconds with gentle shaking by hand before inserting the plate in the Bio-plex 200 plate reader. The Bio-plex Manager software was used for plate analysis and all dilutions were accounted for. The data was exported to the Microsoft Excel software to subtract the readings of the blanks from the corresponding samples.

2.8. Statistical analysis

The Microsoft Excel ‘’Analysis Toolpak’’ add-in was used for statistical analysis. Data analysis was carried out using the Student’s t-test with the alpha value set to 0.05. Following the two-tailed t-test analysis, values less than the alpha value were considered significantly different to the control.

Chapter 3: Results

3.1. TRPS Optimisation

As mentioned in Chapter 1 (Section 2.2), tunable resistive pulse sensing (TRPS) allows the user to determine the size and concentration of particles. The Exoid (TRPS instrument by IZON Science, France) was used in this study (Figure 3.1A). Samples, which are always diluted in an electrolyte such as PBS, are loaded into the upper fluid chamber and the nozzle is inserted (Figure 3.1B, C). What the user aims to achieve is to apply pressure and voltage to pass the particles through a nanopore which is within a membrane

mounted on the Exoid (Figure 3.1D). There are oppositely charged electrodes on either side of the nanopore and when sufficient voltage is applied, this establishes a stable current within the nanopore (Figure 3.1E). As particles pass through the nanopore, they cause volume displacement which results in a rapid temporary decrease in the current and one of these drops in current is called a blockade event (Figure 3.1F). The length of the blockade event (blockade magnitude) as well the frequency of the blockade events are both directly proportional to the particle size and concentration, respectively (Figure 3.1G, H). The system can determine the size and concentration of the particles present in that sample by comparing the blockade magnitude and blockade frequency of the particles in the sample with that of calibration particles. These have a known diameter and concentration. For example, the Calibration Particles Carboxylated 100 (CPC100) particles have a mean diameter of 100 nm and a concentration of $1.7x10^{13}$ particles/ml.

TRPS is extremely challenging and requires training and a deep understanding of the equipment to be able to generate accurate and meaningful data. Thus, before the Exoid could be utilised routinely for sample analysis, a standard operating procedure (SOP) had to be established. To achieve this, 200 nm nanoparticles (CPC200) were analysed.

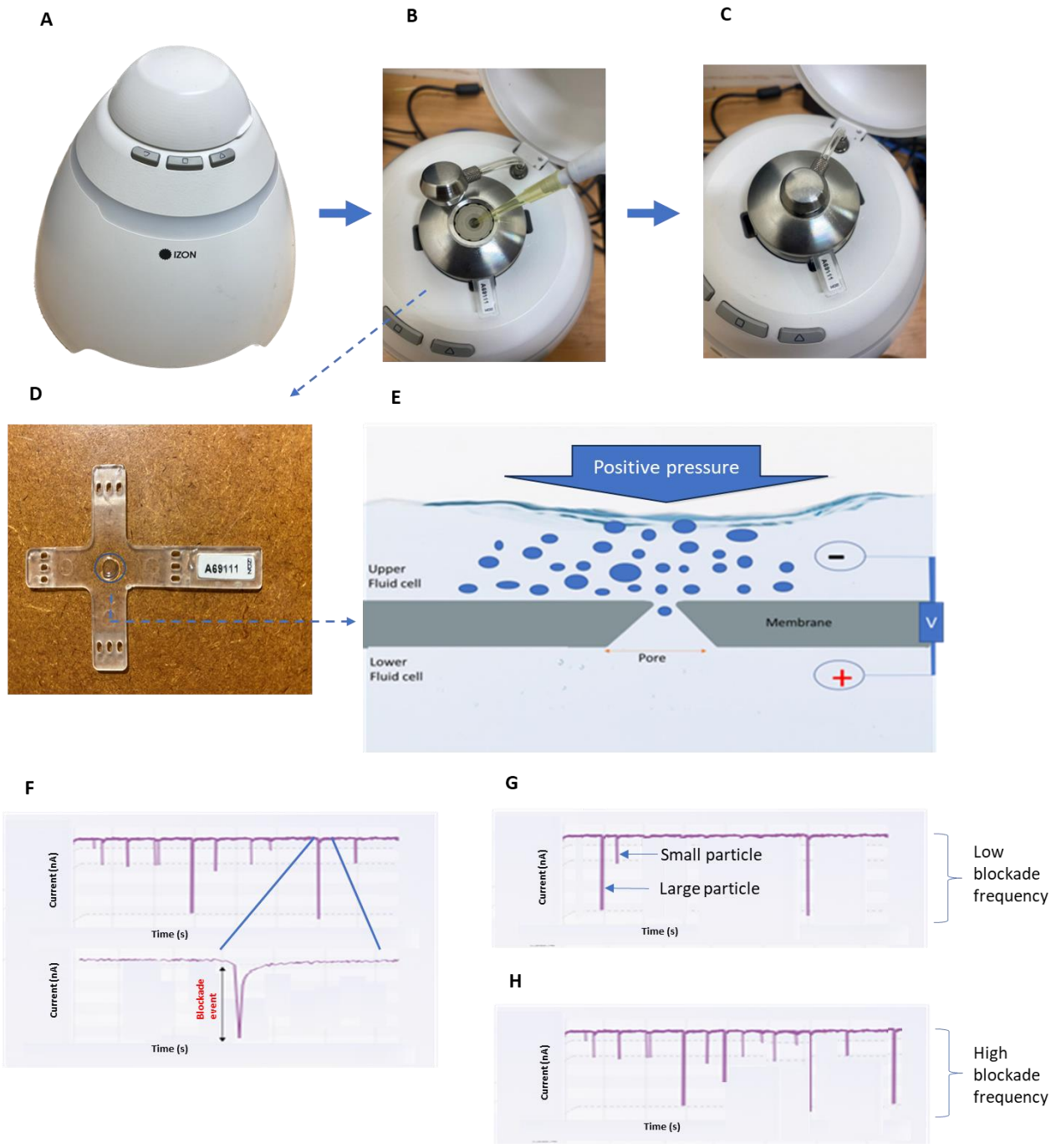

Figure 3.1: Using the Exoid TRPS instrument. A) The Exoid TRPS instrument. B) The sample is loaded into the upper fluid chamber and (C) the pressure nozzle is inserted. D) A nanopore membrane is placed above the lower fluid chamber. E) On either side of the nanopore (in the upper and lower chambers) is fluid electrolyte as well as electrodes. The upper fluid cell has a negative electrode, and the lower fluid cell (under the nanopore) contains the positive electrode. When pressure and voltage are applied it forces particles (shown as blue spheres) through the nanopore. F) As the particles pass through, a temporary drop in the current is caused and this is called a blockade event. G) The length of the blockade event corresponds to the size of the particle. The frequency of the blockade events can be low (G), due low particle concentration, or it can be high (H), due high particle concentration.

3.1.1. Important parameters

Before analysis begins, the user must ensure that the optimum settings have been established. Four crucial parameters are considered in this regard, namely the current, root mean square (RMS) noise, blockade magnitude, and particle rate. All these parameters affect reproducibility as well as how efficiently the system detects particles. However, they will differ depending on the nanopore membrane used so they cannot be standardised and need to be adjusted each time an analysis is performed.

3.1.1.1. Current

When an electrolyte, usually phosphate-buffered saline (PBS), is passed through the nanopore, it enables the establishment of a baseline current with the application of voltage (through the electrodes on opposite sides of the nanopore). It is for this reason that all samples are diluted in the same electrolyte before being analysed on the Exoid. As mentioned previously, when the sample is passed through the nanopore, the particles cause a blockade. For the blockade to be accurately quantified, the baseline current should be kept between 100 nA to 140 nA [183].

The user can control this by adjusting the applied voltage since both the current and voltage are directly proportional (Figure 3.2A). When the current is equal to or less than 0 nA, it means that there is no contact between the electrolyte in the upper fluid cell (above the nanopore, where sample is loaded) and the electrolyte in the lower fluid cell (below the nanopore) (Figure 3.2B). This can be prevented by locating and eliminating any air bubbles as well stretching the nanopore to its maximum diameter and applying maximum pressure to force the electrolyte through. The optimum stretch operation range is 45 mm to 47 mm, but the lower the stretch, the higher the chances that the nanopore will get clogged by larger particles [184]. Although the nanopore can be stretched to a maximum width of 53 mm, it is worth noting that stretching the nanopore membrane more than 48 mm increases the risk of nanopore deformation and ultimate rupture [184, 185]. Once contact has been established between the chambers, applying voltage causes the current to increase (Figure 3.2C).

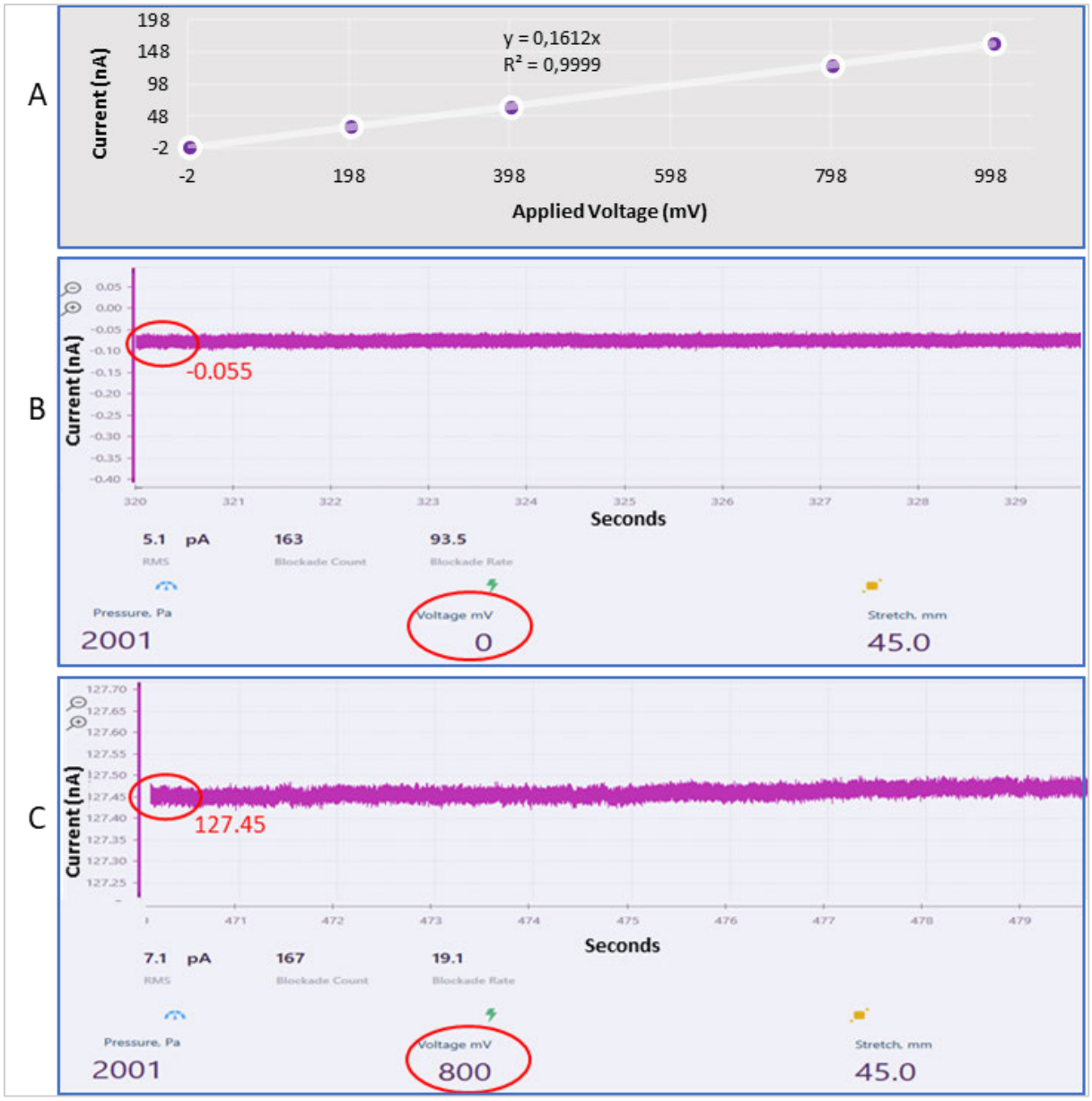

Figure 3.2: Correlation between applied voltage and baseline current. A) Voltage and current are directly proportional. B) Current is -0.055 nA when no voltage is applied. C) Current is an ideal 127.45 nA when 800 mV voltage is applied. The test was conducted using an NP250 nanopore membrane with both the stretch and pressure kept constant. Voltage was applied from 0 to 1000 mV in 200 mV, or 400 mV intervals and the current was recorded at each point.

3.1.1.2. RMS noise

The RMS noise represents the undesirable electrical current that is inherently generated by the Exoid [186]. The user's objective should be to keep the noise levels as low as possible; for optimal results, this value should not exceed 15 pA. Otherwise, any disturbance in current (blockade/resistive pulse) caused by particles passing through the nanopore will not be detected by the system as their signal will be overshadowed by the noise [45]. The presence of air bubbles as well as nanopore clogging (by particles much larger than the nanopore diameter such as clumped nanoparticles and large vesicles or vesicle aggregates) causes an increase in RMS noise. When the nanopore is clogged, not only does the RMS noise increase, but the baseline current displays an erratic pattern (Figure 3.3A). To unclog the nanopore, negative pressure can be applied (Figure 3.3B). Should this not suffice, it can be coupled to applying maximum stretch. Once the particle(s) responsible for the clogging have been dislodged, positive pressure is re-applied, and the system stabilises (Figure 3.3C). Clogging can be prevented by using the Izon coating solution prior to analysis. This solution prevents the binding of particles to the nanopore [187].

Figure 3.3: Unclogging a nanopore. A) Typical profile indicating a clogged nanopore identifiable by unstable baseline current and elevated RMS noise of 31.6 pA. B) Unclogging the nanopore following the application of negative pressure of -1999 Pa causes a large particle to be dislodged and the baseline current stabilises, followed by a decrease in RMS noise to 6.6 pA. C) Once positive pressure reapplied at 2001 Pa, baseline current remains stable with the RMS noise remaining low at 6.5 pA.

Moreover, operating the Exoid near electronic devices such as cell phones and uninterrupted power suppliers (UPS) was also found to cause profound increases in noise (Figure 3.4A, B)

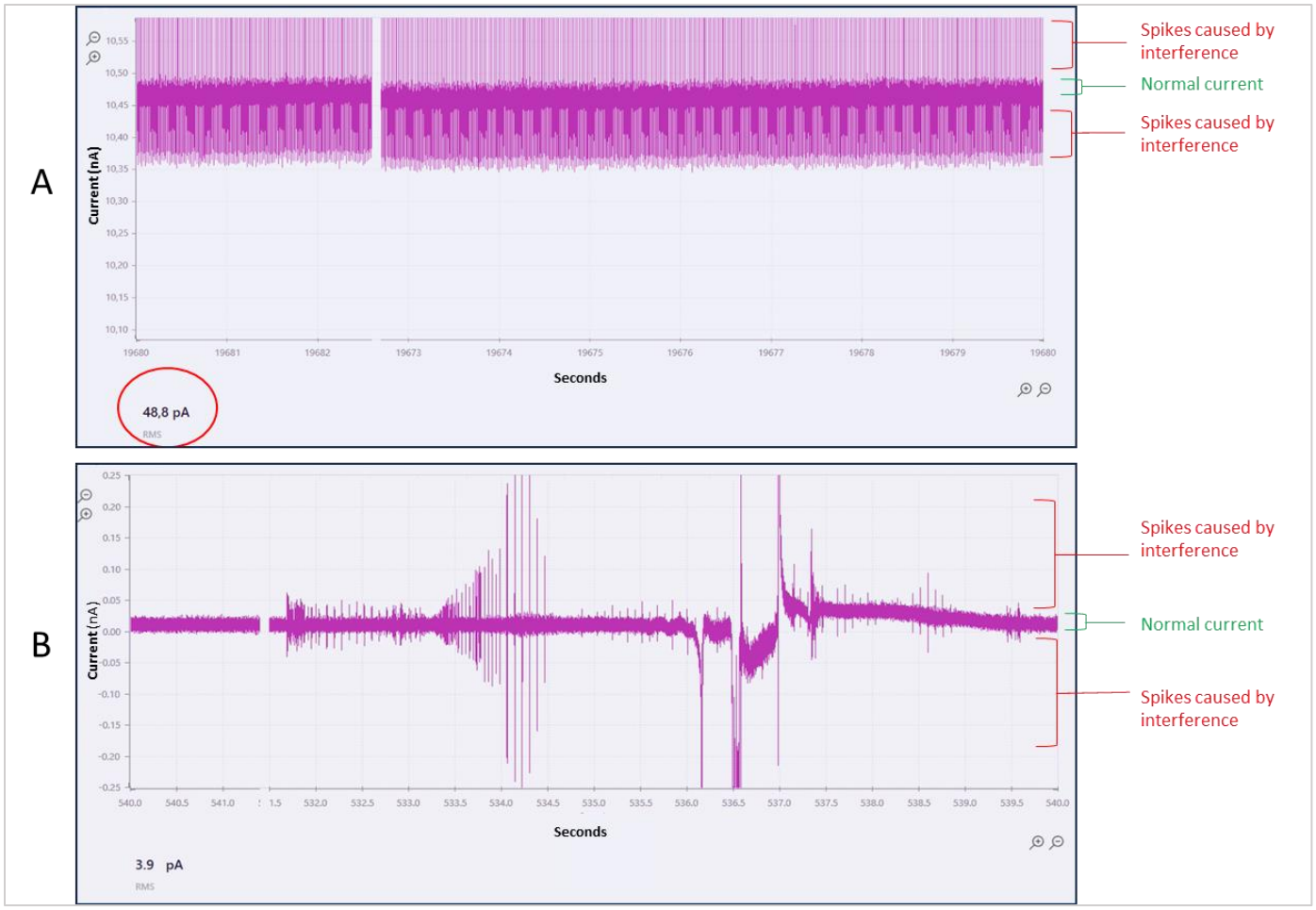

Figure 3.4: Examples of interferences in current and noise due to operating the Exoid near electronic devices. A) Interference (caused by a dedicated uninterrupted power supply during load shedding) disrupting the current, causing a profound increase in RMS noise (48.8 pA). B) Interference (caused by a mobile phone) disrupting the current intermittently, but not the RMS noise (3.9 pA) because no voltage had been applied (current at 0).

3.1.1.3. Blockade magnitude

Since the blockade magnitude corresponds to the size of the particle passing through the nanopore, it is important that it is high enough for the system to detect it. A magnitude of at least 0.2 nA is ideal [187]. Should it be below this value, then the size of the particles may not be easily quantified because the signal will get lost in the RMS noise. This is especially true for smaller particles. To address this, decreasing the nanopore stretch might assist, because decreasing the stretch decreases the size of the nanopore aperture, allowing for even smaller particles to have a bigger impact on the current as

they pass through, resulting in a larger blockade magnitude. However, decreasing the stretch also causes a decrease in the baseline current. This can be countered by applying additional voltage.

3.1.1.4. Particle rate

The particle rate is a measure of the number of particles that pass through the nanopore per minute. The rate is directly proportional to the applied pressure (Figure 3.5). Ideally, this should be between 100 particles/minute to 1500 particles/minute [187]. If the rate is below this range, despite applying sufficient pressure, then a lower dilution of the sample must be used. If it is above this range then the sample needs to be diluted more because when the rate is too high, the likelihood of more than one particle concurrently passing through the nanopore increases. This would result in an overestimation of the particle diameter and an underestimation of the particle concentration.

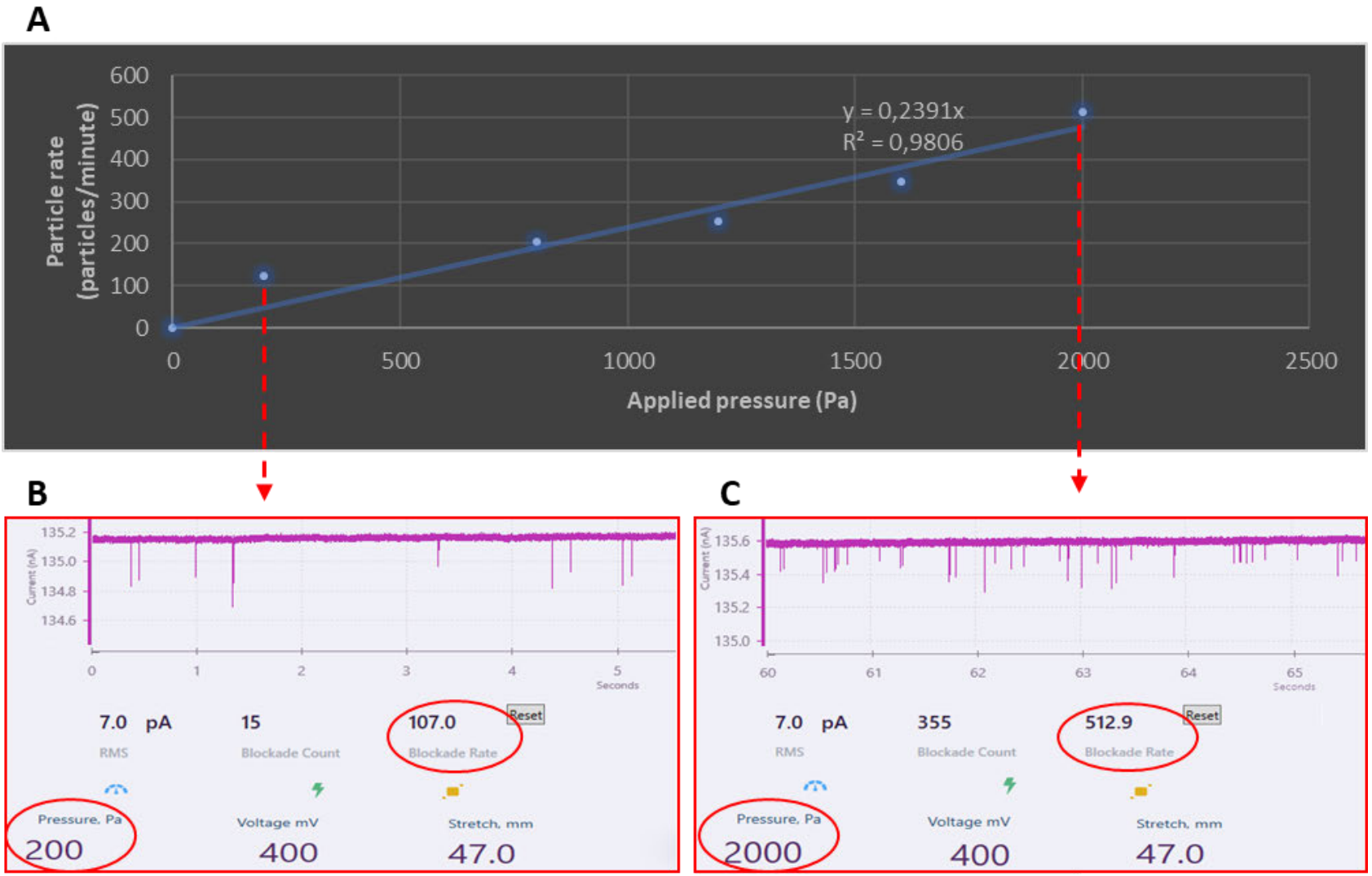

Figure 3.5: Correlation between pressure and the particle rate. Analysis was conducted using a NP250 nanopore membrane and the CPC200 nanoparticles diluted 1 in 50 in PBS. A) Pressure was applied from 0 Pa to 2000 Pa in 200 Pa or 400 Pa increments and the particle rate was recorded at each point. B) At a pressure of 200 PA, the rate was 107.0 particles/minute C) At a pressure of 2000 Pa, the rate was 512.9 particles/minute. The stretch as well as the voltage were kept constant throughout the analysis.

3.1.2. Analysis

Once these parameters have been optimised, analysis can begin. The system is automatically set to measure 500 particles at three different pressures. The user sets the first pressure then the system subsequently carries out the remaining measurements at a pressure that is 200 Pa below the initial set value, and then at a pressure that is 400 Pa above the initial value. It is important to consider that the target 100 particles/minute rate is the minimum rate that must be achieved at the lowest pressure (for example, an initial pressure of 200 Pa is not appropriate, as the system will automatically attempt to apply a second pressure of 0 Pa; therefore, an initial pressure around 400-600 Pa is usually appropriate). The fact that the second pressure applied by the system is 200 Pa less than the initial pressure must also be kept in mind when selecting the starting pressure, as a particle rate plot that is higher than 100 particles/minute must be achieved at all pressures. The particle rate of subsequent measurements will then be between 100 particles/minute and 1500 particles/minute at all three pressures.

The system then applies the same settings to both the calibration sample and the target sample, and a particle rate plot is generated for each (Figure 3.6). This must depict an increase in the particle rate as the pressure increases (Figure 3.6A). If this is not achieved this is reflected as an intersection between the particle rate plots of at least 2 pressures, or a rate that does not increase with increasing pressure (Figure 3.6B). The calibration and measurement must then be repeated at a different starting pressure.

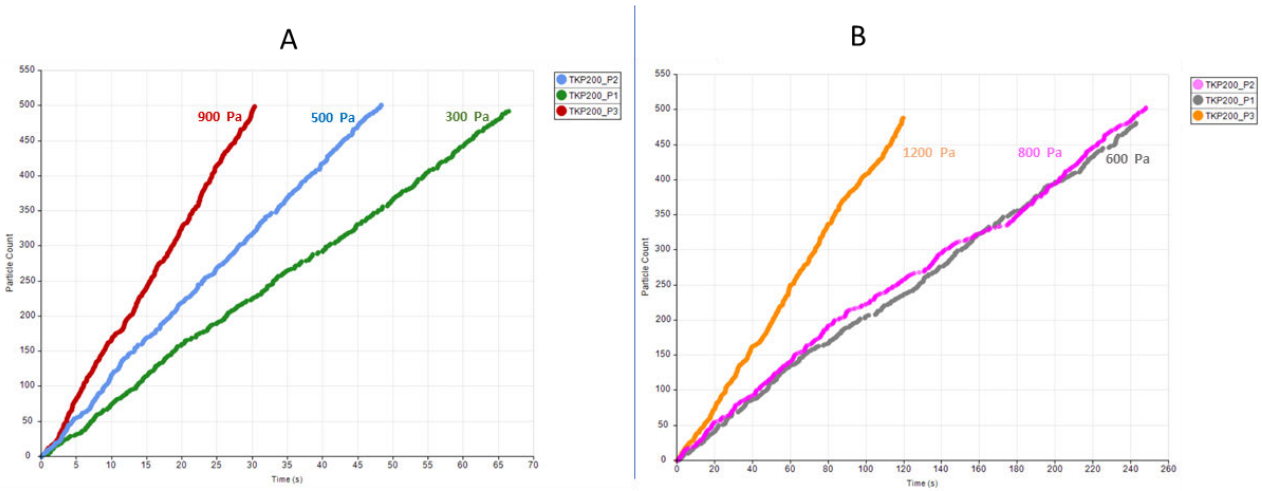

Figure 3.6: Particle rate plots generated using CPC200 calibration particles run at 3 different pressures. A) Depictions of 3 distinct plots with different gradients after analysis was carried out at either pressure 1 (P1), pressure 2 (P2) or pressure 3 (P3). B) Depictions of 3 plots with intersection in of the plots corresponding to the analysis was carried out at P1 and P2

Given the importance of particle rate plots for the system's ability to accurately analyse samples, we determined the effect of intersecting rate plots on the system accuracy. Moreover, during data analysis, the IZON software presents two calibration methods namely ''single pressure calibration'' and ''multipressure calibration''. For this assessment, two types of polystrene nanoparticles with known size and concentration were used. These were the Izon ''Solution S'', and again the CPC200 with respective sizes of 340 and 210 nm as well as concentrations of 1.1 x 10^{11} particles/ml and 8.3 x 10^{13} particles/ml.

3.1.2.1. Size

The Exoid was able to accurately determine the size of particles, within a 1% error, regardless of whether a single pressure or a multipressure calibration method was used (Figure 3.7A). Interestingly, the size could also accurately be determined irrespective of whether the particle rate plots had intersected or not. However, the percentage error increased to 53% under conditions where the particle rate threshold (100 particles/minute) was not achieved during sample analysis, leading to size

underestimation (Figure 3.7A). This emphasises the importance of achieving an appropriate particle rate, in turn achieved through correct dilution practises.

3.1.2.2. Concentration

Large discrepancies were observed in the Exoid's ability to accurately measure the particle concentration under conditions where the rate plots intersected, or the rates achieved were not at threshold (Figure 3.7B). When the particle rate plots are normal (no intersection and appropriate rates achieved) the Exoid could determine the particle concentration within a 15% error. This was true regardless of whether the single pressure or the multipressure calibration method was used (Figure 3.7B). However, intersecting particle rate plots significantly decreased the ability of the Exoid to accurately determine particle concentration. The data suggests that, under these conditions, the system underestimates the particle concentration even when the rate is within the normal range (100-1500 particles/minute) and overestimates it if the analysis is carried out below this range.

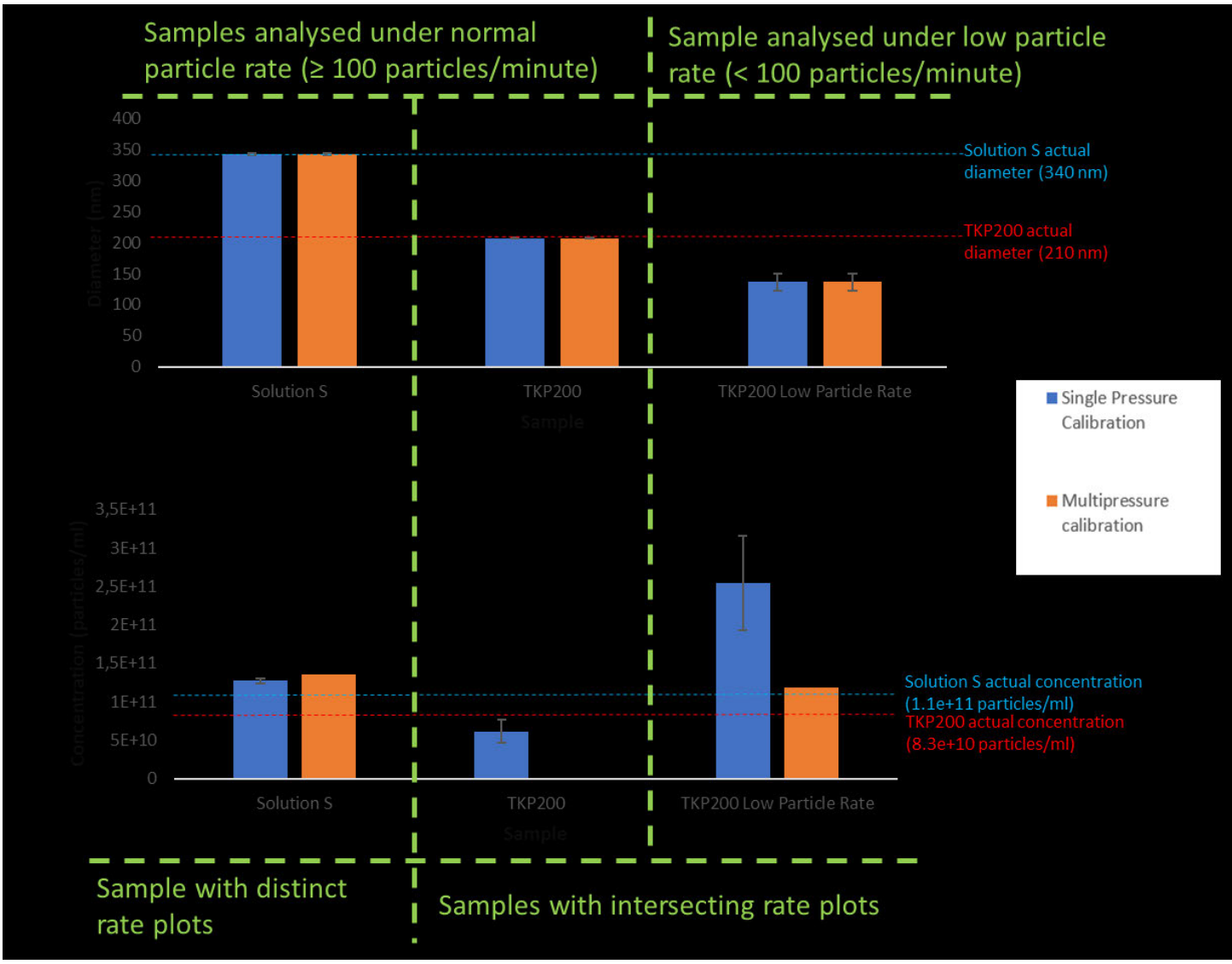

Figure 3.7: Accuracy of the Exoid TRPS equipment. The diameter (A) and concentration (B) of polystyrene nanoparticles (Solution S or CPC200) were estimated under normal particle rates or low rates (< 100 particles/minute). Data analysis was carried out using the single pressure calibration option or multipressure option in the Exoid Izon data suite software. The particle rate plots of each sample were assessed and determined to be distinct or intertwined. All values represent the average of 3 measurements carried out under 3 different pressures.

Moreover, at times the system could not determine the particle concentration using the multipressure calibration option when the particle rate plots had intersecting lines and it gives results as ‘’N/A”. It was noted that the particle rate and the accuracy of the Exoid had a linear relationship. Because when using the single pressure calibration option, three concentrations (for the analysis carried out at the three different pressures) will be generated by the system, it is best only to consider the average of the data generated at

the two highest pressures if a sufficient particle rate could not be achieved the lowest pressure. From these findings, a summary of the workflow to follow to accurately determine the particle size and concentration using the Exoid TRPS approach was established (Figure 3.8).

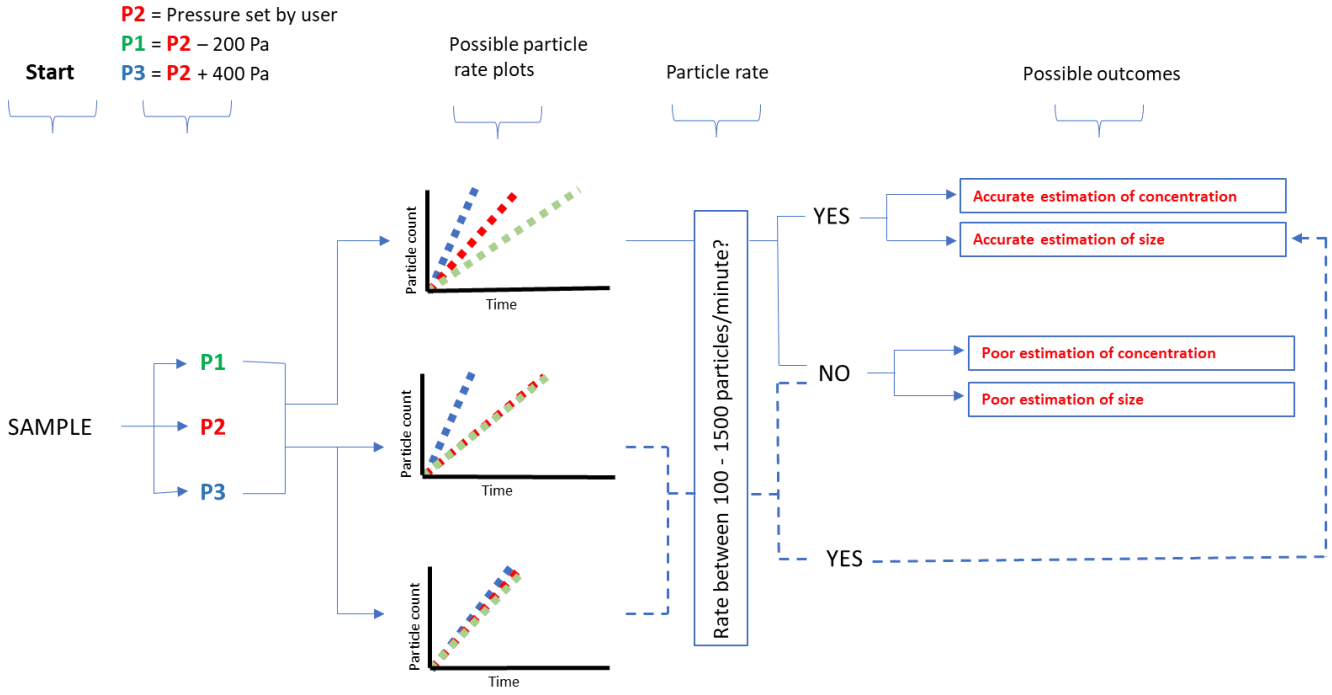

Figure 3.8: Workflow to achieving accurate estimation of particle size and diameter using the Exoid TRPS equipment. The sample is analysed at three pressures and the resulting particle rate plots can have three distinct lines or, two or three of the lines with similar gradients. If the particle rate plot is at least 100 particle/minute, then the sample with distinct lines can be accurately quantified for particle size and concentration. If the rate is less than 100 particles/minute, then there is poor estimation of the particle size and concentration. When the particle rate plot has lines with similar gradients, if the particle rate plot was at least 100 particles/minute, then only the particle size can be measured accurately. However, if the rate was less than 100 particles/minute then neither the size nor the concentration can accurately be measured.

In summary, prior to sample analysis, the user must adjust the nanopore membrane stretch, voltage as well as the pressure to strike a balance such that the current, RMS noise, blockade magnitude, as the particle rate are within their optimum range for accurate particle analysis. The first pressure value is set by the user to achieve an optimum particle rate. The system then sets the next 2 pressure values which are 200 Pa less and subsequently 400 Pa more than the initial pressure; a particle rate plot is then generated. The plot depicts 3 lines which correspond to the 3 different pressures and the rate is directly proportional to the increase in pressure. Should the plots show 3 distinct lines that do not intersect (meaning an increase in pressure resulted in an increase in the particle rate), then the system is able to accurately estimate both the particle size and concentration. However, this is only true if the particles were passing through the nanopore at a rate of at least 100 particles/minute. If the rate is lower than this then the system cannot accurately estimate the size and concentration, irrespective of whether the particle rate plots had distinct lines. Lastly, if the particle rate plot had intersecting lines (meaning an increase in pressure did not increase the particle rate) but the particle rate was at least 100 particles/minute, the system is still able to accurately estimate only the particle diameter and not the concentration.

3.2. Optimisation of the analysis of biological extracellular vesicles using TRPS

Once optimised for particle analysis using commercial polystyrene particles (CPC200), the Exoid was then utilised for the analysis of biological samples. CPC200 are very similar to extracellular vesicles like exosomes in terms of size and charge, however, it was reasonable to suspect that biological samples would perform differently during analysis because biological samples are more heterogenous in nature. Extracellular vesicles (EVs) isolated from a range of UCBS-containing Optiserum represent such biological samples and were subsequently analysed using the Exoid. Batch details are provided in Table 3.1.

Table 3. 1: Age and pregnancy duration of umbilical cord blood donors from which Optiserum batches was produced. Batch numbers refer to the Optiserum batch that was utilised to isolate the EVs.

Sample	Batch Number	Donor age	Week of Pregnancy
1	504	32	36
2	621	30	38
3	797	29	39
5	798	27	39
6	804	27	38
8	807	32	38
9	813	29	37
10	822	35	38
12	828	27	39
13	830	32	38
14	843	30	38
15	872	38	39
16	914	43	38
17	927	38	37
18	929	33	38
19	931	40	39
20	1030	40	37
21	1052	41	38
22	1059	42	38

Briefly, Optiserum (1 ml) was processed following the method described earlier (Chapter 2, Section 2) whereby a final concentration of 5% (v/v) PEG6000 was used to precipitate the exosomes. After the exosomes were pelleted, using the final centrifugation step, the exosome-containing pellet was then resuspended in SFM (1 ml) and stored at -20°C in 100 µl aliquots until needed. Sample 3 (Table 3.1) containing the PEG6000-isolated exosomes from Optiserum batch 797 was used to optimise the Exoid protocol for biological sample analysis.

During EV analysis, frequent nanopore clogging poses a challenge; although nanopore coating can be applied to pre-emptively reduce clogging, we have not found this to be consistently effective. Thus, we chose to filter samples through a 0.22 μm filter before analysis to further address this issue. The data suggested that filtration effectively removed larger particles greater than 300 nm in diameter, as seen by a decrease in maximum diameter (from 776 nm to 291 nm) (Figure 3.9A, B). There was also a decrease in average diameter (from 168 nm to 150 nm), a decrease in mode diameter (134 nm to 116 nm), and a decrease in the d90 value (from 243 nm to 215 nm). Moreover, there was a decrease in the d90/d10 ratio (from 2.2 to 1.89), indicating an increase in sample particle homogeneity following filtration. Interestingly, filtration caused only a slight reduction in vesicle concentration (from 2.62×10^9 particles/ml to 2.23×10^9 particles/ml), confirming that most particles in the sample were not larger than 200 nm in diameter.

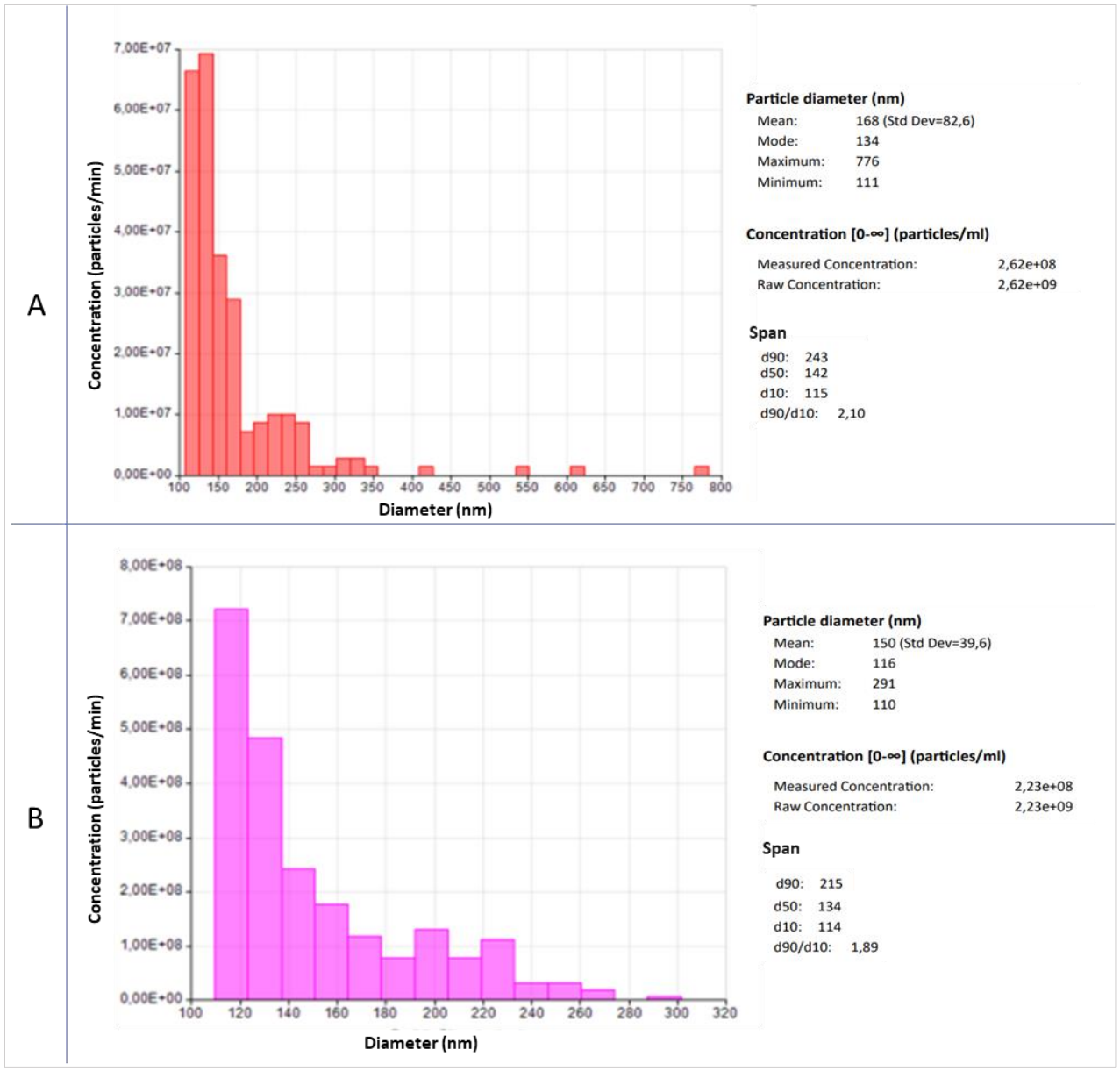

Figure 3.9: Effect of filtration on sample vesicle profile. Exosome-containing samples were analysed using the Exoid TRPS equipment. A) Sample isolated from sample 1 (batch 797) was diluted 10-fold and analysed using the Exoid. B) The same sample was diluted 10-fold but filtered through a 0.2 µm filter before being analysed using the Exoid. Analysis was carried out on the same nanopore membrane.

3.3. Characterisation of UCBS extracellular vesicles

3.3.1. TRPS

We sought to characterise EVs isolated from multiple Optiserum batches (specifically from batch 504, 797, 813, 822, 798, 804, 828, 621, 807 (Table 3.1)), where a sufficient volume of Optiserum was available for EV isolation.

The EV concentration was highly variable (Figure 3.10A). The concentration ranged from 0.3 x 10^9 particles/ml (in Optiserum batch 504) to 10 x 10^9 particles/ml (in Optiserum batch 807). Surprisingly, most of the UCBS-isolated vesicles had a d90 value that was within the generally accepted exosome size range of 30 nm – 150 nm (Figure 3.10B). Only vesicles isolated from batch 797 and 621 were slightly above this range. This was to be expected as samples had been filtered prior to analysis; batch 797 had the highest d90 of 220 nm. All data relating to particle sizes, concentration and population characteristics are provided in Appendix 2.

The EV protein concentration was found to range between 0.48 µg/µl and 1.16 µg/µl. Subsequent analysis to determine whether a correlation exists between total protein concentration and EV number revealed no correlation; for instance, batch 797 and 807 have the same protein concentration, while their EV concentration is 2.2 x 10^9 and 10 x 10^9, respectively (Figure 3.10C). A poor regression correlation of 0.0438 was observed (Figure 3.10D).

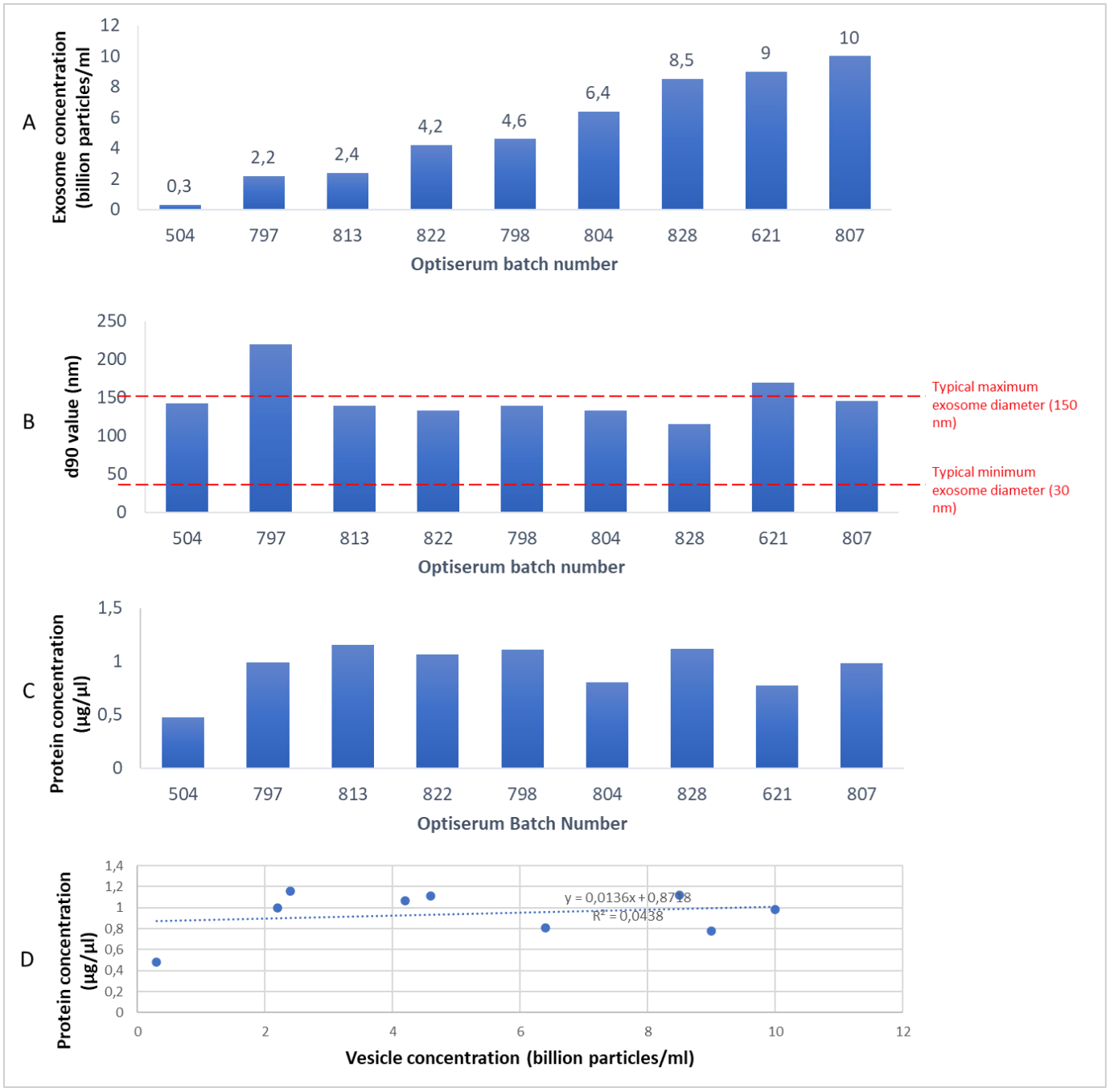

Figure 3.10: EV-containing samples analysed using the Exoid. A) The number of EVs isolated from different Optiserum batches. The vesicle concentration was estimated at 2-3 different pressures. B) The d90 values of the vesicles present in the EV-containing samples. C) Protein concentration of the isolated EVs. D) Correlation between EV numbers and their total protein concentration. TRPS Data analysis was carried out using single pressure calibration.

3.3.2. Transmission electron microscopy

To visualise the isolated EVs and determine whether their morphology is indicative of an exosome (bi-concave/cup-shaped/doughnut-shaped), TEM was utilised. Vesicle-containing samples were either diluted 1/100 in PBS or left undiluted before being mounted as a single drop onto either formvar-coated copper TEM grids (generally used as a golden standard in TEM) or carbon-coated copper grids. This was followed by negative staining using 2% uranyl acetate. Because negative controls (when using TEM) are generally not included in literature, we thought it would be interesting to include them in this study. Two negative controls were chosen; a plain unstained grid, as well as a grid prepared with SFM that had been subjected to the PEG6000 vesicle isolation protocol (Chapter 2, Section 2). The latter was included to determine whether PEG6000 itself, which could contaminate the final EV sample, would create significant background on the TEM images.

On the standard formvar-coated TEM grids, multiple irregularly circular vesicles with diameters ranging from 50 nm to 100 nm were observed (Figure 3.11A). These were within the exosome size range; however, they were too concentrated. Thus, the same sample was diluted 1:100 in an attempt to visualise singular vesicles. Structures with a uniform circular circumference were observed in the diluted sample (Figure 3.11B).

On the formvar and carbon-coated TEM grids, multiple irregularly circular structures with diameters ranging from 50 nm to 100 nm were also observed (Figure 3.11C). However, amongst these were cup-shaped circular structures corresponding to the accepted morphology of exosomes [55, 56]. Again, the sample was diluted 1:100 for better visualisation of single structures and this time the structures identical to exosomes were identified (Figure 3.11D).

Surprisingly, circular structures were also observed in the negative controls (Figure 3.11E, F). These were within the diameter range of 25 nm to 350 nm and had a more defined circumference on the plain grid, suggesting that PEG6000 causes background during TEM.

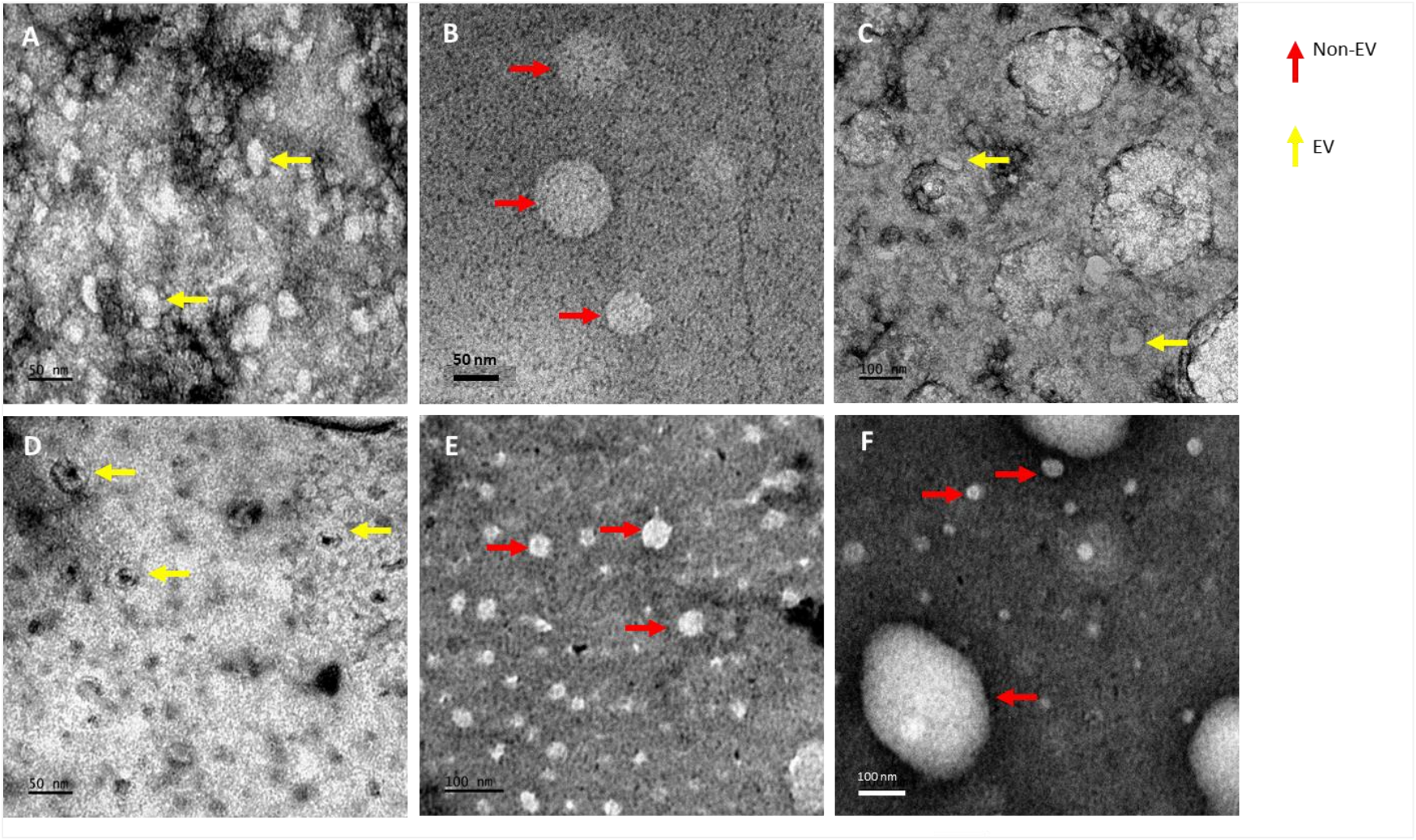

Figure 3.11: Transmission electron micrographs of various samples mounted on different TEM grids. A) Vesicles isolated using PEG6000 from Optiserum and mounted on formvar-coated copper grids B) Vesicles isolated using PEG6000 from Optiserum and diluted 1:100 in PBS before mounting on formvar-coated copper grids C) Vesicles isolated using PEG6000 from Optiserum mounted on formvar and carbon-coated copper grids. D) Vesicles isolated using PEG6000 from Optiserum and diluted 1/100 before being mounted on formvar and carbon-coated grids E) grids Serum-free medium (SFM) that has been subjected to the PEG6000 vesicle isolation protocol and diluted 1/100 before being mounted on formvar-coated copper grids F) Plain non-coated grids. Extracellular vesicles (EVs) and non – extracellular vesicles (non-EVs) were identified.

3.3.3. Internalisation by HEK293 cells

To test EV uptake by cells, HEK293 cells were incubated with PKH26-stained EVs (which will emit a red fluorescence due to the PKH26 dye) followed by immunocytochemistry as described in Chapter 2, Section 6. Briefly, following incubation with EVs, cells were washed to remove excess vesicles that had not been taken up by the target cells and were then incubated with a mouse monoclonal anti-CD81 antibody, followed by the Dylight 488-conjugated secondary antibody (green fluorescence). Lastly, the cell nuclei were stained with the Hoechst nuclear stain (blue fluorescence). EVs (red) that were found to be positive for CD81 (green) could then be confirmed as exosomes. Negative controls included cells that were incubated for 2 hours in SFM (which had been incubated with PKH26, but in the absence of EVs).

A primary antibody control was also included, where, during immunocytochemistry, cells were incubated with PBS lacking the primary anti-CD81 antibody (Figure 3.12). Green fluorescence was not observed in cells incubated in the absence of the mouse monoclocal anti-CD81 primary antibody, therefore the secondary antibody did not result in non-specific staining (Figure 3.12A); nuclei were detected (Hoechst; Figure 3.12B).

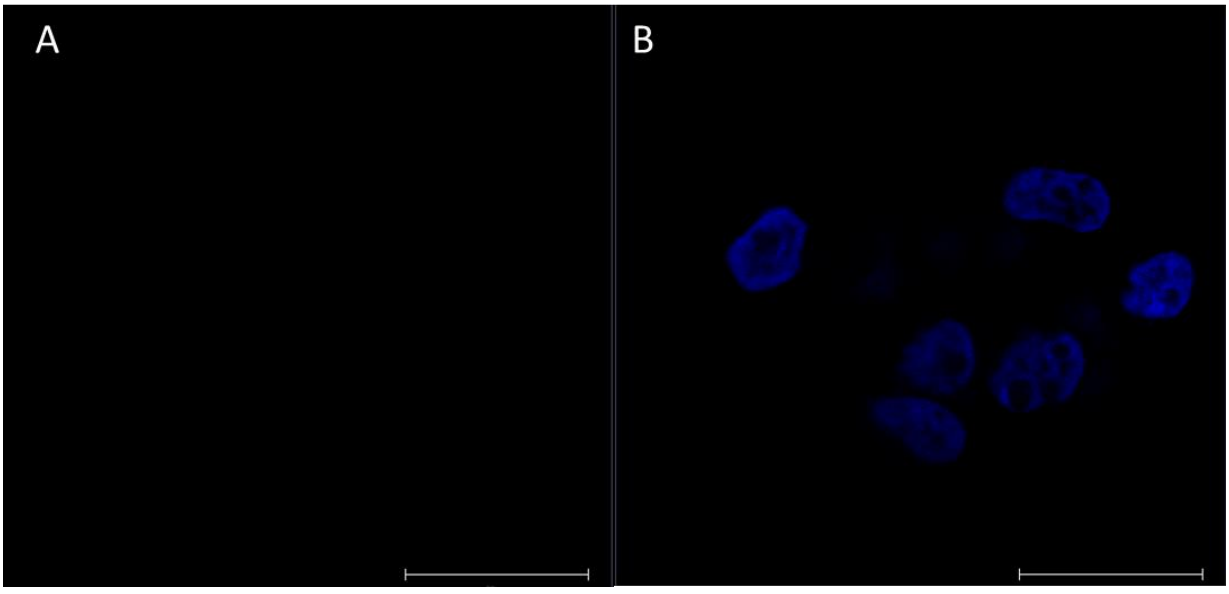

Figure 3.12: HEK293 cells negative CD81 control. Cells were incubated in the absence of the primary mouse anti-CD81 antibody (rather incubated with PBS) before being incubated with the donkey anti-mouse-Dylight 488 antibody. A) No green fluorescence was observed in cells where the nuclei were stained using the blue-fluorescing Hoechst stain (B). Scale bar = 20 µm.

CD81, a transmembrane protein known to be enriched in exosomes and also expressed in HEK293 cells, was detected on the membrane of HEK293 cells in the absence of EVs, confirming the presence of endogenous CD81 on HEK293 cells (Figure 3.13A, B, D) [188]. As expected, red fluorescence was not detected in these cells (Figure 3.13C).

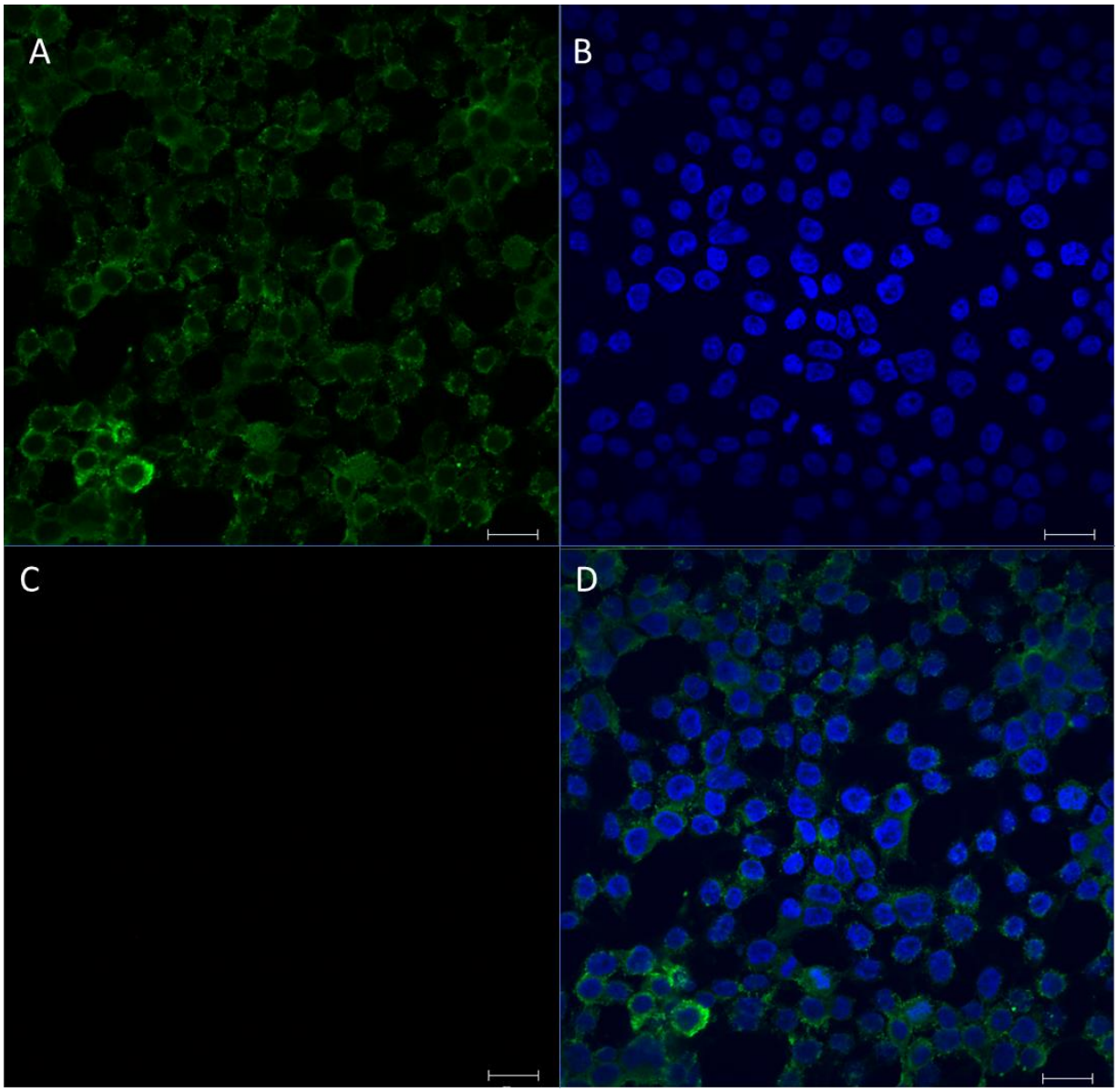

Figure 3.13: HEK393 cells incubated in SFM displaying endogenous CD81. HEK293 cells were incubated for 2 hours in SFM prior to immunocytochemistry with mouse anti-CD81 antibody to demonstrated presence of (A) CD81 (green) and (B) nuclei (blue), but absence of (C) exosomes (red). D) Panels A, B and C were merged. Scale bar 20 µm.

When cells were incubated in the presence of PKH26-stained exosomes, the endogenous CD81 as well the nuclei could still be detected via green and blue fluorescence, respectively (Figure 3.14A, B).

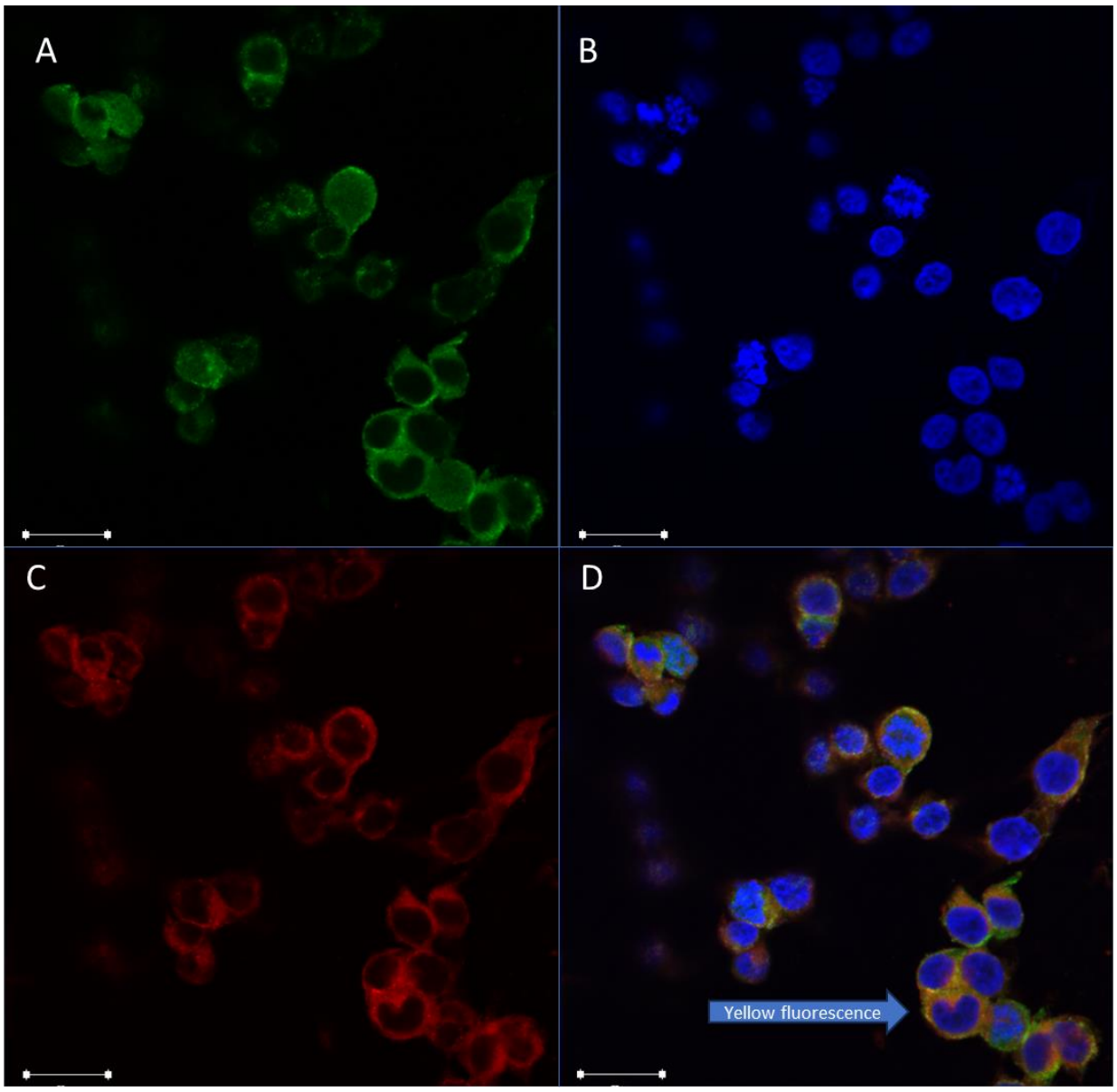

Figure 3.14: Uptake of PKH26-stained exosomes by HEK293 cells. A) Green fluorescence corresponding to the exosome marker CD81. B) Blue fluorescence corresponding with the Hoechst nuclear dye. C) Red fluorescence representing PKH26-positive exosomes D) Overlay of image A, B and C depicting yellow fluorescence indicating colocalisation of green and red fluorescence to shown CD81 positive PKH26-stained exosomes. Scalebar = 20 µm.

In addition, red fluorescence, indicative of the EVs was also detected within the cells (Figure 3.14C). When the images were overlayed, there were regions within the cells

where there was colocalisation of the green and red fluorescence, resulting in the formation of yellow fluorescence (Figure 3.14D). This suggests that the CD81+ EVs have been internalised by HEK293 cells. Furthermore, areas of green fluorescence were also evident; this was also to be expected as HEK293 cells to express CD81 (as confirmed in Figure 3.13). Taken together, the data suggests that the EVs we isolated are in fact exosomes due to their size (as measured by TRPS), morphology (as determined by TEM), uptake and expression of CD81 (as determined by ICC).

3.3.4. Effect on cell proliferation

After confirming the exosome nature of the EVs and their internalisation by HEK293 cells, we sought to examine the effect of UCB serum-derived exosomes on HEK293 cell proliferation. To achieve this, cells were cultured in the presence of increasing numbers of exosomes (isolated from Optiserum batches 798, 813, 807 and 822), ranging from 1 x 10^3 to 1 x 10^8. HEK293 cells were also cultured in the presence (SCM) and absence (SFM) of serum to mimic positive and negative controls respectively.

When the cells were cultured in the presence of 1 x 10^8 exosomes, a significant increase in proliferation was observed, which surpassed the proliferation of cells cultured in SCM (Figure 3.15A). The effect on cell proliferation in response to exosome number less than 1 x 10^8 was variable. For example, the effect of 1 x 10^7 exosomes isolated from Optiserum batch 822 had an effect 1.4-fold less than that of cells cultured in SCM whereas all the other batches were more potent (1.6 - 1.9-fold more). Only when exosomes at a concentration of 1 x 10^4 or less were used, was there no increase in proliferation when compared with SFM. Taken together, 1 x 10^8 exosomes had the highest effect on cell proliferation with a mean relative percentage of 194% (Figure 3.15B). This was significantly higher than both SFM ($p<0.001$) and SCM ($p<0.005$) respectively (Figure 3.15B). Addition of 1 x 10^7 exosomes achieved a mean relative percentage of 145%; this effect was significantly higher than SFM ($p<0.05$), but not significantly higher than SCM. All other exosome concentrations below this number had no statistically significant effect on cell proliferation.

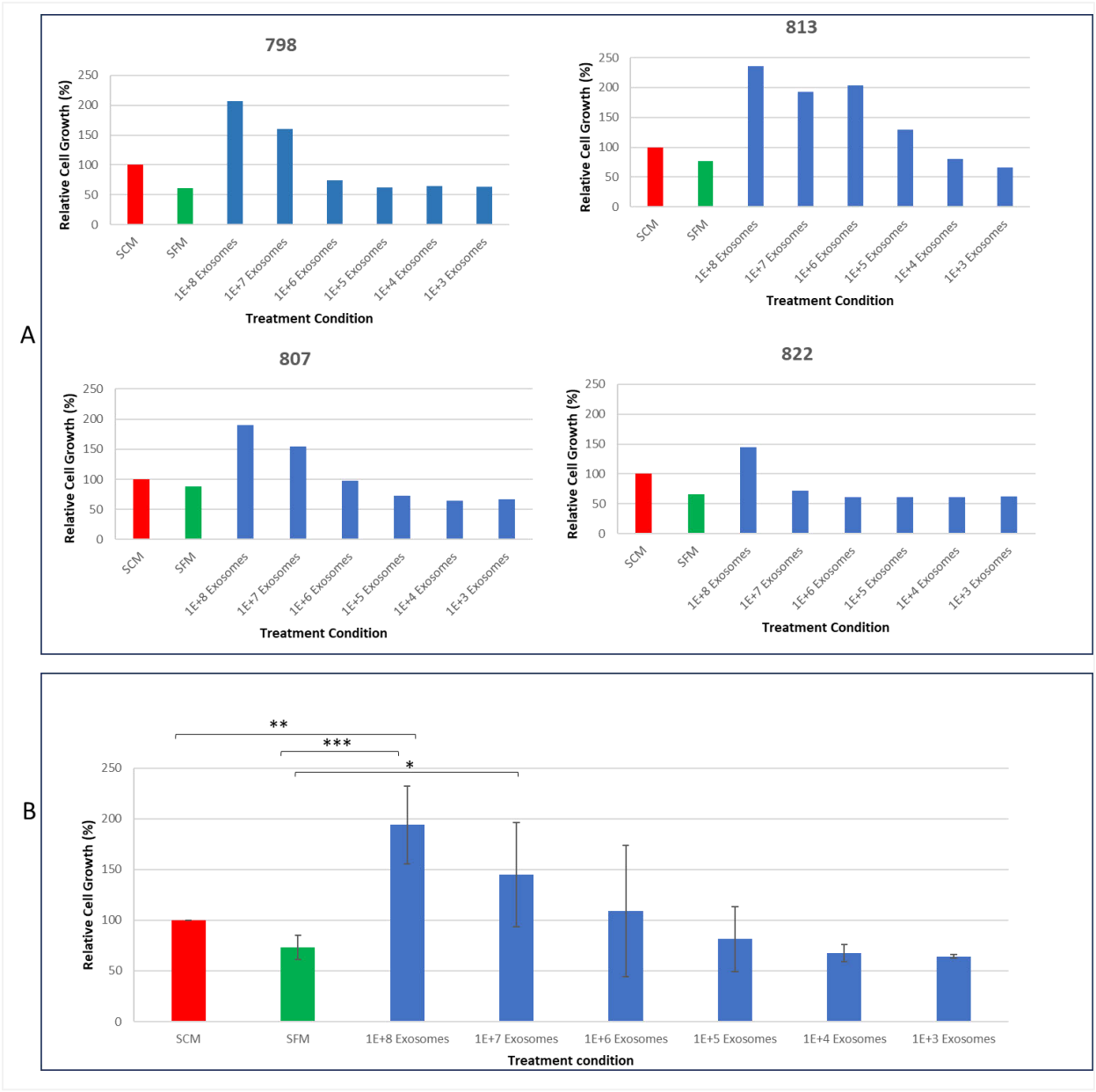

Figure 3. 15: Effect of UCBS-isolated exosomes on HEK293 cell proliferation. Cells were cultured in serum-free medium (SFM) containing increasing numbers of exosomes isolated from different batches (798, 813, 807 or 822), plain SFM, or they were cultured in serum-containing medium (SCM) with 2 to 4 replicates for each batch. The cells were subjected to these treatment conditions for a 24-hour period before the average cell numbers were measured using the MTS assay. The values were displayed as a percentage relative to growth achieved by cells cultured in SCM. A) Effect of exosomes isolated from individual batches on cell proliferation. B) Average effect of exosomes isolated from batches 798, 813, 807 or 822 on HEK293 cell proliferation (n = 4; * = p<0.05; ** = p<0.005; *** = p<0.001)

Surprisingly, when HEK293 cells were cultured in the presence of Optiserum itself (300 µg – 0.3 ug), no significant positive effect on cell proliferation was observed when compared with SFM (Figure 3.16). This suggested that, possibly, the content of the exosomes (when concentrated) could be mediating the positive effect on HEK293 proliferation when compared with the Optiserum (which is a five-fold dilution of umbilical cord blood serum and contains includes the secretome both within and outside the exosome component in the serum).

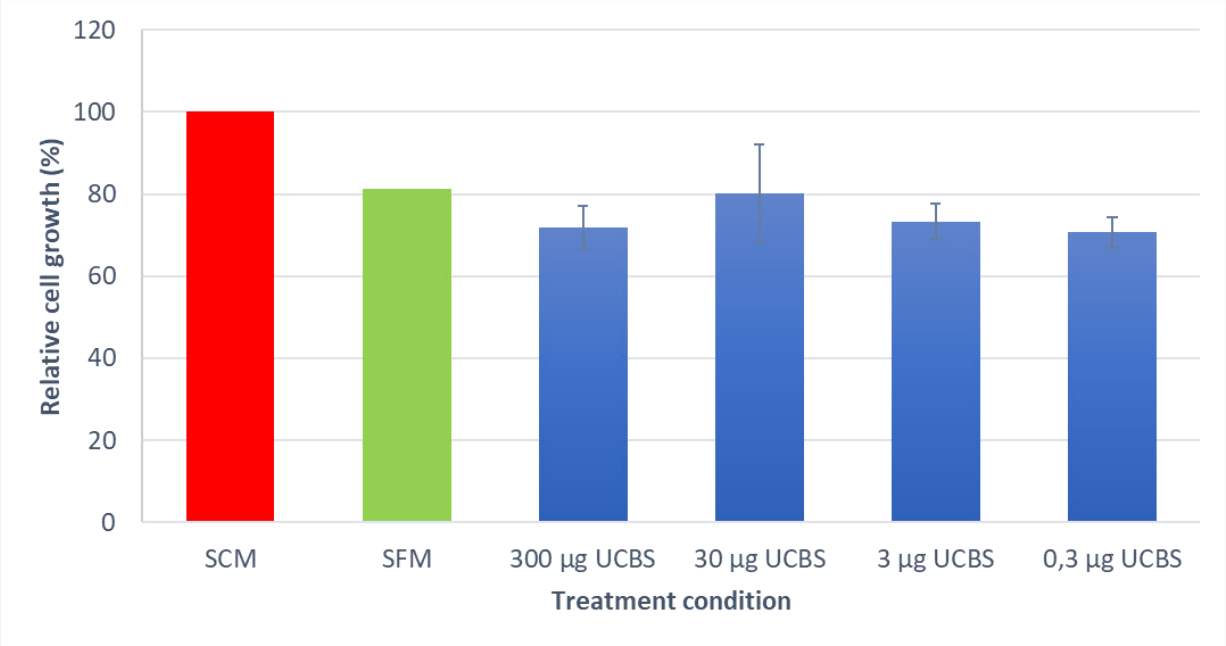

Figure 3.16: Effect of UCBS on cell proliferation. Cells were cultured in either serum-containing medium (SCM), serum-free medium (SFM) or SFM containing varying concentrations of umbilical cord blood serum (UCBS) from four different Optiserum batches. Effects on cell growth were again related to growth observed in SCM.

This suggests that the exosome content/cargo (including nucleic acids, lipids, proteins) should be analysed in more detail. Hence, we began the cargo analysis by focusing on the protein content of exosomes isolated from Optiserum batches.

3.3.5. Protein Content Analysis

Epidermal growth factor (EGF) is a protein known to be found at significant concentrations in UCBS [178]. We therefore sought to first determine whether EGF is enriched in the exosome component. Optiserum and matched samples of isolated exosomes were therefore analysed using an EGF ELISA (Quantikine, R&D Systems; Chapter 2, Section 7.2.1). Briefly, Optiserum samples from different batches (621, 828, 797 and 804) and exosome samples isolated from the same batches were diluted 1:1 with the RD69 diluent before 200 µl of each sample was loaded in duplicate on the 96-well ELISA plate for analysis.

Optiserum was observed to have significantly higher levels of EGF compared to exosomes ($p<0.05$; Figure 3.17A, B). The contents of EGF in exosomes compared to the original Optiserum from which they were isolated ranged from 4 pg/ml to 72 pg/ml and 236 pg/ml to 323 pg/ml, respectively (Figure 3.17A). The mean EGF concentration in exosomes compared to the original Optiserum they were isolated from was significantly lower at 39 pg/ml ± 29 compared with 279 pg/ml ± 36 respectively (Figure 3.17B). It was concluded that exosomes isolated from umbilical cord blood serum are not enriched for EGF.

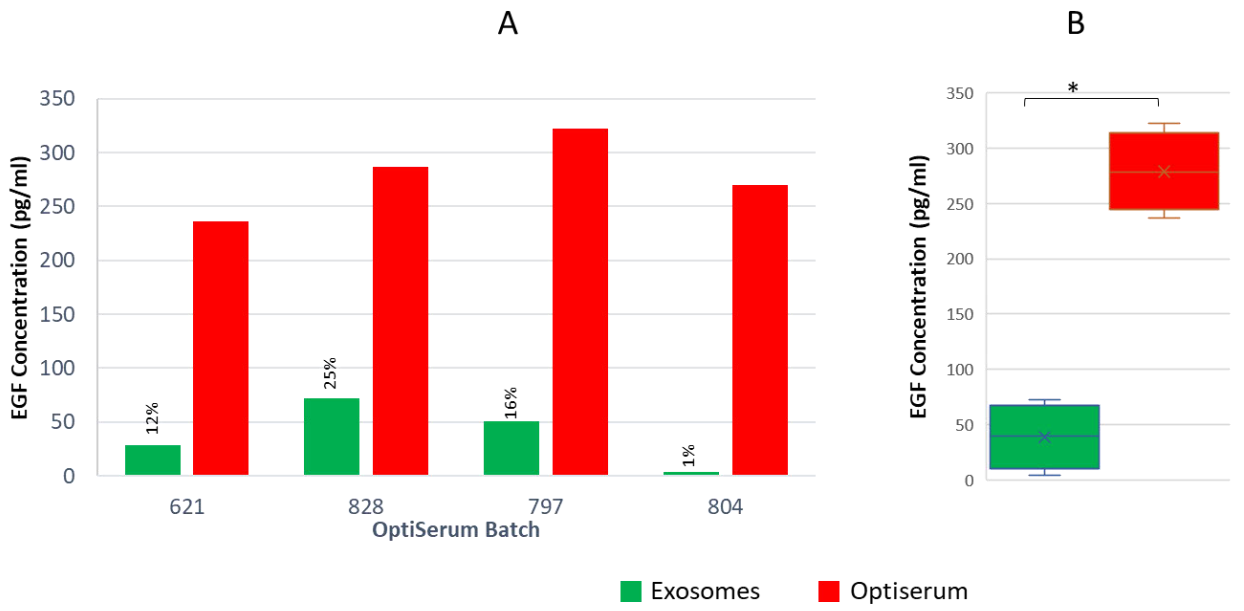

Figure 3.17: Levels of EGF in exosomes compared to the original Optiserum from which they were isolated. A) The EGF levels in the paired samples were measured using ELISA and the percentage values represent the percentage of EGF present in the exosomes compared to the original Optiserum from which it was isolated. B) Generalised comparison of EGF levels in exosomes and Optiserum by averaging the values from the different batches (621, 828, 797 & 804) (n = 4, * = $p < 0.05$)

To gain an understanding of the broader protein cargo of the isolated exosomes, the analysis was expanded to a total of 48 cytokines; the Bioplex 48-plex cytokine screening system described in Chapter 2 Section 2.7.2.2) was utilised to measure the protein content of paired exosomes and UCBS in Optiserum samples from 14 batches.

Following Bioplex analysis, it was found that the following 24 proteins are present at higher levels in Optiserum when compared with the paired isolated exosomes: CTACK, Eotaxin, IL-9, MIP-1b, SCF, MIF, PDGF-bb, RANTES, SCGF-b, TRAIL, IL1-Ra, HGF, TNF-b, SDF-1b, TNF-b, MIG, M-CSF, MCP-1, IP-10, IL-18, IL16, IL-2Ra, G-CSF, and basic FGF (Figure 3.18). Interestingly, there were two proteins that were found to be enriched in exosomes. These were b-NGF and IL-15 (Figure 3.19). Specifically, average b-NGF levels were 48 pg/ml ± 30 in exosomes, but 5 pg/ml ± 7 in Optiserum, while the average IL-15 levels were 1035 pg/ml ± 1060 in exosomes and 526 pg/ml ± 284 in Optiserum (Figure 3.19). Moreover, two other cytokines were present at comparable levels in all 14 tested samples, specifically GRO-a, and TNF-α (Figure 3.20).

Respectively, the average concentration of these two proteins were 1605 pg/ml ± 1151 (in exosomes) compared to 2212 pg/ml ± 380 (in Optiserum), and 91 pg/ml ± 35 (in exosomes) compared to 85 pg/ml ± 32 (in Optiserum).

The remaining 20 tested proteins were not found at detectable levels in either the Optiserum or the isolated exosomes.

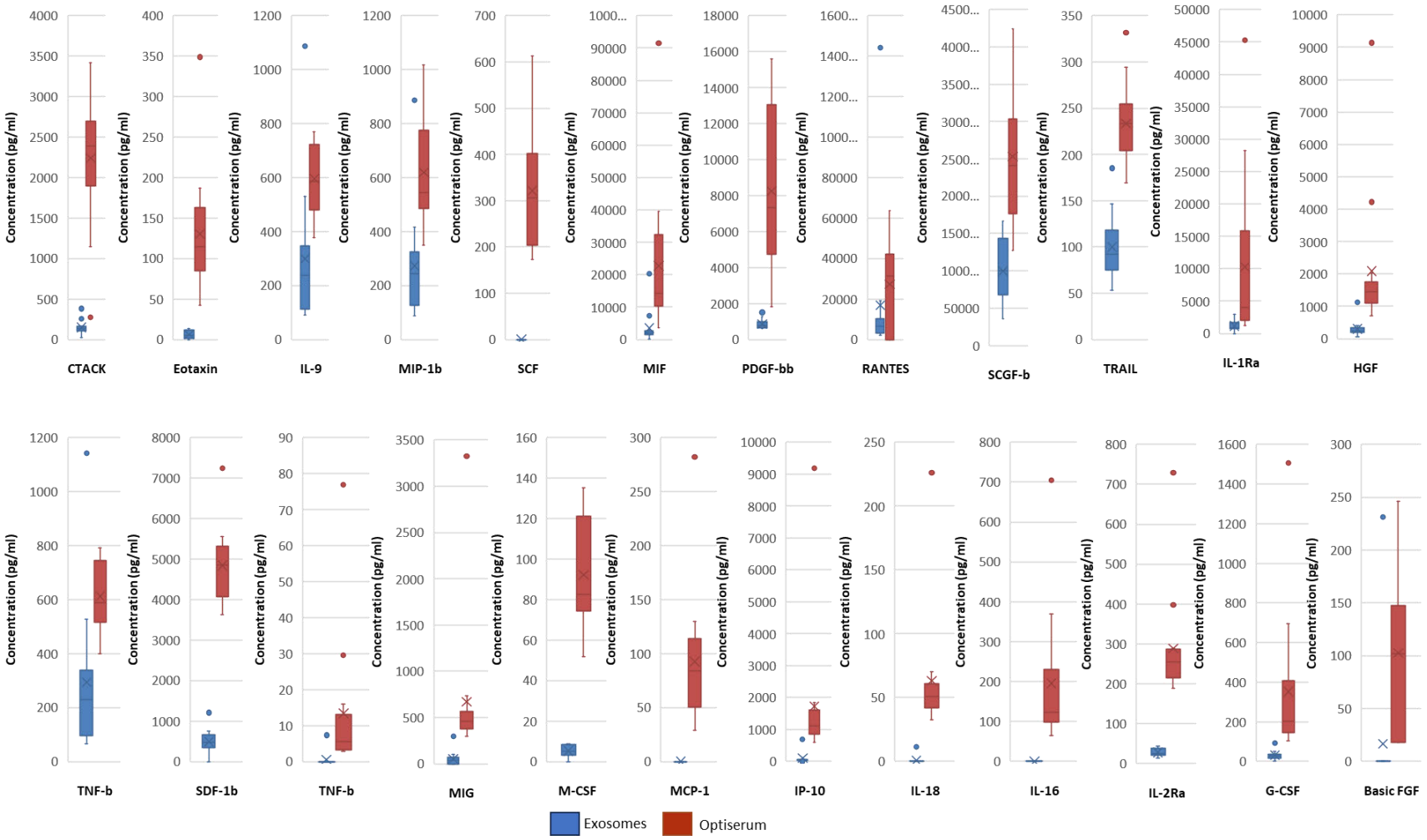

Figure 3.18: Cytokines found in higher levels in Optiserum compared to the exosomes. Cytokine levels were measured in paired exosome and Optiserum samples from 14 different batches (n = 14), using the 48-plex kit.

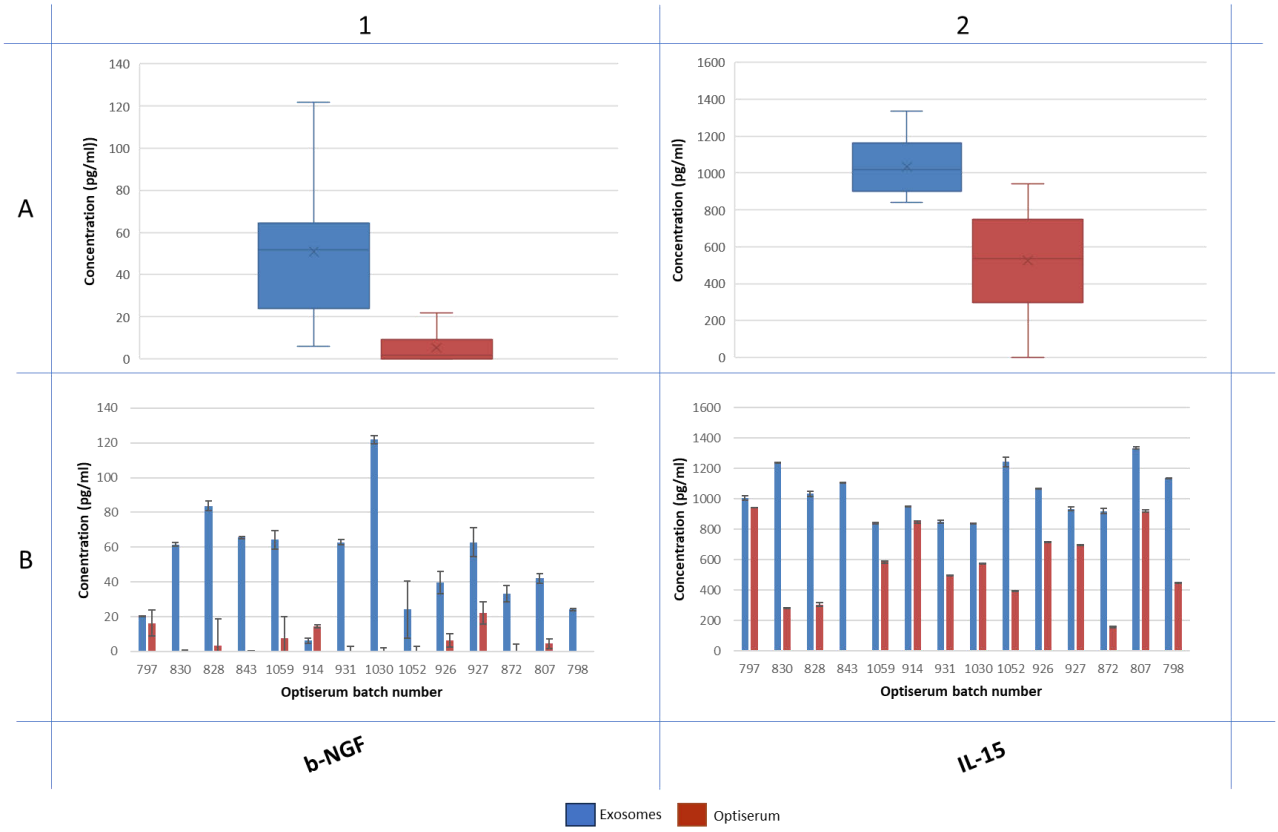

Figure 3.19: Cytokines enriched highly in exosomes compared to the original Optiserum from which they were isolated. Cytokines were measured using the 48-Plex kit (which detects 48 cytokines). A1 – A2) Cytokines present in noticeable levels out of the 48 cytokines measured in paired exosomes and Optiserum samples from 14 different batches (n = 14). B1 – B2) Analysis of cytokine content in individual batches. The error bars were generated using the standard deviation.

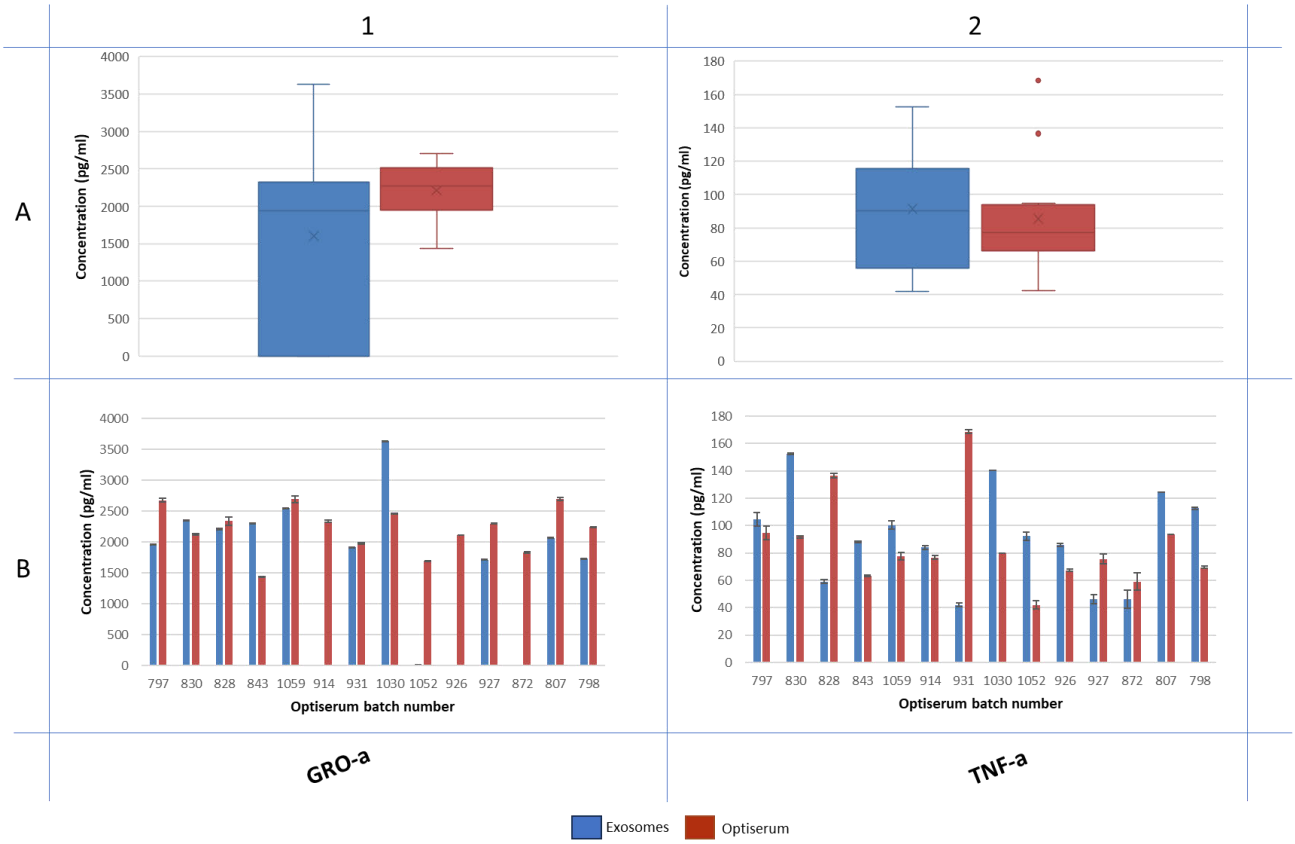

Figure 3.20: Cytokines present in comparable levels in exosomes compared to the original Optiserum from which they were isolated. Cytokines were measured using the 48-Plex kit (which detects 48 cytokines). A1 – A2) Cytokines present in noticeable levels out of the 48 cytokines measured in paired exosomes and Optiserum samples from 14 different batches (n = 14). B1 – B2) Analysis of cytokine content in individual batches. The error bars were generated using the standard deviation.

3.4. Summary

In the current study, extracellular vesicles were isolated from UCBS using PEG6000 precipitation. Samples were characterised using TRPS which analyses nanoparticles using a nanopore approach. Prior to this characterisation of the exosomes an SOP describing the optimal approach to using the Exoid (Izon Science, France) for TRPS was established. The current, RMS noise, blockade magnitude, as well as the particle rate were found to be crucial in the Exoid's ability to accurately analyse particles.

The number of extracellular vesicles isolated from Optiserum (1 ml) was highly variable and could not be correlated with total protein concentration. However, the isolated vesicles were found to be within the exosome size range and were subsequently confirmed to be exosomes following analysis of morphology using TEM and expression of CD81 by immunocytochemistry. These exosomes were internalised by HEK293 cells and were found to promote cell proliferation, as measured by the MTS assay, when used at a concentration of 1×10^8 exosomes.

Subsequent analysis of protein cargo indicated exosome enrichment of b-NGF and IL- 15, while both GRO-a and TNF-a were found to be present at comparable levels in the exosomes and the Optiserum from which they were isolated.

Chapter 4: Discussion

Various studies have supported the hypothesis that the therapeutic properties of UCBS may be attributed to exosomes found within this biological sample. However, little information is available regarding the isolation, cargo and cellular effect of exosomes from UCBS. Moreover, In the current study we aimed to isolate and characterise exosomes from umbilical cord blood serum (UCBS) and determine their effect on cellular proliferation *in vitro.* We successfully isolated EVs from Optiserum (a commercially available product containing UCBS) using PEG6000, characterised these vesicles as exosomes and subsequently analysed the protein cargo as well as determined the effect on cellular proliferation.

A major challenge, when utilising PEG as part of our isolation method, was found to be in the resuspension of the EV-containing pellet after isolation, which often required extended periods of vortex mixing. This could be related to the fact that the resuspension medium was, as is often recommended, cold [189]. Moreover, at times the pellets were invisible, making it impossible to assess whether they had fully resuspended in solution, until TRPS was carried out. This was more challenging due to a lack of descriptive pellet resuspension techniques in literature. Resuspension of the pellet in warm solution (37˚C) is an approach worth considering in future studies because temperature and protein solubility are directly proportional [190].

Characterisation of the PEG-isolated EVs using TRPS was extremely challenging. Despite significant time and effort assigned to study and master the technique, a major hurdle was the constant clogging of the nanopore. This may have been due to the nature of the isolation method; PEG6000 works via a water exclusion mechanism which causes the EVs to tightly compact and possibly clump [119]. One of the strategies used to combat the nanopore clogging was to filter the samples through a 0.22 µl syringe filter before Exoid analysis. Filtration was found to successfully remove large particles (300 – 776 nm) which we believed to be responsible for the clogging. It is unclear whether the large particles observed were aggregates of smaller vesicles or large vesicles such as MVs and apoptotic bodies.

Nonetheless, a fully optimised SOP was successfully established to utilise the Exoid, a TRPS instrument, for EV characterisation. EVs were found to have a mean diameter of 111 $\pm$ 12 nm, well within the exosome size range [5]. Their total concentration was found to range from 0.3 x 10^9 – 10 x 10^9 particles/ml [5]. Considering that the isolation was carried out using Optiserum (a 20% dilution of UCBS), the number of EVs that would be isolated directly from pure UCBS could be substantially higher. When the protein concentration of these vesicles was measured, it was found to have poor correlation with their particle concentration. This was surprising as many studies correlate exosome protein concentration with bioactivities such as cell proliferation [179, 191]. In our study we therefore rather chose to use UCBS EV number when carrying out *in vitro* proliferation assays.

The EVs were further characterised using TEM where cup–shaped structures, generally accepted as characteristic of exosomes, were observed [192]. The cup shape is caused by shrinkage due to air drying during sample mounting and the percentage of cup shaped vesicles in a TEM field of view is generally low (between 14 – 46 %) [193, 194]. This indicates that some exosomes are shielded from the shrinkage, possibly due to clumping. Moreover, the cup-shaped vesicles were more pronounced in samples mounted on carbon-coated grids compared to uncoated grids. This could be due to the fact that both these types of grids are coated with formvar, which is porous, but in addition to the formvar, the carbon-coated grids have an additional carbon membrane. The diameter of these holes ranges from 25 nm to 350 nm. Thus, it is possible that vesicles pass through them during sample mounting. This could be more prevalent in formvar-only grids as they do not have an additional layer like carbon-coated grids. Caution should be taken when interpreting TEM images because the holes in the grid can erroneously be identified as exosomes (not often reported in literature). This is especially true when using lower resolution TEM instruments.

EV uptake by cells and the exosome nature of these EVs was further confirmed using ICC. One of the most common methods of achieving this is to stain the exosome-containing sample using a membrane dye such as the PKH26 red fluorescent linker before incubating them with cells and observing red fluorescence inside the cells.

However, there is a crucial step that is included during the exosome staining, and it is often overlooked. Following staining, the sample is diluted in high protein solution such as BSA to quench the excess dye. This can result in the staining of non-exosomal particles; negative controls to account for this must be included in all studies [71, 72]. In our study, a mouse monoclonal anti-CD81 antibody was used to confirm that the red PKH26-positive vesicles inside the HEK293 cells were in fact exosomes.

Once the internalisation of exosomes by HEK293 cells was confirmed using ICC, their effect on cell proliferation was investigated. We report that exosomes isolated from UCBS have a significant effect on cell proliferation, and to the best of our knowledge, this is a novel finding. The highest number of exosomes tested (1×10^8) almost doubled the proliferation relative to that achieved with the positive control (SCM); there was however high variability between batches. However, it is worth noting that even though no positive effect on cell proliferation was observed when cells were cultured in Optiserum, the Optiserum batches used for these particular experiments were not the same as those from which the exosomes were isolated.

A main contaminant of exosomes, not investigated in this study, is lipoprotein. [195]. Lipoproteins are another type of biological nano-vesicles which are also responsible for transporting cargo to target cells and have been reported in UCBS [196, 197]. Fortunately, when Zhu et al. (2022) recently used high-performance liquid chromatography (HPLC) fractionation to analyse the protein enrichment profiles in UCBS exosomes and compared it to that of maternal serum exosomes they reported that proteins associated with adhesion and biological molecule binding were upregulated and lipoprotein-associated proteins were downregulated [178]. This suggests that lipoproteins are less abundant in UCBS compared to adult serum, however, the lipoprotein component of UCBS exosomes should be investigated in future studies.

Growth factor and cytokine analysis was carried out and revealed that, compared to the Optiserum from which they were isolated, exosomes are enriched in the cytokines b - NGF and lL- 15. These proteins have been reported to have a positive effect on wound healing. For example, b-NGF has been reported to have a therapeutic effect on corneal diseases such neurotrophic corneal ulcers by promoting limbal stem cell proliferation

[198]. This protein has also been reported to promote wound healing by inducing fibrogenesis in conjunctival fibroblast cells [199]. Similarly, intravenous treatment of aged mice with IL-15 was shown to accelerate wound closure [200]. Thus, the therapeutic effects of UCBS could be due to exosome-mediated b-NGF and IL-15 delivery to cells, suggesting that not only can these exosomes be used for direct therapeutic application, but they can potentially be used as drug delivery systems. Future work to test this hypothesis could include culturing cells in media containing these cytokines or exosomes loaded with these cytokines and comparing the growth rate with negative controls.

In conclusion, PEG6000 was effectively used to isolate and characterise exosomes from UCBS. These exosomes were subsequently analysed for the effect on cellular proliferation, where they were found to promote HEK293 cell growth. Protein content analysis revealed that some proteins, particularly b-NGF and IL-15, are enriched in the exosome fraction of UCBS, which may contribute to the positive effect on cellular proliferation. Further research is needed to determine the purity of these exosome samples as well as the mechanism of action related to their pro-proliferative effect. They may have therapeutic value in the context of situations where regeneration is required.

Appendix 1: Labelled Exoid device parts

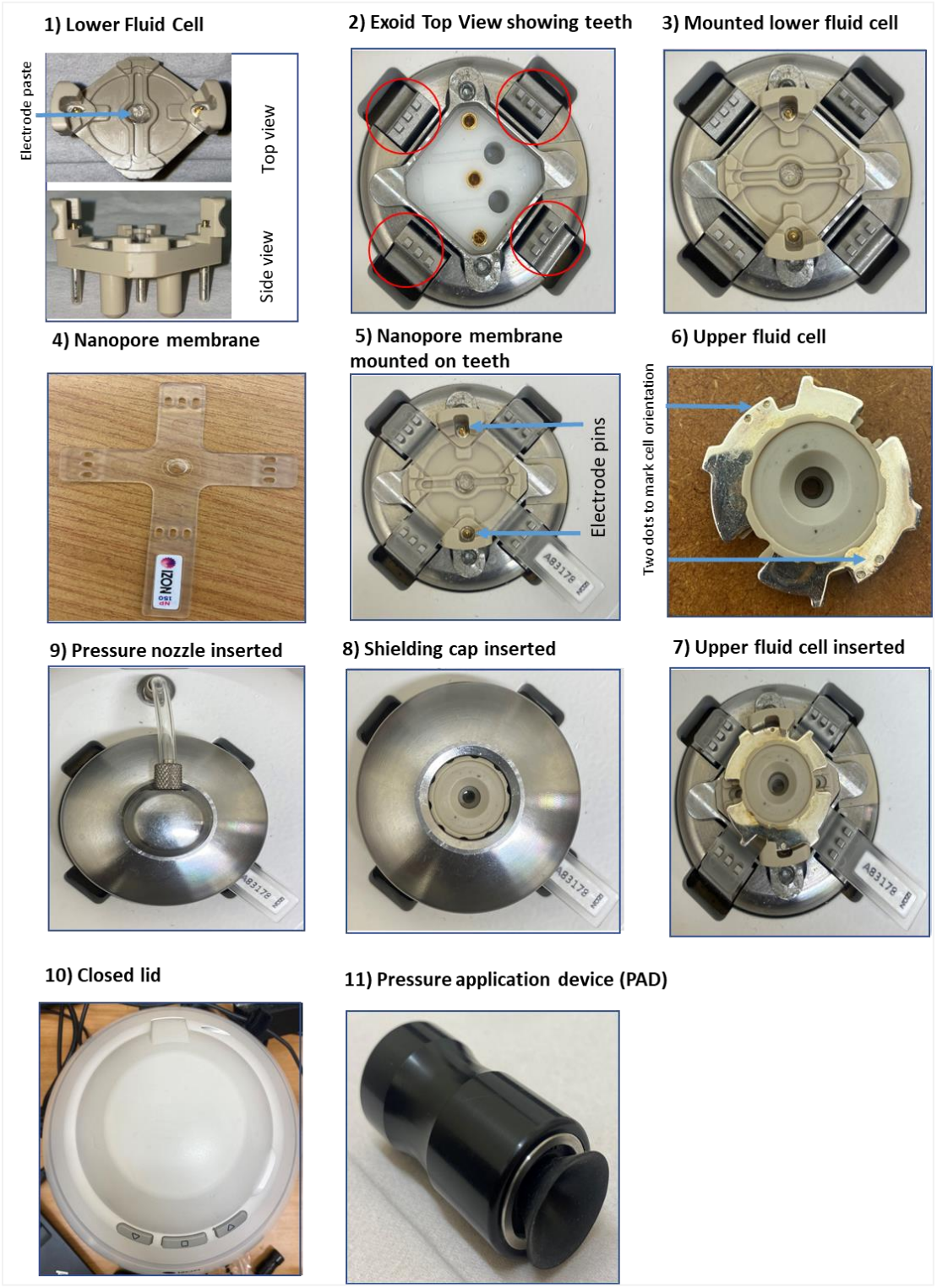

Appendix Figure 1: Main Exoid components required for sample analysis. Diagrams 1-11 depict the necessary parts (in order) that a user should familiarise themselves with in order to begin sample loading and analysis.

References

1. Pan, B.T. and R.M. Johnstone, *Fate of the transferrin receptor during maturation of sheep reticulocytes in vitro: selective externalization of the receptor.* Cell, 1983. **33**(3): p. 967-78.
2. Harding, C. and P. Stahl, *Transferrin recycling in reticulocytes: pH and iron are important determinants of ligand binding and processing.* Biochemical and Biophysical Research Communications, 1983. **113**(2): p. 650-658.
3. Raposo, G., et al., *B lymphocytes secrete antigen-presenting vesicles.* J Exp Med, 1996. **183**(3): p. 1161-72.
4. Harding, C.V., J.E. Heuser, and P.D. Stahl, *Exosomes: looking back three decades and into the future.* J Cell Biol, 2013. **200**(4): p. 367-71.
5. Lin, Y., et al., *Exosomes in disease and regeneration: biological functions, diagnostics, and beneficial effects.* American Journal of Physiology-Heart and Circulatory Physiology, 2020. **319**(6): p. H1162-H1180.
6. Witwer, K.W. and C. Théry, *Extracellular vesicles or exosomes? On primacy, precision, and popularity influencing a choice of nomenclature*. 2019, Taylor & Francis. p. 1648167.
7. Möller, A. and R.J. Lobb, *The evolving translational potential of small extracellular vesicles in cancer.* Nature Reviews Cancer, 2020. **20**(12): p. 697-709.
8. Li, Q., *Role of exosomes in cellular communication between tumor cells and the tumor microenvironment.* Oncology Letters, 2022. **24**(1): p. 1-8.
9. Zhang, J., et al., *Cholesterol content in cell membrane maintains surface levels of ErbB2 and confers a therapeutic vulnerability in ErbB2-positive breast cancer.* Cell Communication and Signaling, 2019. **17**(1): p. 1-12.
10. Sung, B.H., C.A. Parent, and A.M. Weaver, *Extracellular vesicles: Critical players during cell migration.* Developmental cell, 2021. **56**(13): p. 1861-1874.
11. Zaborowski, M.P., et al., *Extracellular Vesicles: Composition, Biological Relevance, and Methods of Study.* Bioscience, 2015. **65**(8): p. 783-797.
12. Keller, S., et al., *Body fluid derived exosomes as a novel template for clinical diagnostics.* Journal of translational medicine, 2011. **9**(1): p. 1-9.
13. Kakarla, R., et al., *Apoptotic cell-derived exosomes: messages from dying cells.* Experimental & Molecular Medicine, 2020. **52**(1): p. 1-6.
14. Brennan, K., et al., *A comparison of methods for the isolation and separation of extracellular vesicles from protein and lipid particles in human serum.* Scientific Reports, 2020. **10**(1): p. 1039.
15. Ratajczak, M.Z. and J. Ratajczak, *Extracellular microvesicles/exosomes: discovery, disbelief, acceptance, and the future?* Leukemia, 2020. **34**(12): p. 3126-3135.
16. Barnette, A. *Flow Cytometry — A Gateway for Discovering More about Small Vesicles*. 2018 16 June 2023; Available from: https://www.bioradiations.com/flow-cytometry-a-gateway-for-discovering-more-about-small-vesicles/.
17. Ståhl, A.L., et al., *Exosomes and microvesicles in normal physiology, pathophysiology, and renal diseases.* Pediatr Nephrol, 2019. **34**(1): p. 11-30.

18. Stahl, P.D. and M.A. Barbieri, *Multivesicular bodies and multivesicular endosomes: the" ins and outs" of endosomal traffic.* Science's STKE, 2002. **2002**(141): p. pe32-pe32.
19. Bobrie, A., et al., *Exosome secretion: molecular mechanisms and roles in immune responses.* Traffic, 2011. **12**(12): p. 1659-1668.
20. Gurung, S., et al., *The exosome journey: From biogenesis to uptake and intracellular signalling.* Cell Communication and Signaling, 2021. **19**(1): p. 1-19.
21. Roxrud, I., H. Stenmark, and L. Malerød, *ESCRT & co.* Biology of the Cell, 2010. **102**(5): p. 293-318.
22. Colombo, M., et al., *Analysis of ESCRT functions in exosome biogenesis, composition and secretion highlights the heterogeneity of extracellular vesicles.* Journal of cell science, 2013. **126**(24): p. 5553-5565.
23. Yang, J., et al., *Plasma-derived exosomal ALIX as a novel biomarker for diagnosis and classification of pancreatic cancer.* Frontiers in Oncology, 2021. **11**: p. 628346.
24. Creutz, C.E., *The annexins and exocytosis.* Science, 1992. **258**(5084): p. 924-31.
25. Phuyal, S., et al., *Regulation of exosome release by glycosphingolipids and flotillins.* Febs j, 2014. **281**(9): p. 2214-27.
26. Jeppesen, D.K., et al., *Reassessment of Exosome Composition.* Cell, 2019. **177**(2): p. 428-445.e18.
27. Urbanelli, L., et al., *Signaling Pathways in Exosomes Biogenesis, Secretion and Fate.* Genes, 2013. **4**(2): p. 152-170.
28. Jankovičová, J., et al., *Tetraspanins, more than markers of extracellular vesicles in reproduction.* International journal of molecular sciences, 2020. **21**(20): p. 7568.
29. Holliday, L.S., L.P.d. Faria, and W.J. Rody Jr, *Actin and actin-associated proteins in extracellular vesicles shed by osteoclasts.* International journal of molecular sciences, 2019. **21**(1): p. 158.
30. Dar, G.H., et al., *Author Correction: GAPDH controls extracellular vesicle biogenesis and enhances the therapeutic potential of EV mediated siRNA delivery to the brain.* Nat Commun, 2021. **12**(1): p. 7357.
31. Wu, R., et al., *Roles of exosomes derived from immune cells in cardiovascular diseases.* Frontiers in Immunology, 2019. **10**: p. 648.
32. Logozzi, M., et al., *Exosomes: a source for new and old biomarkers in cancer.* Cancers, 2020. **12**(9): p. 2566.
33. Rana, S. and M. Zöller, *The functional importance of tetraspanins in exosomes*, in *Emerging Concepts of Tumor Exosome–Mediated Cell-Cell Communication*. 2013, Springer. p. 69-106.
34. Wu, Y., W. Deng, and D.J. Klinke, 2nd, *Exosomes: improved methods to characterize their morphology, RNA content, and surface protein biomarkers.* Analyst, 2015. **140**(19): p. 6631-42.
35. Sokolova, V., et al., *Characterisation of exosomes derived from human cells by nanoparticle tracking analysis and scanning electron microscopy.* Colloids Surf B Biointerfaces, 2011. **87**(1): p. 146-50.
36. Azonano, W., *Reviewing the use of nanoparticle tracking analysis (NTA) for nanomaterial characterization*. 2015.

37. Gardiner, C., et al., *Extracellular vesicle sizing and enumeration by nanoparticle tracking analysis.* Journal of extracellular vesicles, 2013. **2**(1): p. 19671.
38. Zhao, Z., et al., *Isolation and analysis methods of extracellular vesicles (EVs).* Extracellular vesicles and circulating nucleic acids, 2021. **2**: p. 80.
39. Oeyen, E., et al., *Ultrafiltration and size exclusion chromatography combined with asymmetrical-flow field-flow fractionation for the isolation and characterisation of extracellular vesicles from urine.* Journal of Extracellular Vesicles, 2018. **7**(1): p. 1490143.
40. Wu, M., et al., *Isolation of exosomes from whole blood by integrating acoustics and microfluidics.* Proceedings of the National Academy of Sciences, 2017. **114**(40): p. 10584-10589.
41. Maas, S.L., J. De Vrij, and M.L. Broekman, *Quantification and size-profiling of extracellular vesicles using tunable resistive pulse sensing.* JoVE (Journal of Visualized Experiments), 2014(92): p. e51623.
42. Blott, S.J. and K. Pye, *GRADISTAT: a grain size distribution and statistics package for the analysis of unconsolidated sediments.* Earth surface processes and Landforms, 2001. **26**(11): p. 1237-1248.
43. Inc, S., *Use of Silica in Chromatography: Understanding Key Physical Characteristics*. 2021: United States of America.
44. Vogel, R., et al., *A standardized method to determine the concentration of extracellular vesicles using tunable resistive pulse sensing.* Journal of extracellular vesicles, 2016. **5**(1): p. 31242.
45. IzonScience. [cited 2023 16 June 2023]; Available from: https://store.izon.com/products/nanopores%20.
46. Zuba-Surma, E., M. Kucia, and M. Ratajczak, *"Decoding the Dots": The ImageStream system (ISS) as a novel and powerful tool for flow cytometric analysis.* Open Life Sciences, 2008. **3**(1): p. 1-10.
47. Pospichalova, V., et al., *Simplified protocol for flow cytometry analysis of fluorescently labeled exosomes and microvesicles using dedicated flow cytometer.* J Extracell Vesicles, 2015. **4**: p. 25530.
48. De Rosa, S.C., J.M. Brenchley, and M. Roederer, *Beyond six colors: a new era in flow cytometry.* Nature medicine, 2003. **9**(1): p. 112-117.
49. Lucchetti, D., et al., *Measuring extracellular vesicles by conventional flow cytometry: Dream or reality?* International journal of molecular sciences, 2020. **21**(17): p. 6257.
50. Headland, S.E., et al., *Cutting-edge analysis of extracellular microparticles using imagestreamx imaging flow cytometry.* Scientific reports, 2014. **4**(1): p. 1-10.
51. Lässer, C., M. Eldh, and J. Lötvall, *Isolation and characterization of RNA-containing exosomes.* JoVE (Journal of Visualized Experiments), 2012(59): p. e3037.
52. Morales-Kastresana, A. and J.C. Jones, *Flow cytometric analysis of extracellular vesicles*, in *Exosomes and Microvesicles*. 2017, Springer. p. 215-225.
53. Botha, J., H.R. Pugsley, and A. Handberg, *Conventional, high-resolution and imaging flow cytometry: benchmarking performance in characterisation of extracellular vesicles.* Biomedicines, 2021. **9**(2): p. 124.

54. Varga, Z., et al., *Hollow organosilica beads as reference particles for optical detection of extracellular vesicles.* Journal of Thrombosis and Haemostasis, 2018. **16**(8): p. 1646-1655.
55. Hosseini-Beheshti, E., et al., *Exosomes as biomarker enriched microvesicles: characterization of exosomal proteins derived from a panel of prostate cell lines with distinct AR phenotypes.* Molecular & Cellular Proteomics, 2012. **11**(10): p. 863-885.
56. Muller, L., et al., *Tumor-derived exosomes regulate expression of immune function-related genes in human T cell subsets.* Scientific reports, 2016. **6**(1): p. 20254.
57. Szatanek, R., et al., *The Methods of Choice for Extracellular Vesicles (EVs) Characterization.* Int J Mol Sci, 2017. **18**(6).
58. Choi, H. and J.Y. Mun, *Structural analysis of exosomes using different types of electron microscopy.* Applied Microscopy, 2017. **47**(3): p. 171-175.
59. Darvell, B.W., *Chapter 30 - More Chemistry*, in *Materials Science for Dentistry (Tenth Edition)*, B.W. Darvell, Editor. 2018, Woodhead Publishing. p. 771-789.
60. Jung, M.K. and J.Y. Mun, *Sample preparation and imaging of exosomes by transmission electron microscopy.* Journal of visualized experiments: JoVE, 2018(131).
61. Shehadat, S.A., et al., *Optimization of scanning electron microscope technique for amniotic membrane investigation: A preliminary study.* Eur J Dent, 2018. **12**(4): p. 574-578.
62. Nixon, W.C., H.E. Huxley, and A. Klug, *The general principles of scanning electron microscopy.* Philosophical Transactions of the Royal Society of London. B, Biological Sciences, 1971. **261**(837): p. 45-50.
63. Fischer, E.R., et al., *Scanning electron microscopy.* Current protocols in microbiology, 2012. **Chapter 2**: p. Unit2B.2-2B.2.
64. Yuana, Y., et al., *Cryo-electron microscopy of extracellular vesicles in fresh plasma.* Journal of extracellular vesicles, 2013. **2**(1): p. 21494.
65. Cho, B.S., et al., *Exosomes derived from human adipose tissue-derived mesenchymal stem cells alleviate atopic dermatitis.* Stem Cell Res Ther, 2018. **9**(1): p. 187.
66. Dobro, M.J., et al., *Chapter Three - Plunge Freezing for Electron Cryomicroscopy*, in *Methods in Enzymology*, G.J. Jensen, Editor. 2010, Academic Press. p. 63-82.
67. Depelteau, J.S., et al., *An Economical, Portable Manual Cryogenic Plunge Freezer for the Preparation of Vitrified Biological Samples for Cryogenic Electron Microscopy.* Microscopy and Microanalysis, 2020. **26**(3): p. 413-418.
68. Burry, R.W., *Controls for immunocytochemistry: an update.* J Histochem Cytochem, 2011. **59**(1): p. 6-12.
69. Marchenko, S. and L. Flanagan, *Immunocytochemistry: human neural stem cells.* J Vis Exp, 2007(7): p. 267.
70. Kadiu, I., et al., *Biochemical and biologic characterization of exosomes and microvesicles as facilitators of HIV-1 infection in macrophages.* J Immunol, 2012. **189**(2): p. 744-54.

71. Dehghani, M., et al., *Exosome labeling by lipophilic dye PKH26 results in significant increase in vesicle size*. 2019.
72. Pužar Dominkuš, P., et al., *PKH26 labeling of extracellular vesicles: Characterization and cellular internalization of contaminating PKH26 nanoparticles.* Biochimica et Biophysica Acta (BBA) - Biomembranes, 2018. **1860**(6): p. 1350-1361.
73. Van Deun, J., et al., *The impact of disparate isolation methods for extracellular vesicles on downstream RNA profiling.* Journal of extracellular vesicles, 2014. **3**(1): p. 24858.
74. Livshits, M.A., et al., *Isolation of exosomes by differential centrifugation: Theoretical analysis of a commonly used protocol.* Scientific reports, 2015. **5**(1): p. 17319.
75. Yu, L.-L., et al., *A comparison of traditional and novel methods for the separation of exosomes from human samples.* BioMed research international, 2018. **2018**.
76. Webber, J. and A. Clayton, *How pure are your vesicles?* Journal of extracellular vesicles, 2013. **2**(1): p. 19861.
77. Musante, L., et al., *Recovery of urinary nanovesicles from ultracentrifugation supernatants.* Nephrology Dialysis Transplantation, 2013. **28**(6): p. 1425-1433.
78. Momen-Heravi, F., et al., *Current methods for the isolation of extracellular vesicles.* Biological chemistry, 2013. **394**(10): p. 1253-1262.
79. Konoshenko, M.Y., et al., *Isolation of extracellular vesicles: general methodologies and latest trends.* BioMed research international, 2018. **2018**.
80. Cvjetkovic, A., J. Lötvall, and C. Lässer, *The influence of rotor type and centrifugation time on the yield and purity of extracellular vesicles.* Journal of extracellular vesicles, 2014. **3**(1): p. 23111.
81. Liga, A., et al., *Exosome isolation: a microfluidic road-map.* Lab on a Chip, 2015. **15**(11): p. 2388-2394.
82. Onódi, Z., et al., *Isolation of high-purity extracellular vesicles by the combination of iodixanol density gradient ultracentrifugation and bind-elute chromatography from blood plasma.* Frontiers in physiology, 2018. **9**: p. 1479.
83. Tauro, B.J., et al., *Comparison of ultracentrifugation, density gradient separation, and immunoaffinity capture methods for isolating human colon cancer cell line LIM1863-derived exosomes.* Methods, 2012. **56**(2): p. 293-304.
84. Flotte, T.R. and K.I. Berns, *Laboratory techniques in biochemistry and molecular biology*. Vol. 31. 1969: Elsevier.
85. Chen, C.Y., M.C. Hogan, and C.J. Ward, *Purification of exosome-like vesicles from urine*, in *Methods in enzymology*. 2013, Elsevier. p. 225-241.
86. Lamparski, H.G., et al., *Production and characterization of clinical grade exosomes derived from dendritic cells.* Journal of immunological methods, 2002. **270**(2): p. 211-226.
87. Karimi, N., et al., *Detailed analysis of the plasma extracellular vesicle proteome after separation from lipoproteins.* Cellular and molecular life sciences, 2018. **75**: p. 2873-2886.
88. Lobb, R.J., et al., *Optimized exosome isolation protocol for cell culture supernatant and human plasma.* Journal of extracellular vesicles, 2015. **4**(1): p. 27031.

89. Zeringer, E., et al., *Strategies for isolation of exosomes.* Cold Spring Harbor Protocols, 2015. **2015**(4): p. pdb. top074476.
90. Alzahrani, F.A. and I.M. Saadeldin, *Role of exosomes in biological communication systems*. 2021: Springer.
91. Sidhom, K., P.O. Obi, and A. Saleem, *A review of exosomal isolation methods: is size exclusion chromatography the best option?* International Journal of Molecular Sciences, 2020. **21**(18): p. 6466.
92. Cheruvanky, A., et al., *Rapid isolation of urinary exosomal biomarkers using a nanomembrane ultrafiltration concentrator.* American Journal of Physiology-Renal Physiology, 2007. **292**(5): p. F1657-F1661.
93. Diaz, G., et al., *Protein digestion, ultrafiltration, and size exclusion chromatography to optimize the isolation of exosomes from human blood plasma and serum.* JoVE (Journal of Visualized Experiments), 2018(134): p. e57467.
94. Sun, T., et al., *A study of the separation principle in size exclusion chromatography.* Macromolecules, 2004. **37**(11): p. 4304-4312.
95. Baranyai, T., et al., *Isolation of exosomes from blood plasma: qualitative and quantitative comparison of ultracentrifugation and size exclusion chromatography methods.* PloS one, 2015. **10**(12): p. e0145686.
96. Abramowicz, A., P. Widlak, and M. Pietrowska, *Proteomic analysis of exosomal cargo: the challenge of high purity vesicle isolation.* Molecular BioSystems, 2016. **12**(5): p. 1407-1419.
97. Taylor, D.D. and S. Shah, *Methods of isolating extracellular vesicles impact down-stream analyses of their cargoes.* Methods, 2015. **87**: p. 3-10.
98. Mohammad, A.W., D.G. Stevenson, and P.C. Wankat, *Pressure drop correlations and scale-up of size exclusion chromatography with compressible packings.* Industrial & engineering chemistry research, 1992. **31**(2): p. 549-561.
99. Janson, J.C., *Process scale size exclusion chromatography.* Process Scale Liquid Chromatography, 1994: p. 81-98.
100. Stranska, R., et al., *Comparison of membrane affinity-based method with size-exclusion chromatography for isolation of exosome-like vesicles from human plasma.* Journal of translational medicine, 2018. **16**(1): p. 1-9.
101. Karttunen, J., et al., *Size-exclusion chromatography separation reveals that vesicular and non-vesicular small RNA profiles differ in cell free urine.* International Journal of Molecular Sciences, 2021. **22**(9): p. 4881.
102. Batrakova, E.V. and M.S. Kim, *Using exosomes, naturally-equipped nanocarriers, for drug delivery.* Journal of Controlled Release, 2015. **219**: p. 396-405.
103. Benedikter, B.J., et al., *Ultrafiltration combined with size exclusion chromatography efficiently isolates extracellular vesicles from cell culture media for compositional and functional studies.* Scientific reports, 2017. **7**(1): p. 15297.
104. Liangsupree, T., E. Multia, and M.-L. Riekkola, *Modern isolation and separation techniques for extracellular vesicles.* Journal of Chromatography A, 2021. **1636**: p. 461773.
105. Popović, M. and A. de Marco, *Canonical and selective approaches in exosome purification and their implications for diagnostic accuracy.* Transl Cancer Res, 2018. **7**: p. S209-S25.

106. Soda, N., et al., *Advanced liquid biopsy technologies for circulating biomarker detection.* Journal of Materials Chemistry B, 2019. **7**(43): p. 6670-6704.
107. Yang, D., et al., *Progress, opportunity, and perspective on exosome isolation-efforts for efficient exosome-based theranostics.* Theranostics, 2020. **10**(8): p. 3684.
108. Oksvold, M.P., A. Neurauter, and K.W. Pedersen, *Magnetic bead-based isolation of exosomes.* RNA Interference: Challenges and Therapeutic Opportunities, 2015: p. 465-481.
109. Ludwig, A.-K., et al., *Precipitation with polyethylene glycol followed by washing and pelleting by ultracentrifugation enriches extracellular vesicles from tissue culture supernatants in small and large scales.* Journal of extracellular vesicles, 2018. **7**(1): p. 1528109.
110. Andreu, Z., et al., *Comparative analysis of EV isolation procedures for miRNAs detection in serum samples.* Journal of extracellular vesicles, 2016. **5**(1): p. 31655.
111. García-Romero, N., et al., *Polyethylene glycol improves current methods for circulating extracellular vesicle-derived DNA isolation.* Journal of translational medicine, 2019. **17**: p. 1-11.
112. Arakawa, T. and S.N. Timasheff, *Mechanism of polyethylene glycol interaction with proteins.* Biochemistry, 1985. **24**(24): p. 6756-6762.
113. Kalarikkal, S.P., et al., *A cost-effective polyethylene glycol-based method for the isolation of functional edible nanoparticles from ginger rhizomes.* Scientific Reports, 2020. **10**(1): p. 1-12.
114. Shieh, T.-M., et al., *Optimization Protocol of the PEG-Based Method for OSCC-Derived Exosome Isolation and Downstream Applications.* Separations, 2022. **9**(12): p. 435.
115. Lobb, R. and A. Möller, *Size exclusion chromatography: a simple and reliable method for exosome purification.* Extracellular Vesicles: Methods and Protocols, 2017: p. 105-110.
116. He, X., et al., *Utilizing DNase I and graphene oxide modified magnetic nanoparticles for sensing PD-L1 in human plasma.* Sensor Review, 2021. **41**(3): p. 229-234.
117. Peterson, M.F., et al., *Integrated systems for exosome investigation.* Methods, 2015. **87**: p. 31-45.
118. Kim, J., Z. Tan, and D.M. Lubman, *Exosome enrichment of human serum using multiple cycles of centrifugation.* Electrophoresis, 2015. **36**(17): p. 2017-2026.
119. Weng, Y., et al., *Effective isolation of exosomes with polyethylene glycol from cell culture supernatant for in-depth proteome profiling.* Analyst, 2016. **141**(15): p. 4640-4646.
120. Greening, D.W., et al., *A protocol for exosome isolation and characterization: evaluation of ultracentrifugation, density-gradient separation, and immunoaffinity capture methods.* Proteomic profiling: Methods and protocols, 2015: p. 179-209.
121. Filipović, L., et al., *Affinity-based isolation of extracellular vesicles by means of single-domain antibodies bound to macroporous methacrylate-based copolymer.* New Biotechnology, 2022. **69**: p. 36-48.

122. Bellotti, C., et al., *High-grade extracellular vesicles preparation by combined size-exclusion and affinity chromatography.* Scientific Reports, 2021. **11**(1): p. 1-13.
123. Chen, J., et al., *Review on strategies and technologies for exosome isolation and purification.* Frontiers in Bioengineering and Biotechnology, 2022. **9**: p. 811971.
124. *National Institutes of Health (USA)*. [cited 2023 12 January 2023]; Available from: https://clinicaltrials.gov/ct2/results?cond=exosomes&term=&cntry=&state=&city=&dist=.
125. Maharajan, N., et al., *Regenerative therapy using umbilical cord serum.* in vivo, 2021. **35**(2): p. 699-705.
126. Hu, W., et al., *Released exosomes contribute to the immune modulation of cord blood-derived stem cells.* Frontiers in immunology, 2020. **11**: p. 165.
127. Song, Y., et al., *Exosomal miR-146a contributes to the enhanced therapeutic efficacy of interleukin-1β-primed mesenchymal stem cells against sepsis.* Stem cells, 2017. **35**(5): p. 1208-1221.
128. Kim, Y.-J., et al., *Exosomes derived from human umbilical cord blood mesenchymal stem cells stimulates rejuvenation of human skin.* Biochemical and Biophysical Research Communications, 2017. **493**(2): p. 1102-1108.
129. Ganceviciene, R., et al., *Skin anti-aging strategies.* Dermato-endocrinology, 2012. **4**(3): p. 308-319.
130. Gimona, M., et al., *Manufacturing of human extracellular vesicle-based therapeutics for clinical use.* International journal of molecular sciences, 2017. **18**(6): p. 1190.
131. Osaki, M. and F. Okada, *Exosomes and their role in cancer progression.* Yonago acta medica, 2019. **62**(2): p. 182-190.
132. Huang, T. and C.-X. Deng, *Current progresses of exosomes as cancer diagnostic and prognostic biomarkers.* International journal of biological sciences, 2019. **15**(1): p. 1.
133. Zhou, Y., et al., *The role of exosomes and their applications in cancer.* International Journal of Molecular Sciences, 2021. **22**(22): p. 12204.
134. Shaji, J. and V. Patole, *Protein and peptide drug delivery: oral approaches.* Indian journal of pharmaceutical sciences, 2008. **70**(3): p. 269.
135. Betker, J.L., et al., *The potential of exosomes from cow milk for oral delivery.* Journal of pharmaceutical sciences, 2019. **108**(4): p. 1496-1505.
136. Samuel, M., et al., *Oral administration of bovine milk-derived extracellular vesicles induces senescence in the primary tumor but accelerates cancer metastasis.* Nature Communications, 2021. **12**(1): p. 3950.
137. Wong, A.D., et al., *The blood-brain barrier: an engineering perspective.* Frontiers in neuroengineering, 2013. **6**: p. 7.
138. Banks, W.A., et al., *Transport of Extracellular Vesicles across the Blood-Brain Barrier: Brain Pharmacokinetics and Effects of Inflammation.* International journal of molecular sciences, 2020. **21**(12): p. 4407.
139. Daraee, H., et al., *Application of liposomes in medicine and drug delivery.* Artificial cells, nanomedicine, and biotechnology, 2016. **44**(1): p. 381-391.
140. Alvarez-Erviti, L., et al., *Delivery of siRNA to the mouse brain by systemic injection of targeted exosomes.* Nat Biotechnol, 2011. **29**(4): p. 341-5.

141. Haney, M.J., et al., *Macrophage-derived extracellular vesicles as drug delivery systems for triple negative breast cancer (TNBC) therapy.* Journal of Neuroimmune Pharmacology, 2020. **15**: p. 487-500.
142. Pascucci, L., et al., *Paclitaxel is incorporated by mesenchymal stromal cells and released in exosomes that inhibit in vitro tumor growth: a new approach for drug delivery.* J Control Release, 2014. **192**: p. 262-70.
143. Haney, M.J., et al., *Exosomes as drug delivery vehicles for Parkinson's disease therapy.* Journal of controlled release, 2015. **207**: p. 18-30.
144. Luan, X., et al., *Engineering exosomes as refined biological nanoplatforms for drug delivery.* Acta Pharmacologica Sinica, 2017. **38**(6): p. 754-763.
145. Podolak, I., A. Galanty, and D. Sobolewska, *Saponins as cytotoxic agents: a review.* Phytochemistry Reviews, 2010. **9**: p. 425-474.
146. Li, Y.-J., et al., *Gemcitabine loaded autologous exosomes for effective and safe chemotherapy of pancreatic cancer.* Acta biomaterialia, 2020. **101**: p. 519-530.
147. Xi, X.M., S.J. Xia, and R. Lu, *Drug loading techniques for exosome-based drug delivery systems.* Pharmazie, 2021. **76**(2): p. 61-67.
148. Haney, M.J., et al., *TPP1 delivery to lysosomes with extracellular vesicles and their enhanced brain distribution in the animal model of batten disease.* Advanced healthcare materials, 2019. **8**(11): p. 1801271.
149. Tian, Y., et al., *A doxorubicin delivery platform using engineered natural membrane vesicle exosomes for targeted tumor therapy.* Biomaterials, 2014. **35**(7): p. 2383-2390.
150. Fu, S., et al., *Exosome engineering: Current progress in cargo loading and targeted delivery.* NanoImpact, 2020. **20**: p. 100261.
151. Sato, Y.T., et al., *Engineering hybrid exosomes by membrane fusion with liposomes.* Sci Rep, 2016. **6**: p. 21933.
152. Benjakul, S. and F. Bauer, *Physicochemical and enzymatic changes of cod muscle proteins subjected to different freeze–thaw cycles.* Journal of the Science of Food and Agriculture, 2000. **80**(8): p. 1143-1150.
153. Kueltzo, L.A., et al., *Effects of solution conditions, processing parameters, and container materials on aggregation of a monoclonal antibody during freeze-thawing.* J Pharm Sci, 2008. **97**(5): p. 1801-12.
154. Ali, S., et al., *Effect of multiple freeze–thaw cycles on the quality of chicken breast meat.* Food chemistry, 2015. **173**: p. 808-814.
155. Ong, S.G.M., et al., *Evaluation of extrusion technique for nanosizing liposomes.* Pharmaceutics, 2016. **8**(4): p. 36.
156. Donoso-Quezada, J., S. Ayala-Mar, and J. González-Valdez, *State-of-the-art exosome loading and functionalization techniques for enhanced therapeutics: a review.* Critical reviews in biotechnology, 2020. **40**(6): p. 804-820.
157. Busatto, S., et al., *A Simple and Quick Method for Loading Proteins in Extracellular Vesicles.* Pharmaceuticals, 2021. **14**(4): p. 356.
158. Manikandan, M., et al., *Altered levels of miR-21, miR-125b-2*, miR-138, miR-155, miR-184, and miR-205 in oral squamous cell carcinoma and association with clinicopathological characteristics.* Journal of Oral Pathology & Medicine, 2015. **44**(10): p. 792-800.

159. Mahesh, G. and R. Biswas, *MicroRNA-155: a master regulator of inflammation.* Journal of Interferon & Cytokine Research, 2019. **39**(6): p. 321-330.
160. Nie, H., et al., *Use of lung-specific exosomes for miRNA-126 delivery in non-small cell lung cancer.* Nanoscale, 2020. **12**(2): p. 877-887.
161. Jeong, K., et al., *Exosome-mediated microRNA-497 delivery for anti-cancer therapy in a microfluidic 3D lung cancer model.* Lab on a Chip, 2020. **20**(3): p. 548-557.
162. Faruqu, F.N., L. Xu, and K.T. Al-Jamal, *Preparation of exosomes for siRNA delivery to cancer cells.* JoVE (Journal of Visualized Experiments), 2018(142): p. e58814.
163. Kuate, S., et al., *Exosomal vaccines containing the S protein of the SARS coronavirus induce high levels of neutralizing antibodies.* Virology, 2007. **362**(1): p. 26-37.
164. Newcomb, J.D., et al., *Umbilical cord blood research: current and future perspectives.* Cell Transplant, 2007. **16**(2): p. 151-8.
165. Allison, B.J., et al., *Is Umbilical Cord Blood Therapy an Effective Treatment for Early Lung Injury in Growth Restriction?* Frontiers in Endocrinology, 2020. **11**: p. 86.
166. Chang, J.W., et al., *Therapeutic effects of umbilical cord blood-derived mesenchymal stem cell transplantation in experimental lupus nephritis.* Cell Transplant, 2011. **20**(2): p. 245-57.
167. Allan, D.S., *Using umbilical cord blood for regenerative therapy: Proof or promise?* STEM CELLS, 2020. **38**(5): p. 590-595.
168. Nagarajan, M., et al., *Regenerative Therapy Using Umbilical Cord Serum.* In Vivo, 2021. **35**(2): p. 699.
169. Rhéaume, M.-E., et al., *Preparation and growth factor characterization of cord blood-derived plasma, serum, growth factor-rich plasma and induced serum.* Cytokine, 2022. **149**: p. 155756.
170. Maharajan, N., et al., *Regenerative Therapy Using Umbilical Cord Serum.* In Vivo, 2021. **35**(2): p. 699-705.
171. Giannaccare, G., et al., *Umbilical Cord Blood and Serum for the Treatment of Ocular Diseases: A Comprehensive Review.* Ophthalmol Ther, 2020. **9**(2): p. 235-248.
172. Yoon, K., et al., *Therapeutic effect of umbilical cord serum eyedrops for the treatment of dry eye associated with graft-versus-host disease.* Bone marrow transplantation, 2007. **39**(4): p. 231-235.
173. Tovar, A.A., I.A. White, and A.L. Sabater, *Use of Acellular Umbilical Cord-Derived Tissues in Corneal and Ocular Surface Diseases.* Medicines, 2021. **8**(2): p. 12.
174. Yoon, K.-C., et al., *Application of umbilical cord serum eyedrops for recurrent corneal erosions.* Cornea, 2011. **30**(7): p. 744-748.
175. Esquenazi, S., et al., *Use of autologous serum in corneal epithelial defects post-lamellar surgery.* Cornea, 2005. **24**(8): p. 992-997.
176. Rijken, P.J., et al., *Epidermal growth factor induces rapid reorganization of the actin microfilament system in human A431 cells.* Journal of Cell Science, 1991. **100**(3): p. 491-499.

177. Boonstra, J., et al., *The epidermal growth factor.* Cell biology international, 1995. **19**(5): p. 413-430.
178. Versura, P., et al., *Cord blood serum-based eye drops: the impact of donor haematological and obstetric factors on the variability of epidermal growth factor levels.* Blood Transfusion, 2014. **12**(Suppl 1): p. s44.
179. Zhong, X.Q., et al., *Umbilical Cord Blood-Derived Exosomes From Very Preterm Infants With Bronchopulmonary Dysplasia Impaired Endothelial Angiogenesis: Roles of Exosomal MicroRNAs.* Front Cell Dev Biol, 2021. **9**: p. 637248.
180. Huang, Y.-J., et al., *Umbilical cord blood plasma-derived exosomes as a novel therapy to reverse liver fibrosis.* Stem Cell Research & Therapy, 2021. **12**(1): p. 568.
181. Hu, Y., et al., *Exosomes from human umbilical cord blood accelerate cutaneous wound healing through miR-21-3p-mediated promotion of angiogenesis and fibroblast function.* Theranostics, 2018. **8**(1): p. 169-184.
182. Jia, L., et al., *Maternal and umbilical cord serum-derived exosomes enhance endothelial cell proliferation and migration.* The FASEB Journal, 2018. **32**(8): p. 4534-4543.
183. IzonScience. *TRPS Fundamentals*. [cited 2023 16 June 2023]; Available from: https://support.izon.com/what-do-each-of-the-tunable-parameters-do.
184. Coumans, F.A., et al., *Reproducible extracellular vesicle size and concentration determination with tunable resistive pulse sensing.* Journal of extracellular vesicles, 2014. **3**(1): p. 25922.
185. IzonScience. *qNano user manual*. [cited 2023 15-05-2023]; Available from: https://f.hubspotusercontent30.net/hubfs/4136435/Manuals,%20Technical%20Notes%20and%20Customer%20Support/qNano/qnano-user-manual-QN1-OQ-014.pdf.
186. Daintith, J., *A dictionary of physics*. 2014, Oxford University Press.
187. IzonScience. *The Exoid training practical mudule*. [cited 2023 16 June 2023]; Available from: https://files.izon.com/hubfs/Manuals,%20Technical%20Notes%20and%20Customer%20Support/Exoid/exoid-training-manual-EX1-OQ-003.pdf.
188. Ashraf Malik, M., et al., *CD81(+) Exosomes Play a Pivotal Role in the Establishment of Hepatitis C Persistent Infection and Contribute Toward the Progression of Hepatocellular Carcinoma.* Viral Immunol, 2019. **32**(10): p. 453-462.
189. Van De Vlekkert, D., et al., *Isolation, Purification and Characterization of Exosomes fromFibroblast Cultures of Skeletal Muscle.* Bio Protoc, 2020. **10**(7): p. e3576.
190. Pelegrine, D.H.G. and C.A. Gasparetto, *Whey proteins solubility as function of temperature and pH.* LWT - Food Science and Technology, 2005. **38**(1): p. 77-80.
191. Hu, Y., et al., *Exosomes from human umbilical cord blood accelerate cutaneous wound healing through miR-21-3p-mediated promotion of angiogenesis and fibroblast function.* Theranostics, 2018. **8**(1): p. 169.
192. Tang, Y., Y. Zhou, and H.-J. Li, *Advances in mesenchymal stem cell exosomes: a review.* Stem Cell Research & Therapy, 2021. **12**(1): p. 71.

193. Malenica, M., et al., *Perspectives of Microscopy Methods for Morphology Characterisation of Extracellular Vesicles from Human Biofluids.* Biomedicines, 2021. **9**(6).
194. Rikkert, L.G., et al., *Quality of extracellular vesicle images by transmission electron microscopy is operator and protocol dependent.* J Extracell Vesicles, 2019. **8**(1): p. 1555419.
195. Busatto, S., et al., *Considerations for extracellular vesicle and lipoprotein interactions in cell culture assays.* J Extracell Vesicles, 2022. **11**(4): p. e12202.
196. Nagasaka, H., et al., *Unique character and metabolism of high density lipoprotein (HDL) in fetus.* Atherosclerosis, 2002. **161**(1): p. 215-23.
197. Averna, M.R., et al., *Lipids, lipoproteins and apolipoproteins AI, AII, B, CII, CIII and E in newborns.* Biol Neonate, 1991. **60**(3-4): p. 187-92.
198. Kolli, S., et al., *The Role of Nerve Growth Factor in Maintaining Proliferative Capacity, Colony-Forming Efficiency, and the Limbal Stem Cell Phenotype.* Stem Cells, 2019. **37**(1): p. 139-149.
199. Esposito, G., et al., *Nerve Growth Factor (NGF) modulates in vitro induced myofibroblasts by highlighting a differential protein signature.* Scientific Reports, 2021. **11**(1): p. 1672.
200. Wong, W., et al., *The exercise cytokine interleukin-15 rescues slow wound healing in aged mice.* J Biol Chem, 2019. **294**(52): p. 20024-20038.